Title
Visual cue representation without movement or task demands in the rodent hippocampus.

Author
Purandare, Chinmay

Publication Date
2021

Peer reviewed|Thesis/dissertation

UNIVERSITY OF CALIFORNIA

Los Angeles

Visual cue representation without movement or task demands in the rodent hippocampus.

A dissertation submitted in partial satisfaction
of the requirements for the degree
Doctor of Philosophy in Bioengineering

by

Chinmay Purandare

2021

ABSTRACT OF THE DISSERTATION

Visual cue representation without movement or task demands in the rodent hippocampus

by

Chinmay Purandare

Doctor of Philosophy in Bioengineering

University of California, Los Angeles, 2021

Professor Kalyanam Shivkumar, Co-Chair

Professor Mayank Mehta, Co-Chair

Rodent hippocampus is believed to be critically involved in generating selectivity to allocentric space, call place cells, which are abstract and prospective. Such responses are thought to require both distal visual cues and self-motion cues. In primates, however, hippocampal neurons encode object-place association without any locomotion requirement.

In this thesis, we developed a simple experimental design of a moving bar of light to investigate the representation of distance, angle, and movement direction of this distal visual cue in hippocampal region CA1. Nonspecific olfactory and auditory cues were eliminated using a previously described virtual reality (VR) system, where the subject was body-fixed but allowed

to run on a spherical treadmill. Our results demonstrate that a moving bar of light can reliably modulate the activity of majority of hippocampal place cells, without any task demand, memory, reward contingency or locomotion requirements. Visual cue representation was retrospective in nature, as would be expected from the hierarchical position of hippocampus in the visual circuit, unlike place cells, which are prospective.

Our unique VR design allowed us to dissociate the contributions of distal visual cues and head movements on hippocampal firing. In addition to the visual cue encoding described above, we found that a third of the neurons showed selective responses with respect to head movements. This head movement selectivity was inversely related to the visual cue selectivity and was also found in experiments where the animal performed navigational tasks in the VR. These results suggest that multisensory association present in the real world plays a stronger role in hippocampal firing than navigational demands tied to virtual navigation**.**

We also analyzed single unit responses from multiple hippocampal regions (including CA1) in a publicly available dataset of head fixed mice viewing repeated presentations of movie-like, streaming visual stimuli. Hippocampal responses were selective to different frames of the movie and this selectivity reduced substantially when the frames were presented in a shuffled fashion.

These results suggest that the rodent hippocampus can encode features of simple as well as complex visual stimuli without active engagement or reward contingencies, similar to other cortical areas involved in visual processing. On the other hand, spatial selectivity can occur in body fixed environments with only head movements, with mis-matched as well as absent distal visual cues. Taken together, our work furthers the understanding of multi-sensory contributions to hippocampal firing.

The dissertation of Chinmay Purandare is approved.

Robijn Bruinsma

Dario Ringach

Kalyanam Shivkumar, Committee Co-Chair

Mayank Mehta, Committee Co-Chair

University of California, Los Angeles

2021

TABLE OF CONTENTS

TABLE OF FIGURES

Main Figures

Extended Data Figures

ACKNOWLEDGEMENTS

I am thankful to my advisor, Mayank Mehta, starting with the opportunity to work in this lab in the summer of 2015. I have deeply enjoyed my time here and cherished the process of research and the joys of discovery. I attribute my scientific temper, ability to work independently, and attention to detail to my experiences in this lab, and I am thankful for his patience, guidance, and support.

I thank the members of the lab, Dr. Shonali Dhingra, Krishna Choudhary, Mina Shahi, Dr. Karen Safaryan, Thuc To, Rodrigo Rios, Dr. Jason Moore, and Dr. Aditya Singh for being friends and for their love, support, and guidance in this endeavor. I particularly want to thank Shonali for teaching me rodent surgery and electrophysiology and for the immense help with experiments which made this work possible. I also thank Cliff Vuong, Ayaka Hachisuka and a host of undergraduate researchers as well as former members of the lab whose efforts yielded the data I used in my research.

I thank my committee for giving me guidance through their expertise and encouraging me to pursue these projects. Additional thanks go to Dr. Dario Ringach and Dr. Alcino Silva for their input for the work presented in Chapter 2. I am also thankful to the team at Allen Institute for Brain sciences (Seattle) for publicly sharing the data presented in Chapter 4.

Most importantly, I thank my parents, Madhuri and Sudheer Purandare who have been wonderful in supporting my ambitions my entire life. They share this achievement with me. I also thank my partner Deepika Dixit. I would never have been able to take on this enormous task if not for their support, love, and encouragement.

Chapter 2 is adapted from

Chinmay S. Purandare, Shonali Dhingra, Rodrigo Rios, Cliff Vuong, Thuc To, Ayaka Hachisuka, Krishna Choudhary, Mayank R. Mehta. **Moving bar of light generates angle, distance and direction selectivity in place cells** (*Submitted*)
Author Contributions are as follows**:**

M.R.M. and **C.S.P.** designed the experiments. **S.D., C.S.P., R.R., C.V., T.T., A.H.** and **K.C.** performed the experiments. **C.S.P.** developed the stimuli and performed the analyses with input from **M.R.M. M.R.M.** and **C.S.P** wrote the manuscript with critical input from **S.D.** and other authors.

Chapter 3 is adapted from

Chinmay S. Purandare, Mayank R. Mehta. **Hippocampal representations for real world space during virtual environment navigation** *(In preparation for publication)*

Chapter 4 is adapted from

Chinmay S. Purandare, Mayank R. Mehta. **Streaming visual stimuli elicit selective responses in rodent hippocampus** *(In preparation for publication)*

VITA

EDUCATION

2016 - 2018	M.S.	Bioengineering, UCLA (3.69/4)
2012 - 2016	B.Tech.	Indian Institute of Technology (IIT) Bombay, India.
	Major	Mechanical Engineering (8.87/10)
	Minor	Systems and Control Engineering

RESEARCH MANUSCRIPTS

1. Moving bar of light generates angle, distance, and direction selectivity in place cells (Under review at *Nature*)
2. Hippocampal representations for real world space during virtual environment navigation (*In preparation for publication*. Presented at SfN 2018 & 2019, iNAV 2020)
3. Streaming visual stimuli elicit selective responses in rodent hippocampus *(In preparation for publication)*
4. Excitation inhibition balance in rodent hippocampus during virtual environment navigation (*In preparation for publication*)

AWARDS & FUNDING

2020	Jessamine K. Hilliard Neurobiology Graduate Student Award
2016 - 2017	UCLA Graduate Division University Fellowship

TEACHING EXPERIENCE

2020	Teaching Assistant, Physics for Life Sciences Majors	UCLA
2020	Winter Course on Computational Brain Research	IIT-Madras, India
2018, 2019	Teaching Assistant, Neurophysics: Brain-Mind Problem	UCLA

CHAPTER 1: INTRODUCTION

Hippocampus is one of the most well-studied brain regions in mammals. In their seminal work on 'Patient H.M.', Milner[1] and colleagues found that surgical lesion of hippocampus (undertaken to relieve epileptic seizures) led to severe anterograde amnesia. H.M. had reasonably good memory of events up to 5 years and earlier from the surgery but could not form new episodic memories. On the other hand, he could learn new motor skills, suggesting that the damage to hippocampus was tied to the loss of episodic or declarative memory but not so much to the loss of procedural memory.

Synaptic plasticity is one of the most widely accepted neural mechanisms of learning and memory. Synapses, the connections between 2 neurons, strengthen or weaken over time. Repeated pairing of the 'driving' or presynaptic neuron, coupled with the depolarization of the 'downstream' or post-synaptic neuron leads to changes in the efficacy of the driving neuron to make the downstream neuron fire. Relative timing is critical; typically, connections become stronger when the presynaptic neuron fires before but within few milliseconds of the post synaptic neuron. Cellular studies of synaptic plasticity were also first conducted on the hippocampal circuitry. Bliss and Lomo[2] studied long term potentiation on the synapses forming on dentate granule cells from the perforant path. Repeated potentiation of the perforant path fibers for less than 30 seconds resulted in larger post synaptic depolarization of the granule cells, which was maintained for long periods of time (30 mins to 10 hours).

These clinical and cellular observations led to numerous experiments in rodents as well as primates studying the role of hippocampus in formation and recollection of memory. Monkeys can be trained to associate a given object with a particular location, even using a single training trial[3]. But such object-place memory is impaired with bilateral hippocampus lesion, even if they continue to have object recognition memory. One of the first experimental protocols for object-place association in rodents is the Morris Water Maze (MWM)[4] task. Rats were required to swim in a circular pool and search for an elevated platform which allowed them to escape and stop swimming (Fig 1.1). Wild type rats readily learnt this place-navigation task and could navigate to the platform within 30 training trials, even if they started at a novel starting location.

On the other hand, hippocampus lesioned rats were unable to remember the location of the hidden platform, hence showing deficits of object (escape platform) in place (quadrant of the water pool) memory.

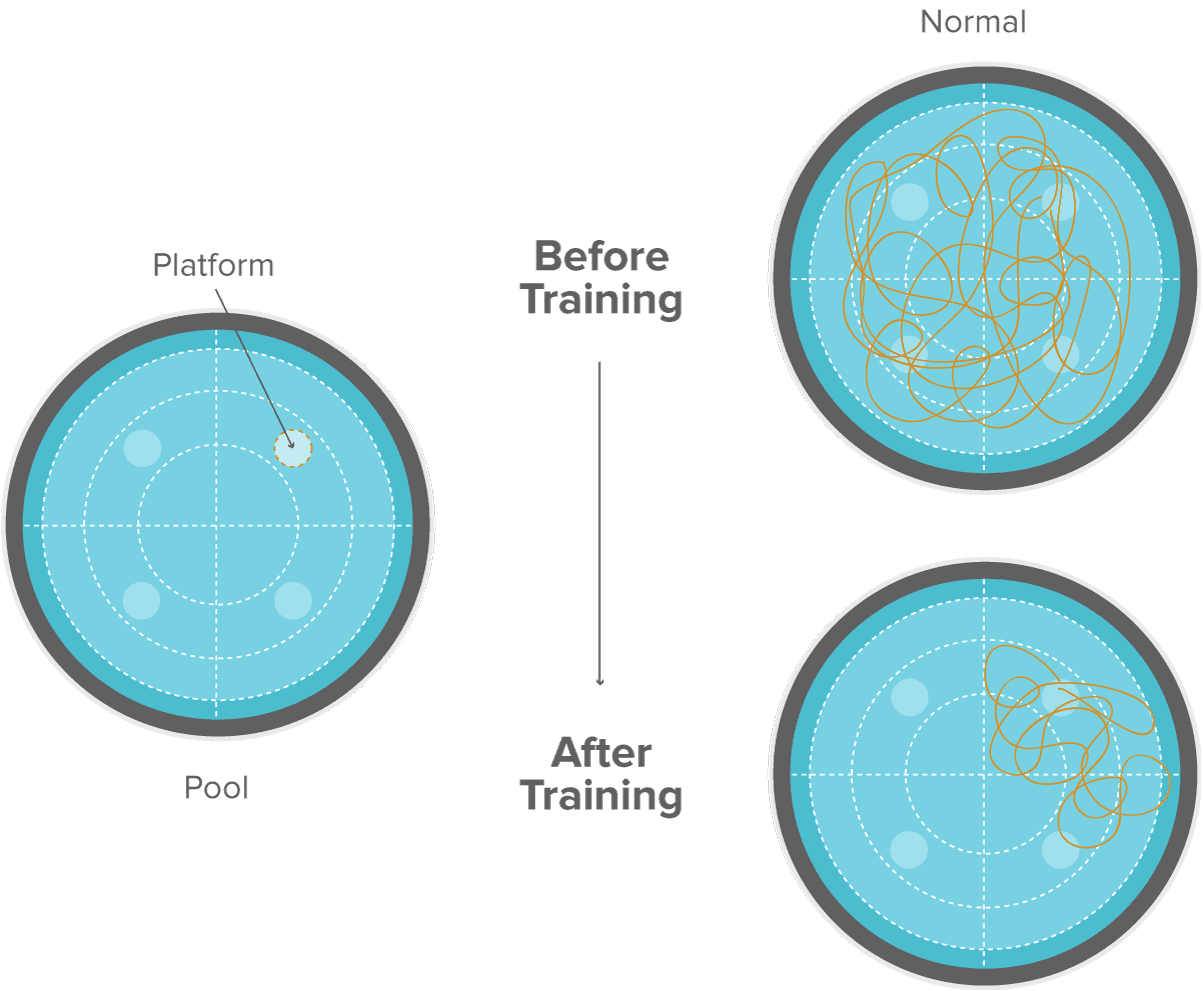

Fig 1.1 | Morris Water Maze (MWM) task. Mice spend more time in the target quadrant where the escape platform is located after repeated training in the MWM task.

Rodent hippocampus is now believed to be centrally involved in spatial memory and considered the seat of 'internal GPS'. Neural responses in hippocampus and adjacent regions enable the encoding of an allocentric, abstract, Euclidean map of space. The formation of such a cognitive map is supported by single unit firing in hippocampus which is selective for the current location of the animal. O'Keefe and Nadel[5] demonstrated the existence of such 'place cells'; neurons which fire in a restricted region of space and are silent at other locations (Fig 1.2).

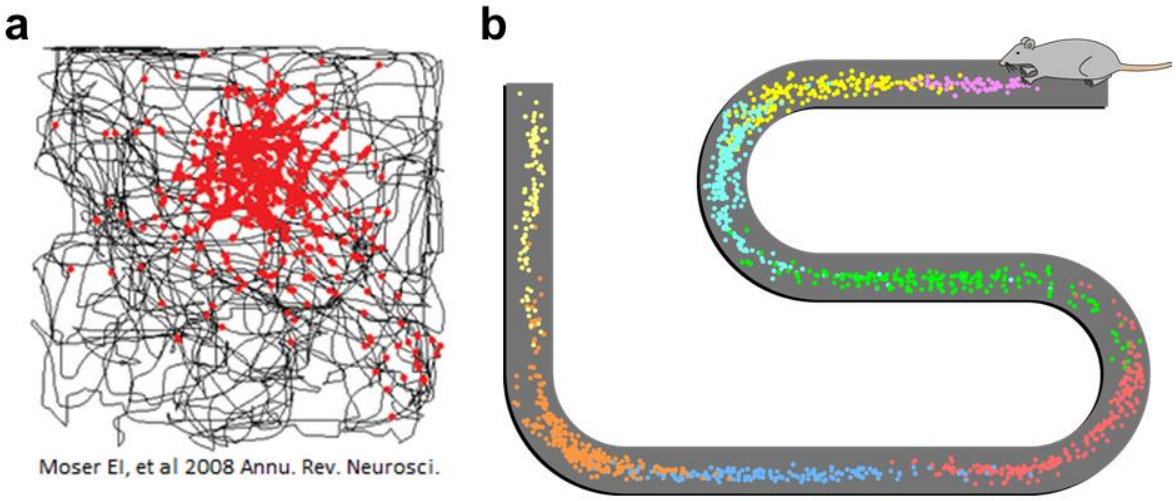

Fig 1.2 | Illustration of place cells (a) Spikes from a single hippocampal neuron in red are localized to a subset of the space explored, called the place field of that unit. Path taken by the animal in a two-dimensional arena are depicted in gray. Vast majority of CA1 hippocampal neurons show place fields as this example neuron, and hence are often called 'place cells'. **(b)** Illustration of a one dimensional track with different place cell spikes shown in different colors along the track (Source: Wikipedia).

What sensory information do these hippocampal neurons use to form such a map of space? Landmark cues, like distal visual cues, are believed to influence hippocampal firing. When rats ran in a circular environment with a single cue card on one of the walls, the rotation of the cue card caused a proportional rotation of the place cell firing activity, also called the 'place field' of the neuron[6] (Fig 1.3). But place cells are seen in blind rats as well[7], whose place fields are controlled by the location of accessible landmarks of different shapes and sizes which were placed inside the testing arena. This result suggests that in addition to the visual cues, olfactory (smell) and tactile (touch) properties of objects affect hippocampal firing. More interestingly, blind rats had place cells even at locations away from these cues, which were taken to suggest that once landmarks have been established, hippocampal firing can use internally generated self-motion information to build a spatial map.

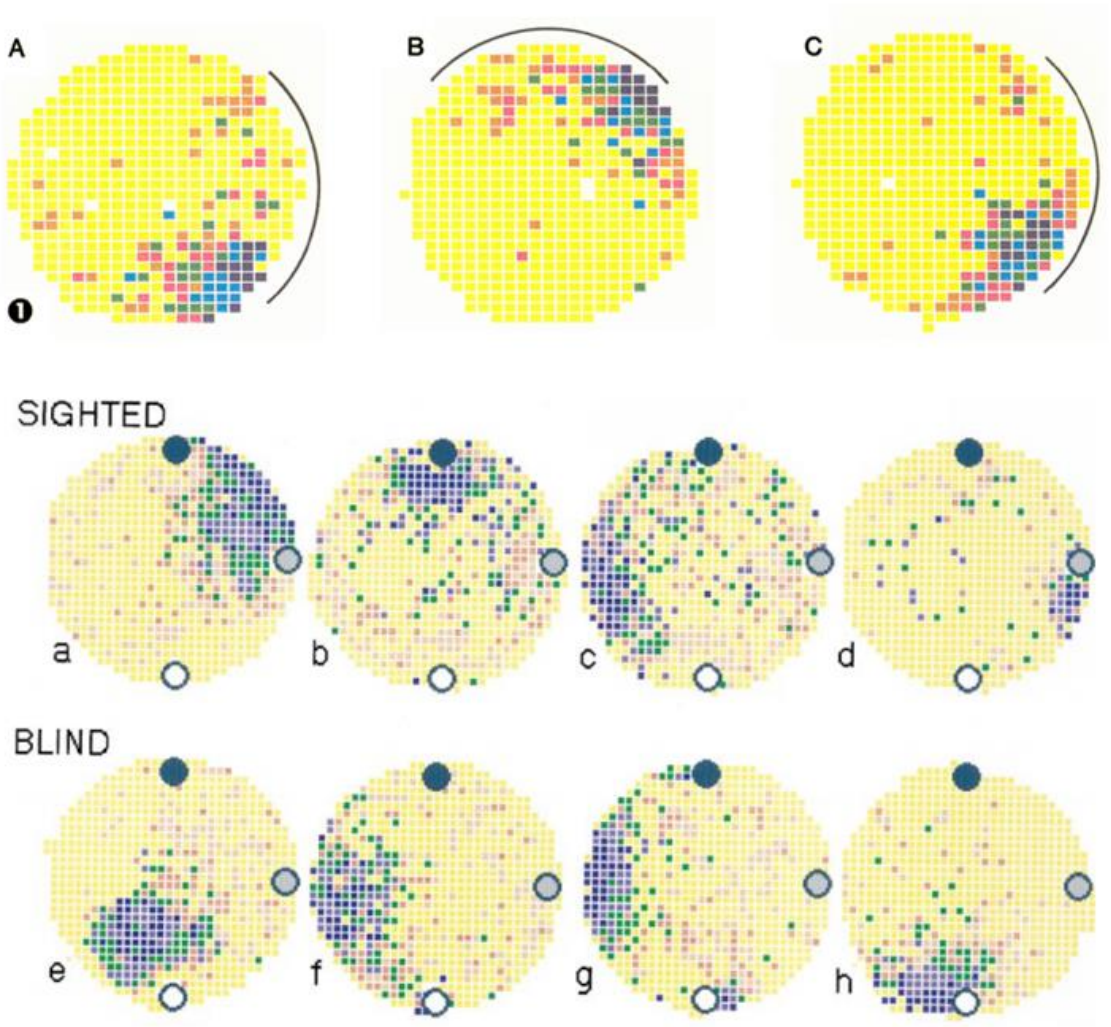

Fig 1.3 | Relationship between visual cues and spatial coding. Top row: The firing of a hippocampal neuron followed the rotation of a cue card on the wall (illustrated by the arc on the right in the first session (A) and later moved by 90º to the north of the testing arena (B). **Middle and bottom row:** Instead of distal visual cue, similar experiments using objects placed inside the arena led to place fields in sighted as well as blind rats. (Adapted from Save et. al. *Journal of Neuroscience* 1998[7])

Apart from landmark and cue-based navigation, path integration is the other leading theory of spatial encoding in rodent hippocampus. According to this theory, self-motion cues can be integrated over time to compute current position from an initial starting point. The first

demonstration of the use of a path integration system in mammals was shown in gerbils[8,9]. Female gerbils searched for her cubs in dark, but upon successful retrieval of the pups, returned back in a straight-line path (Fig. 1.4). This observation was later corroborated with the presence of head direction cells in post-subiculum (which is synapse downstream from hippocampus CA1) which could enable the encoding of cardinal direction in the allocentric frame using vestibular cues[10]. Another contributing class of cells is the grid cells in entorhinal cortex, which have a grid-like structure of repeating place fields at regular intervals but with different spatial periodicities[11]. The entorhinal cortex is one of the major inputs to CA1 and their input can be combined in a sigmoidal fashion to cause spatial firing of place cells (Fig 1.5). It has also been suggested that hippocampal single unit firing is part of a pre-configured network which uses self-motion to keep track of allocentric space[12]. According to this theory, distal visual cues or other landmarks can be used to reset the system and correct the errors which will build up in the position estimate over time.

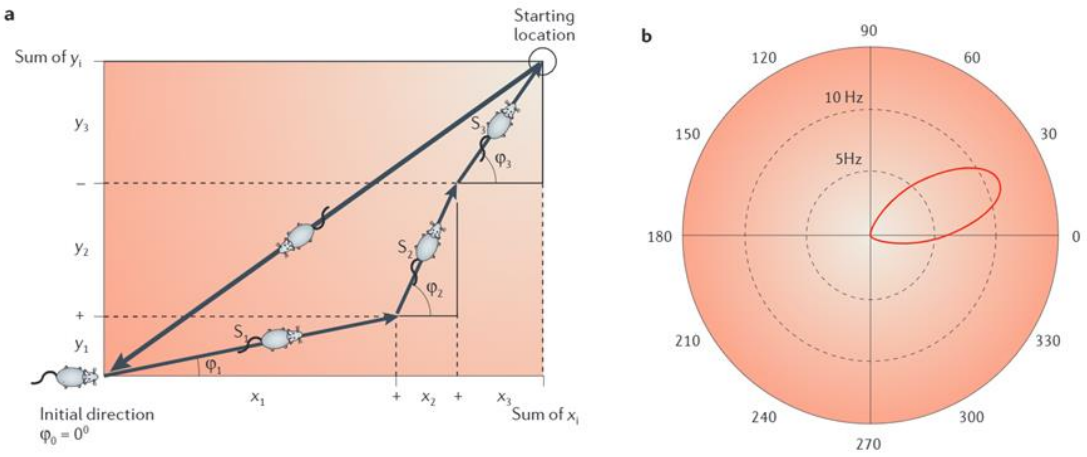

Fig 1.4 | Path integration in mammals and head direction cells (a) Illustration of path integration, where outward motion along different directions can be 'integrated' to compute an effective displacement vector from the initial position. On the return trajectory, animals use this direct path. **(b)** Example firing rate response of a head direction cell, which selectively fires when the animal faces ~30^o with respect to the experimental room.

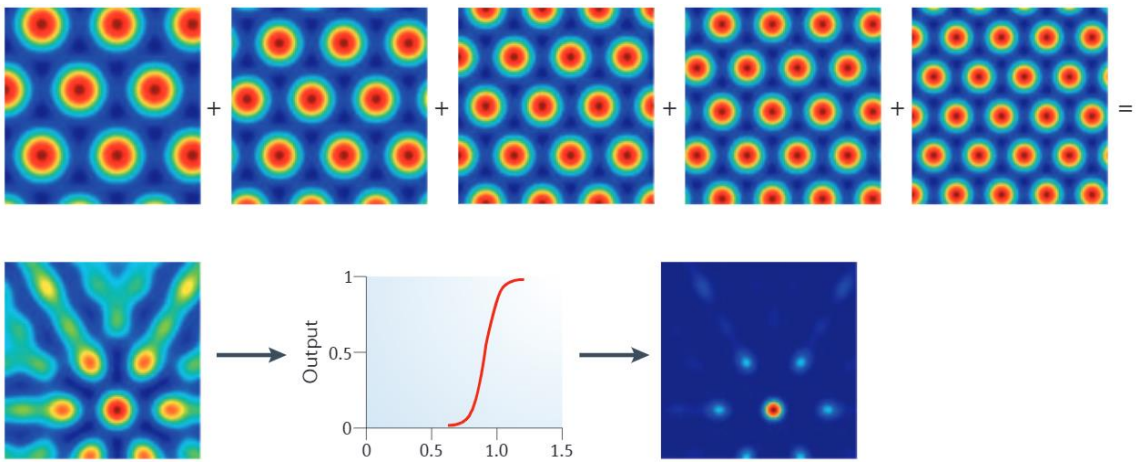

Fig 1.5 | A model of place cell firing as a summation of grid cell activity. Linear summation of multiple grid cells with different spatial periodicities leads to a single peak, where they overlap. A simple thresholding operation on this summation can lead to a single region of maximal firing as seen for place cells.

Virtual reality (VR) environments have recently emerged as a popular choice of experimental setup to dissociate the contribution of distal visual cues and other proximal cues, like tactile and olfactory cues. The exact design of VR and the choice of self-motion cues used to manipulate the visual scene affect the response of hippocampal place cells. In rodent studies of Aronov and Tank[13], the animal ran of a styrofoam ball, but was afforded 360^o turning, and the visual world moved with him. In such a design, the range of vestibular cues during VR exploration are quite similar to that in free foraging in real world (RW) environments (Fig 1.6). Intact spatial firing was observed in the animals foraging for reward in such a virtual environment, even if they were physically in the same space in the experimental room. On the other hand, prior work from our lab[14] reported the loss of spatial selectivity in VR if 2-dimensional navigation is accompanied by incomplete vestibular signal, resulting from body fixation, which does not allow a 360^o turn. But this impaired vestibular signal seems to be sufficient for selectivity to position along linear paths, where active turning is largely avoided. Hence selective responses in hippocampus CA1 seem to require intact and full range of self-motion cues, particularly for navigation of two-dimensional paths.

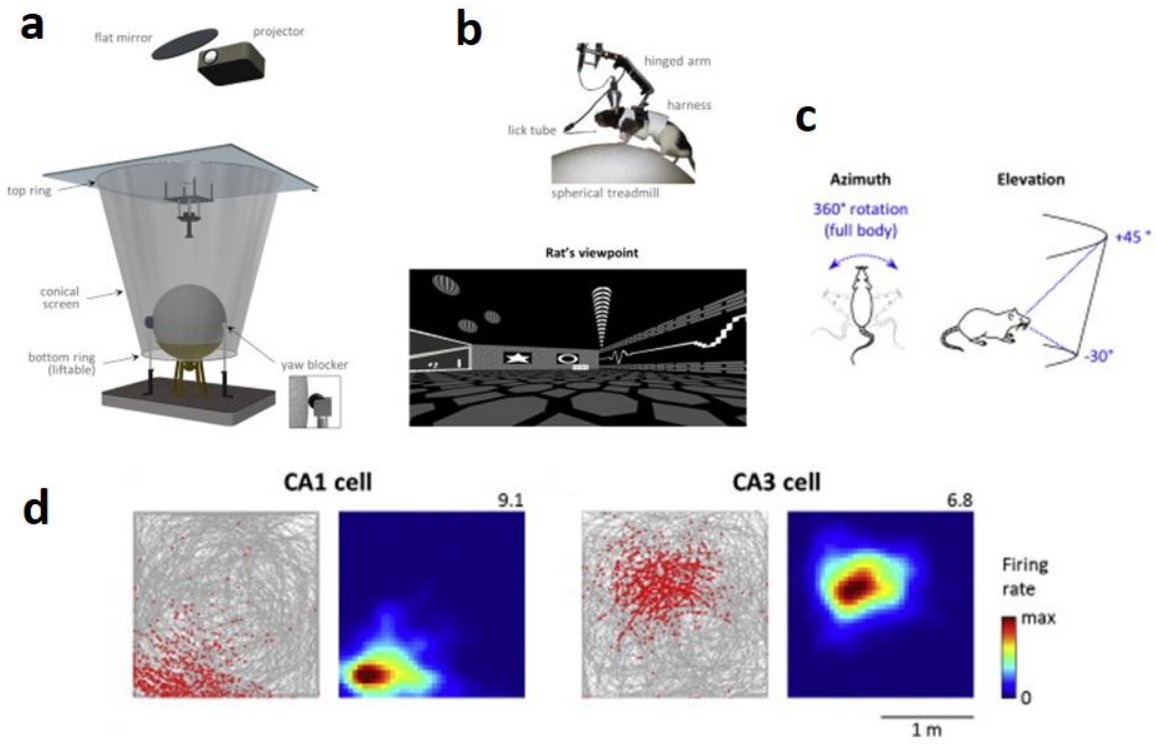

Fig 1.6 | Place cells in VR with complete rotational freedom (a) VR setup from experiments of Aronov and Tank[13] (Neuron 2014). The overhead projector creates a VR environment all around the animal, who can run on the spherical treadmill. The treadmill is installed with a 'yaw-blocker' which prevents the treadmill rotating around. **(b) & (c)** Instead the animal, along with the lick tube turns around, hence having the complete range of turning movements. **(d)** Intact spatial selectivity, evidenced by place cells in CA1 and CA3 was reported in such a VR system.

Recent work has also shown that hippocampal neurons are involved in the encoding of location of 'others', called social place cells. In these experiments, an observer rat[15] or bat[16] viewed another animal (termed demonstrator) in an observational learning task. In these experiments, the 'observer' animal was required to navigate a variation of the T-maze, based on which arm/side the demonstrator animal navigated to. Neurons in CA1 were found to be encoding for the location of the demonstrator animal for both bats and rats. But in similar experiments where the rats were passively observing another animal run back and forth on a linear track[17], hippocampal activity did not show selectivity for the demonstrator animal's position suggesting that task demands or a memory component are crucial for encoding the position of others in hippocampus.

In addition to the now well-accepted role in navigation, rodent hippocampus has recently been shown to encode non-spatial information. Rats were trained to perform an auditory frequency detection task where they held onto a lever while a frequency swept from 2 to 22 kHz, and had to release the lever in a small range of sound frequency for rewards[18]. They found that ~40% of CA1 hippocampal neurons showed selective firing during this non-spatial task, where different neurons fired at different epochs of the experiments (press the lever, release the lever, and corresponding to different frequencies). As a control, they repeated the sound frequency sweeps, without the requirement for level press and release. In this passive playback condition, selectivity in hippocampus was lost, suggesting that task demands, and memory requirements play an important role in hippocampal encoding of a non-spatial dimension (Fig 1.7). Similar experiments[19,20] showed that hippocampal units showed sensory correlates (preferential firing during high frequency or low frequency tones) during working memory or reference memory tasks, but not during passive stimulation without memory task.

What is the minimum combination of sensory, self-motion cues and memory demands which are necessary and sufficient to drive selective responses in hippocampus? Prior work has shown that direction selectivity in the hippocampus can be causally controlled by distal visual cues. The virtual environment was varied, ranging from a rich set of distal visual cues on all walls, to a visual environment with all 4 walls which were black[21]. Although there was no task demand tied to the visual cues on the wall, hippocampal firing was modulated by these cues in a causal manner. The use of body-fixed VR caused the proximal cues to be unpaired with the visual cues on the walls and vestibular signal was minimized since the animal could not completely turn around. This suggests that active locomotion, paired with visual cues is sufficient to drive selective responses in hippocampus to this one-dimensional metric of direction. On the other hand, active navigation itself was insufficient, since in the absence of cues on the wall, directional selectivity was lost (Fig 1.8).

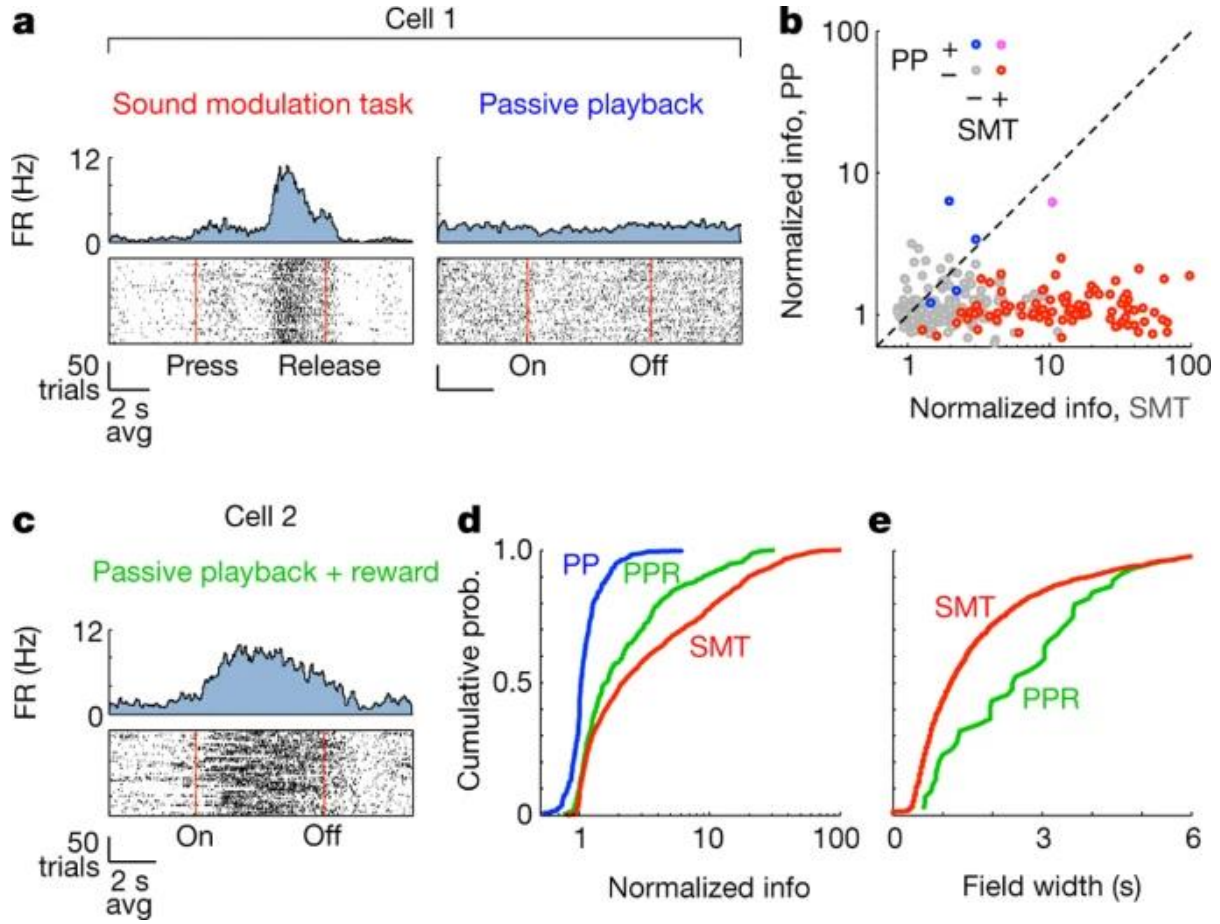

Fig 1.7 | **Hippocampal selectivity to a non-spatial dimension (a)** Activity of the same CA1 neuron during the SMT and during passive playback (PP) of acoustic stimuli that matched those in the SMT. Top, PSTHs. Bottom, raster plots, with time linearly warped between the onset and the offset of the sound. On, sound onset; off, sound offset. **(b)** Firing rate modulation of all 295 CA1 neurons recorded during the SMT and passive playback. 'Normalized info' is the mutual information between spikes and the phase of the task, divided by the average value from samples with shuffled spike timing. Points are colored according to whether the cell was modulated by SMT and/or passive playback. **(c)** Activity of a neuron during passive playback of acoustic stimuli that were followed by rewards (PPR). **(d)** Cumulative histograms of the normalized information in the three tasks (295 cells for SMT and passive playback and 248 cells for PPR). Task modulation of activity is stronger during PPR than during passive playback and even stronger during the SMT. **(e)** Cumulative histograms of the field durations during SMT

and PPR. Activity shows more temporally precise task modulation during the SMT. (Adapted from Aronov et. al. *Nature* 2017[18])

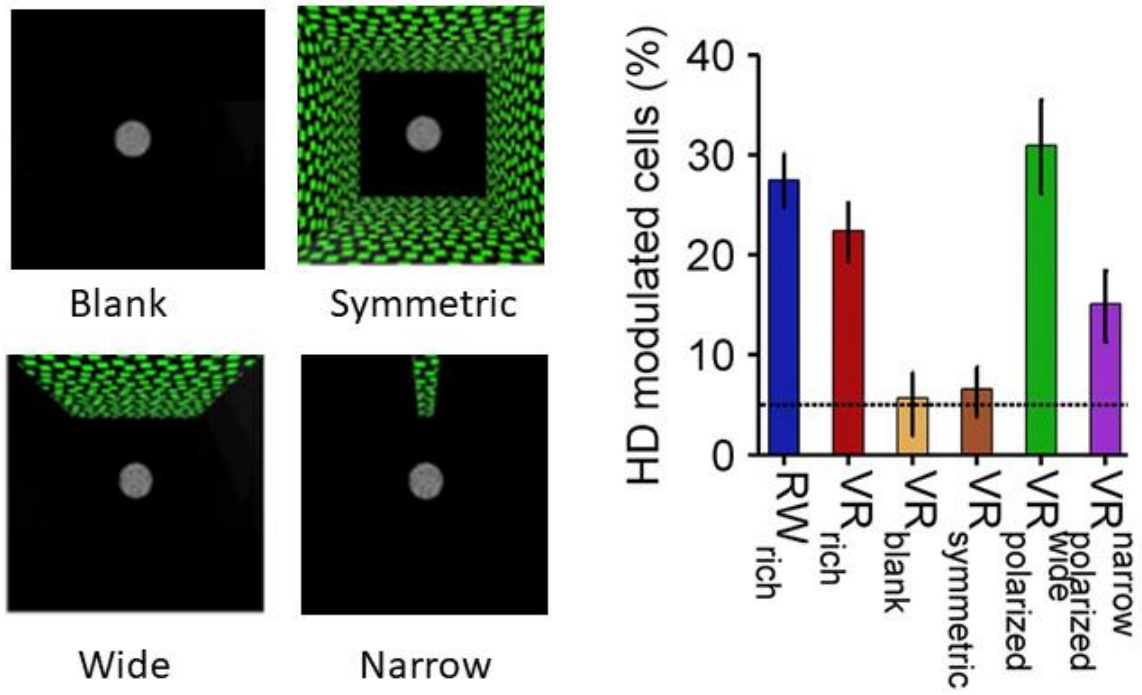

Fig 1.8 | Causal control of hippocampal directionality by distal visual cues. Left - Illustration of the experimental setup with variety of visual cues on the walls **Right -** Selectivity for head direction (HD) was at chance level when the visual cues did not provide directional information, as for the blank and symmetric experiments even though the animal actively navigated the virtual room. (Adapted from Acharya et. al. *Cell* 2015[21])

In the present work, we considered the complementary experiment. Instead of a stationary visual cue presented while the animal is mobile, we rotated a bar of light (similar to the 'narrow' strip in Fig 1.8) while the animal was held a fixed distance from the visual cue. These experiments and their results are described in Chapter 2.

Although body fixed, the rats were able to move their head around. The range of head movements was small and could not explain the selectivity we report for the bar of light. But would hippocampal neurons show selective responses to the position of the head with respect to

the body, regardless of distal visual cues? To answer this, we looked at the recordings from rats performing active foraging in VR, where the range and frequency of head movements was larger, since the animal would actively scan the virtual environment to navigate. These analyses are detailed in Chapter 3.

In Chapter 4, we analyzed hippocampal responses to repeated presentation of a 30 second clip of a movie from a publicly available dataset. Here, the animal was head fixed, removing the confounding effects of head movements. We report single units from all parts of the hippocampus which are selective to the visual information presented on the screen, similar to the selectivity seen in visual areas, like lateral geniculate nucleus and primary visual cortex.

CHAPTER 2: VISUAL CUE DISTANCE, ANGLE AND DIRECTION ENCODING WITHOUT TASK, MEMORY OR NAVIGATION DEMANDS

Abstract

Primary visual cortical neurons selectively respond to the position and motion direction of specific stimuli retrospectively, without any locomotion or task demand. At the other end of the visual circuit is the hippocampus, where in addition to visual cues, self-motion cues and task demand are thought to be crucial to generate selectivity to allocentric space in rodents that is abstract and prospective. In primates, however, hippocampal neurons encode object-place association without any locomotion requirement. To bridge these disparities, we measured rodent hippocampal responses to a vertical bar of light in a body-fixed rat, independent of behavior and rewards. When the bar revolved around the rat at a fixed distance, more than 70% of dorsal CA1 neurons showed stable modulation of activity as a function of the bar's angular position, while nearly 40% showed canonical angular tuning, in a body-centric coordinate frame, termed Stimulus Angle Cells or Coding (SAC). The angular position of the oriented bar could be decoded from only a few hundred neurons' activity. Nearly a third of SAC were also tuned to the direction of revolution of the bar and most of these responses were retrospective. SAC were invariant with respect to the pattern, color, speed and predictability of movement of the bar. When the bar moved towards and away from the rat at a fixed angle, neurons encoded its distance and direction of movement, with more neurons preferring approaching motion. Thus, a majority of neurons in the hippocampus, a multisensory region several synapses away from the primary visual cortex, encode non-abstract information about stimulus-angle, distance and direction of movement, in a manner similar to the visual cortex, without any locomotion, reward or memory demand. We posit that these responses would influence the cortico-hippocampal circuit and form the basis for generating abstract and prospective representations.

Introduction

Sensory cortical neurons generate selective responses to specific stimuli, in the egocentric (e.g. retinotopic) coordinate frame, without any locomotion, memory or rewards[22]. In contrast, the hippocampus is thought to contain an abstract, allocentric cognitive map, supported by spatially selective place cells[23], grid cells[24] and head direction cells[10]. Such robust hippocampal responses are thought to require both distal visual cues[5] and self-motion cues[14,25], e.g. via path

integration[12], which requires specific sets of self-movements. In addition, the angular and linear optic flow generated by locomotion could contribute to hippocampal activity, but this has not been directly tested. Recent studies have shown significant modulation of hippocampal activity by an auditory[18–20,26] or a social stimulus[15,16]. These tasks required specific actions, rewards or memory to generate selectivity. The stimulus related hippocampal activity modulation reduced to chance level when task demand and stimulus locked rewards were omitted[17–20]. In particular, no study has investigated if hippocampal neurons can encode the angular position and direction of movement of a visual stimulus without bodily movements; it is commonly thought that such compass information requires locomotion[12,21,27]. To understand hippocampal function, it is necessary to know if place cells encode information about the angular position and motion direction of a specific moving visual stimulus, like sensory cortices, regardless of movement, memory or reward.

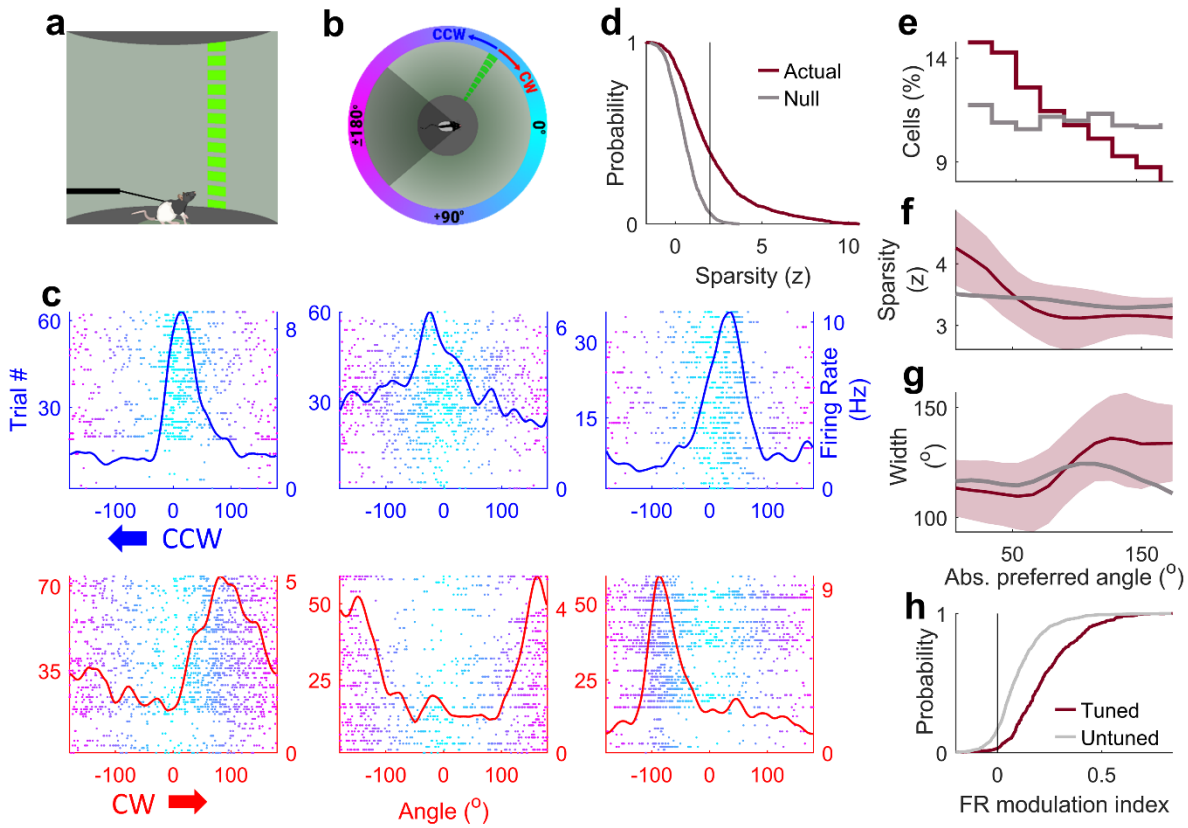

Fig. 2.1 | Hippocampal response to a revolving bar of light: (**a**) Schematic of the experimental setup and (**b**) Top-down view. The rat's head is at the center of a cylinder. A green-striped bar of light (13 ° wide) revolves around the rat at a fixed distance in two

directions (clockwise (CW) or counterclockwise (CCW)). Rat's putative field of view is 270°, with the area (dark gray) behind him being invisible to him. (**c**) Raster plots. Trial number (y-axis on the left) and firing rates (y-axis on the right) of six CA1 neurons as a function of the angular position of the bar (x-axis, 0° in front of the rat and ±180° behind). Bold arrows underneath show the direction of revolution (top panels, Counterclockwise (CCW); bottom panels, Clockwise (CW)). (**d**) Cumulative distribution function (CDF) of strength of tuning (z-scored sparsity, see methods) for 1191 active CA1 putative pyramidal cells (response with higher tuning chosen between CCW and CW, (d) through (f)). The actual data shows significantly greater (KS-test p=1.26x10^{-89}) tuning than the shuffled data (Gray line for (**d**) through (**g**)). 39% of neurons showed significant (z>2, vertical black line) tuning. (**e**) Distribution of tuned cells as a function of the preferred angle (angle of maximal firing). There were twice as many tuned cells at forward angles than behind. (**f**) Median z-scored sparsity and its variability (SEM, shaded area, here and subsequently) of tuned cells as a function of their preferred angle. (Correlation coefficient r=-0.28 p=1.5x10^{-9}). (**g**) Median value of the full width at quarter maxima across the ensemble of tuned responses increased as a function of preferred angle of tuning. (r=+0.15 p=1.3x10^{-3}). (**h**) CDF of firing rate modulation index within versus outside the preferred zone (see methods) for tuned cells was significantly different (Two-sample KS test p=1.9x10^{-50}) than untuned cells.

To address these questions, rats were gently held in place on a large spherical treadmill, surrounded by a cylindrical screen[28]. They were free to move their heads around the body, but not fully turn their body. They were given random rewards to keep them motivated, similar to typical place cell (e.g. random foraging) experiments. The only salient visual stimulus was a vertical bar of light, 74cm tall, 7.5cm wide, 33cm away from the rat, thus subtending a 13° solid angle. In the first set of experiments, the bar revolved around the rat at a constant speed (36°/s), without any change in shape or size (Fig. 2.1a, b), independent of rat's behavior or reward delivery. The bar's revolution direction switched between CW (clockwise) and CCW (counterclockwise) every four revolutions. In subsequent experiments, when we varied the identity, movement and trajectory of the bar, selective responses were found in all cases.

Stimulus angle coding (SAC) in large fraction of CA1 neurons

We measured the activity of 1191 putative pyramidal neurons (with firing rate above 0.2Hz during the experiment) from the dorsal CA1 of 8 Long Evans rats in 149 sessions using tetrodes (see methods[29]). Many neurons showed clear modulation of firing rate as a function of the bar position (Fig. 2.1c), with substantial increase in firing rates in a limited region of visual angles. We call this stimulus angle coding (SAC) or stimulus angle cells. Across the ensemble of neurons, 464 (39%) showed significant (sparsity (z)>2, corresponding to $p < 0.023$, see methods, see Extended Data Fig. 2.1 for other metrics) stimulus angle tuning in either the CW or CCW direction (Fig. 2.1d).

Like the primary visual cortical responses and hippocampal place cells, most tuning curves were unimodal (Extended Data Fig. 2.2) with a single preferred angle where the firing rate was the highest. But virtually no neurons showed an off response (a significant decrease in firing rate). The preferred angles spanned the entire range, including angles behind the rat (Fig. 2.1e). These responses resembled striate cortical neurons in many ways[22,30]. More neurons encoded the positions in front of the rat (0^o) and there was a gradual, two-fold decline in the number of tuned cells for angles behind ($\pm 180^o$). The strength of SAC (Fig. 2.1f, see methods) was much larger near 0^o compared to 180^o. The width of the tuning curves also increased gradually as a function of the absolute preferred angle from 0^o to 180^o (114^o vs 144^o Fig. 2.1g), and was quite variable at every angle, spanning on average about a third of the visual field, similar to place cells on linear tracks[31,32].

Hippocampal place cells on 1D tracks have high firing rates within the field and virtually no spiking outside[31]. In contrast, the firing rates of SAC were often nonzero outside the preferred angle of SAC, as evidenced by modest values of the firing rate modulation index (Fig. 2.1h, see methods). On the other hand, these broad SAC tuning curves resembled the directional tuning of CA1 neurons recently reported in the real world and virtual reality[21], with comparable fraction of neurons showing significant angular tuning. SAC trial to trial variability was quite large, but comparable to recent experiments in visual cortex of mice under similar conditions[33]. Notably, the variability in the mean firing rate across trials was small and unrelated to the degree of angular tuning. However, the trial-trial variability of the preferred angle was quite large and predictive of the degree of SAC of a neuron (Extended Data Fig. 2.3).

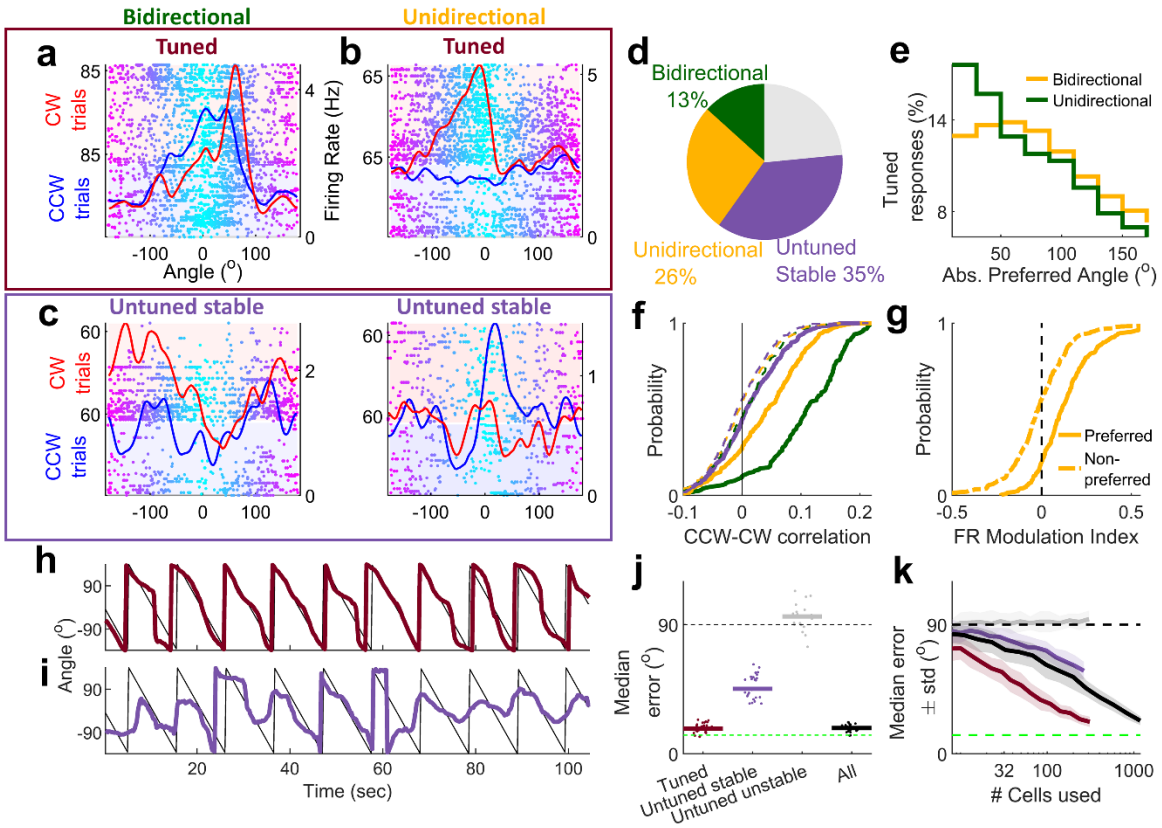

Fig. 2.2 | Directionality, stability and ensemble decoding of SAC. (**a**) Example of a bi-directional cell, showing significant (z>2) tuning (maroon) in both CCW and CW directions. (**b**) Similar to (a), but for a uni-directional cell, showing significant tuning in only one direction (CW here). CCW (blue) and CW (red) trials have been grouped together for ease of visualization, but experimentally were presented in alternating blocks of four trials each. (**c**) Example cells showing stable responses (lavender) with multiple peaks that did not have significant sparsity (z<2) (bi-directional stable, left; unidirectional stable (CCW), right). (**d**) Relative percentages of cells. (**e**) Percentage of tuned responses as a function of the absolute preferred angle, for bidirectional and unidirectional populations are significantly different from each other (two-sample KS test p=0.04). (**f**) Correlation coefficient of CCW and CW responses for different populations of cells, (two sample KS test green, bidirectional, $p=3.3\times10^{-27}$, orange, unidirectional $p=7.0\times10^{-27}$, lavender, untuned stable, $p=4.4\times10^{-4}$. Dashed curves indicate respective shuffles. (**g**) Firing rate modulation index for uni-directionally tuned cells (see methods), for angles around the response peak (preferred zone) was significantly different from zero (t-test $p=4.1\times10^{-35}$), but not outside preferred zone (t-test p=0.35). (**h**) Example

decoding of 10 randomly chosen trials (gray) using all tuned cells in the CCW direction (maroon); all other trials were used to build the population-encoding matrix. **(i)** Same as (h) but using the untuned-stable responses (lavender). (**j**) Median error between stimulus angle and decoded angle over 30 instantiations of 10 trials each for actual and shuffle data. The decoding errors for tuned (median=17.6º) and untuned stable (median=45.2º) are significantly less than that of shuffle (non-parametric rank sum test $p<10^{-150}$ for both populations). Green dashed line indicates width of the visual cue; black dashed line indicates median error expected by chance. (**k**) Sample iteration showing decoding error decreases with increase in the number of responses used for decoding, for populations of all (black), tuned (maroon) and untuned stable (lavender) cells, but not for untuned unstable cells (gray).

Revolution direction selectivity of SAC

In the primary visual cortex, majority of neurons respond selectively to the angular position of the oriented bar, regardless of its movement direction, and a minority of neurons are sensitive to the movement direction of the bar[22]. But, majority of hippocampal neurons on linear tracks are highly directional[29,31]. Further, in both areas, if a neuron is active in both directions, then it shows significant and stable modulation in both directions.

To bridge these discrepancies, we inspected the selectivity, directionality, and stability (see methods) of the SAC. The degree of tuning varied continuously across neurons with no clear boundary between tuned and untuned neurons (Extended Data Fig. 2.4).To examine the tuning properties across this population we separated the neurons according to their degree of tuning in the two movement directions, as commonly done[17]. Some neurons were bidirectional, with significant (z>2) SAC in both movement directions (Fig. 2.2a, Extended Data Fig. 2.5). However, a larger subset of neurons was unidirectional, with significant (z>2) angle selectivity in only one movement direction (Fig. 2.2b, Extended Data Fig. 2.5). For the tuned direction, SAC were stable, showing consistent firing rate modulation as a function of angle across trials. Surprisingly, there were many untuned-stable neurons (see methods), which showed consistent, significantly stable spiking across trials, but the SAC, quantified by z-scored sparsity, was not significantly different than chance (Fig. 2.2c, Extended Data Fig. 2.6). Across the ensemble, about 13% (154) of neurons were bidirectional, 26% (310) were unidirectional, and 35% (421)

were untuned-stable (Fig. 2.2d, Extended Data Fig. 2.6). Thus, the vast majority (74%, 885) of hippocampal pyramidal neurons were consistently influenced by the angular position and direction of the revolving bar. However, unlike visual cortex, far more SAC neurons were unidirectional, and unlike hippocampal place cells and visual cortex, far greater number of neurons showed untuned but stable responses. The majority of tuned neurons had their preferred angle around 0^o, i.e., in front of the rat (Fig. 2.2e) and this bias was greater for the bidirectional cells.

We then examined the differences in firing rates and tuning properties between the two movement directions. For both the unidirectional and bidirectional cells, the firing rate was substantially different between the two directions of movement (Extended Data Fig. 2.7). Further, the mean firing rates of neurons was invariably larger in the direction in which the stimulus angle tuning was greater, compared to the less tuned, or untuned, direction (Extended Data Fig. 2.7). This disparity in firing rates between the tuned and untuned directions arose largely from the increase in firing rate within the preferred zone ($\pm 90^o$ around the preferred angle) in the tuned direction (Fig. 2.2g). Higher rate cells were more likely to be bidirectional than unidirectional, even when the contribution of firing rates differences to strength of tuning were factored out (Extended Data Fig. 2.8). Finally, the tuning curves in the CW and CCW directions were significantly correlated for bidirectional cells (Fig. 2.2f). This was true, although to a smaller extent, for unidirectional cells and untuned-stable cells, but not for the untuned unstable cells.

Population vector decoding of SAC

In addition to individual cells showing stable stimulus angle encoding, we found that the population responses were also coherent for tuned and untuned-stable populations (Extended Data Fig. 2.9, see methods). Ensemble of a few hundred place cells is sufficient to decode the rat's position using population vector decoding[34]. Using similar methods, we decoded the position of the bar using different ensembles of SAC (see methods).

The ensemble of 310 tuned cells (CCW), with a short temporal window of 250ms, could decode the position of the oriented bar with a median accuracy of 17.6^o (Fig. 2.2h, j) comparable to the bar width (13^o). This is qualitatively similar to the spatial decoding accuracy of place cells[34,35].

Additionally, the 266 untuned but stable cells could also decode the position of the bar significantly better than chance, but the median error was 45.2^{o} (Fig. 2.2i, j) which is larger than that for the tuned cells. The unstable cells did not contain significant information about the bar position. Decoding performance improved when using a larger number of tuned or untuned stable cells, but not when using more unstable responses (Fig 2.2k). Thus the ensemble of untuned stable cells contained significant SAC information, even though these individual cells did not[36]. This was not the case for the untuned unstable cells.

Most neurons show retrospective SAC

Under most conditions, visual cortical neurons respond to the stimulus with a short latency, i.e. retrospectively, whereas most hippocampal bidirectional cells on linear tracks are prospective, i.e. they fire before the rat approaches the place field from the opposite movement directions[29,35,37]. However, we found that the converse was true for these hippocampal bidirectional SAC (Extended Data Fig. 2.10). Here (example cell, Fig. 2.3d), the preferred angle in the CCW direction lagged behind that in the CW direction, i.e., in both directions the neuron responded to the bar after it had gone past a specific angle, which is a retrospective response. Hence, we computed the circular difference between the preferred angle between the CW and CCW directions (bidirectional population response, Fig. 2.3a-b), which were predominantly positive. Are only the peaks of SAC retrospective or do the entire tuning curves have lagged responses? To address this, we computed the cross correlation between the entire tuning curves between the CW and CCW directions. Majority (80%) of neurons showed maximum correlation at positive latency. Thus, most neurons responded to the oriented bar retrospectively, i.e., with a lag.

The median latency to response was 276.2ms (leading to 19.9^{o} median shift in cross correlation Fig. 2.3f). This retrospective coding was evident across the entire ensemble of bidirectional cells, such that the population vector overlap between the CW and CCW directions was highest at values slightly shifted from the diagonal (Fig. 2.3h, see methods).

Additional experiments using a photodiode showed that this lag could not be explained by the latencies in the recording equipment (Extended Data Fig. 2.11, equipment latency of 38.9ms was removed from all numbers reported herein). In fact, retrospective tuning was found even for the

unidirectional cells, even though the tuning was not significant in one of the revolution directions, resulting in weaker correlations (Fig. 2.3i-k). The range of latencies was larger for the unidirectional cells than bidirectional cells (Fig 2.3f, j), but median latency in cross correlations (19.9^{o}, or 276.2ms temporal latency of response) was comparable to bidirectional cells. Thus, the retrospective coding does not arise due to difference in tuning strengths. The larger range of latencies and weaker correlations for unidirectional cells could arise because significant tuning is present in only one direction. Small but significant temporal bias was observed in the untuned-stable cells but not for the unstable cells (Extended Data Fig. 2.12).

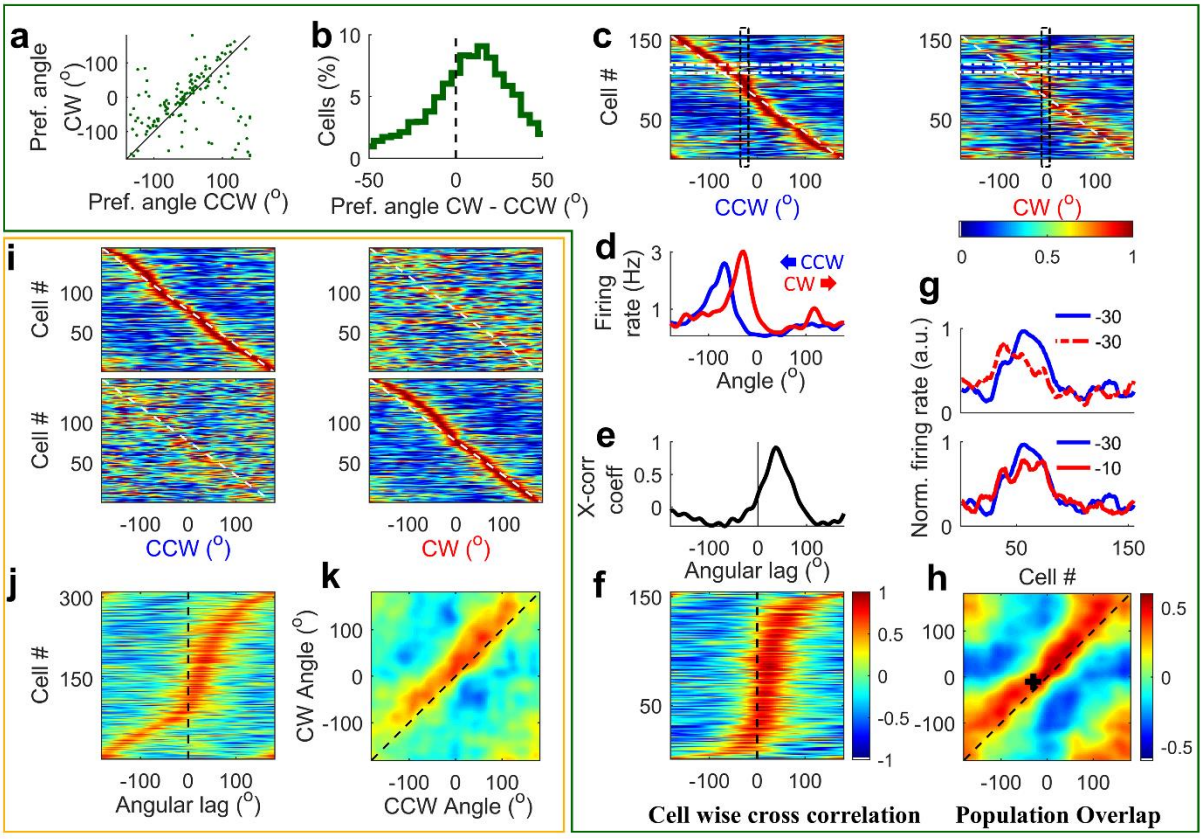

Fig. 2.3 | Retrospective nature of stimulus angle coding (SAC). (**a**) For bidirectional tuned cells, the peak angle in the CW (y-axis) direction was greater than that in the CCW (x-axis). (**b**) Histogram of difference (CW-CCW, restricted to ±50^{o}) of the peak angles in two directions of a cell was significantly (t-test, p=0.003) positive indicating a retrospective shift. (**c-g**) For bidirectional cells: (**c**) Stack plots of normalized population responses of cells, sorted according to the peak angle in the CCW (left). The corresponding responses of cells in the CW direction (right). (**d**) Example cell showing

retrospective latency between the CCW (blue) and CW (red) tuning curves, corresponding to the horizontal white boxes in (c). (**e**) Cross correlation between the CCW and CW responses in (d) had a maximum at positive latency (+27°). (**f**) Cell wise cross correlations between CW and CCW tuning curves, sorted according to their peak-lag. Majority (80%) of lags were positive, i.e., retrospective. The ensemble median lag of 19.9° ±49.8° was significantly positive (Circular median test at 0°, p=4.8x10^{-16}). (**g**) The firing rate, averaged across the entire ensemble of bidirectional cells at -30° in the CCW direction was misaligned with the ensemble averaged responses in the CW direction at the same angle (top), but better aligned with the ensemble averaged responses in the CW direction at -10° (bottom, vertical boxed in (c)), showing retrospective response. **(h)** Population vector overlap of SAC across all cells. At all angles, these population vector correlation coefficients had a peak at a positive lag (CW peak–CCW peak, median=+54.3° ±25.3° t-test p=0.007) showing a retrospective shift. Black marker (+) indicates the correlation coefficient between the population responses at black boxes, i.e., the population response in (g). (**i**) Same as (c) for uni-directional cells with CCW tuned cells (top row) and CW tuned cells (bottom row) sorted according to their SAC peak in the tuned direction. (**j**) Same as in (f) Cross correlations from the uni-directional tuned cells were combined and sorted according to the peak-lag. Majority (67%) of the cross correlations had a significantly positive lag (median latency=19.9°±86.1°, circular median test at 0°, p=1.8x10^{-10}). (**k**) Same as (h) for unidirectional cell population vector cross-correlation. For all angles the population vector cross correlation coefficients had a peak at a positive lag (CW peak–CCW peak, median= +56.2° ±23.7° t-test p=0.001) showing retrospective coding, which was not significantly different from the retrospective lag in bidirectional cells (KS-test, p=0.28).

Invariance of SAC tuning

When the distal visual cues are changed by even a small amount, hippocampal CA1 neurons show remapping, i.e. large changes in place cells' firing rate, degree of spatial selectivity and the preferred location or receptive field[38,39]. On the other hand, primate hippocampal neurons show selectivity to a combination of object identity and its retinotopic position[40].

To address this in a systematic fashion we recorded the responses of the same set of neurons, on the same day to bars of light with different visual features (see methods), without any other changes in stimuli or behavior. In one experiment, we changed the stimulus minimally (green-black stripes vs green-black checkered pattern 2.4a, e-g). Neural firing rates, strength of SAC, preferred tuning location and tuning curve profiles were largely invariant and comparable to spontaneous fluctuations (Fig. 2.4a, see methods). To further test this invariance, we changed the vertical bar substantially by changing both color and pattern (green-black horizontal stripes vs blue with one vertical black line 2.4b). This resulted in significantly more changes in all measures of SAC, though this too was far less than expected by chance. Thus, unlike complete remapping with change in visual cues, SAC was invariant to substantial changes in visual cues.

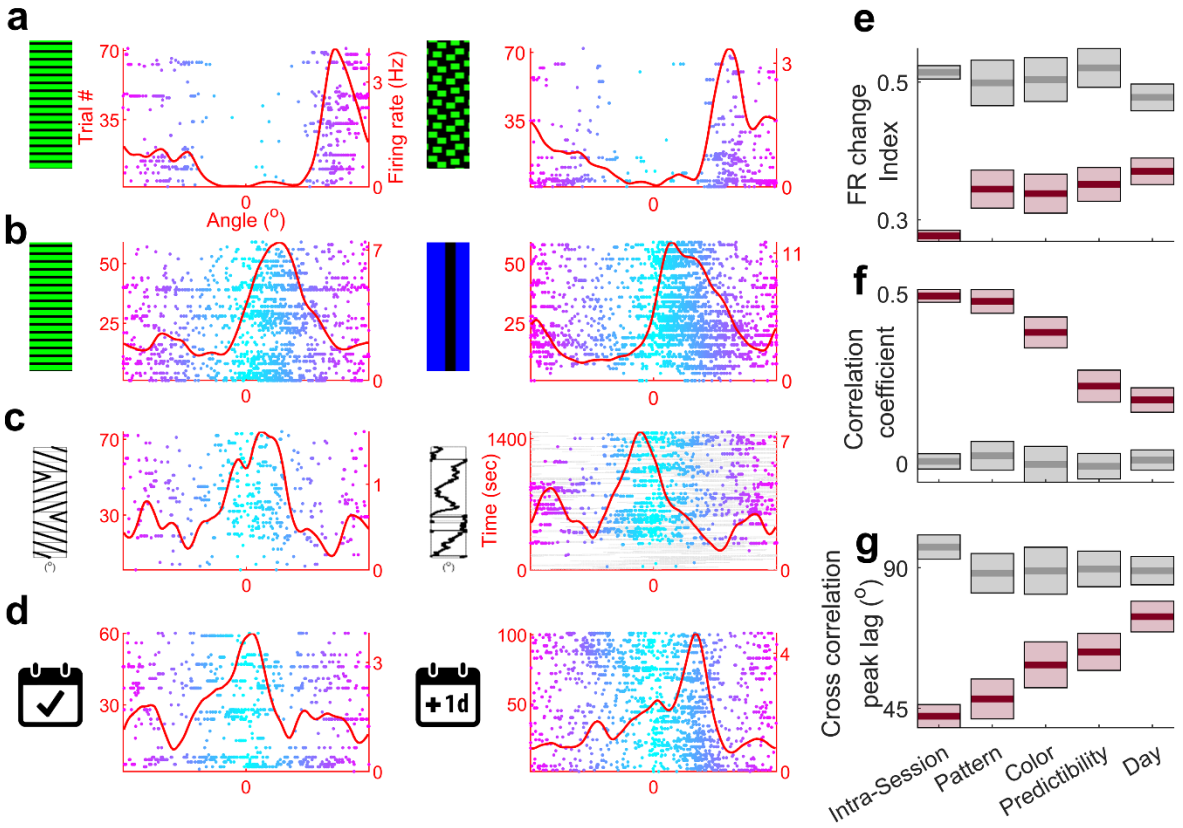

Fig. 2.4 | Dependence of SAC on stimulus pattern, color, movement predictability and time. (**a**) Response of the same cell shows similar SAC for green striped pattern (left) and green-checkered pattern (right). **(b)** Similar to (a), but for changes of stimulus color, green and blue, and pattern (horizontal vs vertical stripe). **(c)** same as (a), but for changes to predictability of the stimulus, termed 'systematic' (left) for predictable

movement of the stimulus, as compared to 'random' (right, see methods). **(d)** Same as (a), but for the same cell's response to the same systematic stimulus across 2 days. (**e)** Firing rate remapping, quantified by FR change index (mean ± SEM), was significantly ($p< 8x10^{-6}$) smaller for the actual data (dark-pink) than for shuffle data (gray) for all conditions. **(f)** Similar to (e), but correlation coefficient between the tuning curves across different conditions (mean values: pattern=0.48, color =0.39, predictability =0.28, day=0.19. All correlations were significantly greater (t-test $p<7.7x10^{-9}$) than shuffle. **(g)** Same as (e), using angular lag in cross correlation to quantify amount of shift between tuning curves across the two conditions (pattern=48°, color=59°, predictability=63°, day=74°). All were significantly lesser (t-test $p<0.003$) than shuffle. All example cells here are chosen from CW condition for clarity.

Sequential tasks can influence neural selectivity in the hippocampus[14,41] and visual cortex[42]. Hippocampal neurons also show selectivity in sequential, non-spatial tasks[15,16,18] and sequential versus random goal-directed paths induce place field remapping[43]. Hence, the above experiments did not include any systematic behavior or rewards related to the moving bar. To compute the contribution of the sequential movement of the bar of light to SAC, we designed experiments where the movement of the vertical bar was less predictable. The bar moved only 56.7° in one direction on average, and then abruptly changed speed and direction. We call this the randomly moving bar paradigm (Fig. 2.4c). Here, 26% neurons showed significant SAC, which was far greater than chance, though lesser than the systematic condition (Extended Data Fig. 2.14). The other results were qualitatively similar to systematically moving bar of light, including the percentage of unidirectional, bidirectional and untuned-stable cells. (Extended Data Fig. 2.14). Thus, the SAC cannot arise entirely from sequential movement of the bar, and the retrospective latencies were unaffected (Extended Data Fig. 2.13) by systematic or random motion of the bar. To directly ascertain the effect of predictability on SAC, we separately analyzed the randomly moving bar data in the first 1-second after stimulus direction flip, and an equivalent subsample of data from later when the stimulus had moved in the current direction for at least 3 seconds (Extended Data Fig. 2.14, see methods). SAC was similar in these two conditions. Further, SAC were not systematically biased by the angular movement speed of stimulus, nor did hippocampal firing encode stimulus speed beyond chance (Extended Data Fig. 2.14).

Recent studies have reported spontaneous, slow remapping of place cells over several days[44]. We measured the activity of the same cells for more than one day, and measured changes in SAC without any changes in stimuli or their predictability. There was substantial remapping across two days, evidenced by very low correlation between the tuning curves of the same neuron across two days (Fig. 2.4d). This was not due to difference in novelty, because rats had experienced this stimulus for at least one week.

There was a consistent pattern of remapping across these experiments, as measured by the correlation coefficient of the tuning curves (Fig. 2.4f). The smallest change in tuning curves occurred with the smallest change in stimulus, i.e., pattern change. Greater change with change in color, even greater change with alteration in stimulus predictability and the largest change occurred spontaneously across two days. This occurred due two mechanisms. First, the preferred tuning angle rotated across different conditions, with the lowest amount of change for pattern change, larger for color, followed by predictability and time. Second, even when this change in the preferred tuning angle was factored out, similar pattern of changes in correlations persisted (Extended Data Fig. 2.14).

Overlapping neural populations encode stimulus angle, distance, and spatial position.

During spatial exploration majority of rodent hippocampal neurons show spatially selective responses, aka place cells. What is the relationship between SAC vs spatial selectivity of neurons? In additional experiments we measured the activity of the same set of CA1 neurons, on the same day, during the SAC protocol and while rats freely foraged for randomly scattered rewards in two-dimensional environments (Fig 2.5a, see methods). Out of 341 pyramidal cells, 56% were active in both experiments, whereas 29% and 15% were active only during exploration or during SAC, respectively. Firing rates during exploration and SAC experiments were strongly correlated (Extended Data Fig. 2.15). Of the population of cells active in both experiments, 44% showed significant tuning to both spatial position and stimulus angle, whereas 51% showed significant tuning to only space. The strength of tuning was significantly correlated between these two experiments (Fig. 2.5c). Thus, the majority of SAC cells were also place cells.

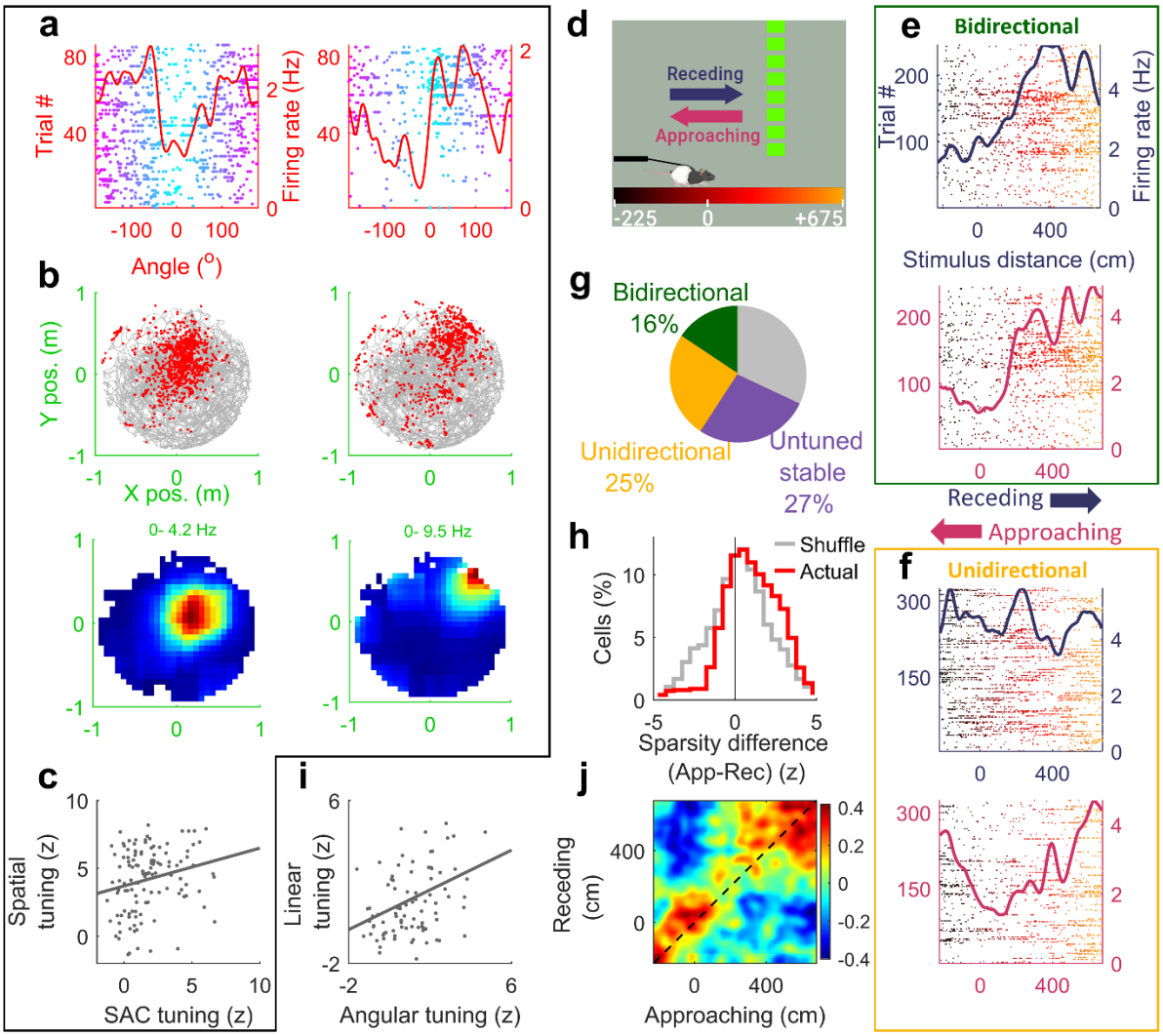

Fig. 2.5 | Overlapping neural populations encode stimulus angle, distance, and spatial position. (**a)** Two cells recorded on the same day showing significant SAC in the revolving bar of experiment and **(b)** spatial selectivity during free foraging in two-dimensional maze. Top panel shows the position of the rat (grey dots) when the spikes occurred from that neuron (red dots). Bottom panel shows the firing probability or rate at each position. **(c)** Strength of SAC and spatial selectivity measured by z-scored sparsity were significantly correlated (r=+0.22 p=0.014). **(d)** Schematic of the stimulus distance experiment. The same green stripped bar moved between -225cm to +675cm in 10 seconds, towards and away from the rat at a fixed angle (0º). **(e)** Raster plots and firing rates of a bidirectional cells with significant tuning to the approaching (pink, top) as well as receding (dark blue, bottom) movement of the bar of light. Trial number (y-axis on the

left) and firing rates (y-axis on the right) **(f)** Same as (e), but for a unidirectional cell, tuned for stimulus distance only during the approaching stimulus movement. **(g)** Pie chart depicting fraction of cell tuned (bidirectional and unidirectional) as well as untuned but stable, similar to Figure 2. **(h)** Stimulus distance tuning is higher during approaching epochs, even after down sampling spike trains to have same firing rate (t-test actual p=4.6x10^{-4}, shuffle p=0.7). **(i)** For same cells recorded in angular and linear stimulus movement experiments, tuning was positively correlated (r=0.36 p=5x10^{-4}). **(j)** Population vector overlap computed using all cells, between responses in approaching and receding stimulus movement shows retrospective response, with maxima at values above the diagonal, similar to Fig. 2.3(h).

Spatial exploration involves not only angular optic flow but looming signals too. Hence, we measured 147 place cells where the stimulus moved towards or away from a body-fixed rat, completing one lap in 10 seconds, without any change in angular position (illustration - Fig 2.5d, example cells - Fig. 2.5e, f). The firing rates of 41% of neurons showed significant modulation as a function of the stimulus distance (Fig. 2.5g) and 27% of cells had untuned but stable responses. Neurons not only encoded distance but also direction of movement, with 17% and 8% of neurons showing significant tuning to only the approaching (coming closer) or receding (moving away) bar of light, respectively. Neural firing rates were very similar for approaching and receding stimuli, but stimulus distance coding was much stronger for approaching movements (Fig 2.5h). For matched cells recorded in both stimulus distance and angular experiments (see methods), firing rates (Extended Data Fig. 2.15) as well as the strength of tuning were correlated, suggesting that the same population of neurons can encode both distance and angle (Fig. 2.5i). The preferred distance (i.e., the position of maximal firing) for the bidirectional cells, was not uniform but bimodal, with majority of neurons active near the rat (0 cm) or farthest away (500cm), and very few neurons representing the intermediate distances (Extended Data Fig. 2.15). Retrospective response was also seen in these experiments, with the population overlap between approaching and receding responses shifted to values above the diagonal (Fig. 2.5j, Extended Data Fig. 2.15) corresponding to a retrospective shift of 70.6cm or 196.1ms.

Discussion

These results demonstrate that a moving bar of light can reliably modulate the activity of majority of hippocampal place cells, without any task demand, memory, reward contingency or locomotion requirements (see Extended Data Fig. 2.16 for reward related controls, 2.17 for behavior related controls and 2.18 for GLM estimates). Neurons encoded both the angular position and linear distance of the bar of light, with respect to the rat. In addition, neurons were selective to the direction of angular or linear movement. Thus, these responses provided a vectorial representation of the stimulus positions around the rat. Only a few hundred neurons were sufficient to accurately decode the angular position of visual stimulus. Positions in front of the rat and near him were overrepresented. Majority of neurons that encoded the bar position were also spatially selective during real world exploration and the strength of SAC and spatial tunings were correlated across neurons. However, unlike place cells that remap when the behavior is sequential vs. random[43], the stimulus angle tuning was relatively unchanged when the predictability or sequential nature of stimuli was altered. Even more striking, while place cells are predictive or prospective [35,37,45], including in virtual reality setup similar to that used here[29] the stimulus angle tuning was retrospective in nature (Extended Data Figure. 2.10).

These results have similarities and important differences compared to recent findings of social neurons in the hippocampus [15,16] where a small subset of neurons encoded the linear position of a demonstrator animal. However, those experiments required strong training, task, or reward. Without these behavioral requirements there was no significant modulation of hippocampal activity[17–20]. Other experiments showed that a small subset of hippocampal neurons could respond to sensory cues during auditory discrimination task, but robust responses required stimulus locked rewards and behavior[18,19,26]. Thus, hippocampal selectivity in those experiments cannot be attributed solely to the stimulus position. In contrast, in our experiments, the neural responses can be attributed solely to the stimulus angle. Indeed, the stimulus angular tuning was relatively invariant to changes in the pattern or color of the bar of light, or the randomness of stimulus movement. Further, a majority of neurons showed significant modulation in our experiments, enough to decode the bar position from a few hundred neurons. The differences between the prior results and ours could be because the hippocampus is involved in creating spatial representations from the visual cues and our experiments created stimulus movement

while eliminating nonspecific cues. This is supported by the strong correlation between the degree of visual stimulus angle position tuning and allocentric spatial tuning across neurons.

These results show that during passive viewing, rodent hippocampal activity patterns fit the visual hierarchy[46]. For example, the SAC show similar angular dependence as visual cortex, e.g. larger tuning curve width for more peripheral stimuli, and over-representation of the nasal compared to temporal positions[30]. This nasal-temporal magnification increases with increasing processing stages from the retina to thalamus and striate cortex[30], but the hippocampal magnification we report is much smaller. Further, like the visual cortex, hippocampal neurons too showed retrospective responses, but with larger response latency, suggesting visual cortical inputs reached hippocampus to generate SAC. The larger latency is consistent with the response latencies in the human hippocampus[47] and the progressive increase in response latencies in the cortico-entorhinal-hippocampal circuit during Up-Down states[48–50]. However, there were no off responses in the SAC and the tuning curves were broader and more unidirectional than in the primary visual cortex. This could arise due to processing in the cortico-hippocampal circuit, especially the entorhinal cortex[50], or due to the contribution of alternate pathways from the retina to the hippocampus[51].

Hippocampal spatial maps are thought to rely on the distal visual cues[5]. Rats can not only navigate using only vision in virtual reality, but they preferentially rely on vision[28]. Robust hippocampal coding for visual cue position, angle and movement direction reported here without any movements further supports these findings. But these findings cannot be explained by path integration. Instead, they can be explained by a refinement of the multisensory-pairing hypothesis[14,21]. In the absence of any correlation between physical stimuli, rewards and internally generated self-motion, hippocampal neurons can generate robust, invariant, non-abstract responses to as the visual stimulus angle, distance and direction, akin to cortical regions. Consistently, these responses are retrospective in nature, similar to cortical responses, with additional latency. However, these responses are less robust than place cells. Visual cues combined with uncorrelated locomotion cues can generate direction head-selectivity but not spatial selectivity[21], whereas consistency between locomotion, reward and visual cues generates spatial selectivity in the hippocampus[13,14] and primary visual cortex[42]. Place cells robustly respond to not only visual[52,53] but also multisensory cues on the track[37,45,54] and to self-motion

cues[14,29,55]. We hypothesize that the greatly enhanced correlations between all the cues could be encoded more robustly via synaptic plasticity to generate anticipatory or prospective coding of absolute position[31,56]. This is further supported by the finding that robust responses and prospective coding were also seen in purely visual virtual reality, but for relative distance, not absolute position, since only the optic flow and locomotion cues were correlated at identical distance[29]. Thus, the retrospective coding of moving stimulus angle, position and direction could form the basis for generating a wide range of invariant, anticipatory spatial maps via multisensory associations.

Methods

Subjects

Eight adult male Long-Evans rats (3 months old at the start of experiments) were individually housed on a 12-hour light/dark cycle. Their total food intake (15-20 g of food per day) and water intake (25-35 ml of water per day) were controlled and monitored to maintain body weight. Rats received 10-12ml of water in a 20-minute experiment. All experimental procedures were approved by the UCLA Chancellor's Animal Research Committee and were conducted in accordance with USA federal guidelines.

Experimental apparatus

Rats were body restricted with a fabric harnesses as they ran on an air-levitated spherical treadmill of 30cm radius. The rat was placed at the center of a cylindrical screen of radius 33cm and 74 cm high. Visual cues were projected on the screen. Although the rat was free to run and stop voluntarily, his running activity was decoupled from the projector and hence had no effect on the visual cues. Body restriction allowed the rat to scan his surroundings with neck movements. Running speed was measured by optical mice recording rotations of the spherical treadmill at 60Hz. Head movement with respect to the harnessed and fixed body was recorded at 60Hz using an overhead camera tracking two red LEDs attached to the cranial implant using the methods described before[29]. Rewards were delivered at random intervals (16.2 sec ±7.5s, 2

rewards, 200ms apart) to keep the rats motivated and the experimental conditions similar to typical place cell experiments.

Behavioral pre-training

All experiments were conducted in acoustically- and EMF-shielded rooms. The rats were conditioned to associate a tone with sugar-water reward. They were gently body-fixed in the apparatus that allowed them to move their heads with respect to the body, but the body could not turn around. In order for the rats to remain calm in the apparatus for long periods, they were trained to navigate in a visually rich virtual maze where a suspended, striped pillar indicated rewarded position. After surgery, rats were exposed to the revolving bar environment for the first time, where the movement of the rat had no impact on the movement of the revolving bar. Six out of eight rats never experienced virtual reality after the revolving bar experiments began.

Experiment Design

The salient visual stimulus was a 13 degrees wide vertical bar of light which revolved around the rat at a constant speed (10s per revolution) without any change in shape or size (Fig 2.1A). We used three different textures of visual cues as shown in Fig. 4. The results were qualitatively similar for all of them hence the data were combined. Each block of trials consisted of four clockwise (CW) or four counterclockwise (CCW) revolutions of the bar of light. There were 13-15 blocks of trials in each session. During the random bar of light experiment, the bar revolved at one of the six speeds: $\pm 36^{o}$, $\pm 72^{o}$, or $\pm 108^{o}$ per second and spanning angles ranging 30^{o} to 70^{o} at any given speed, before changing the speed at random. Reward dispensing was similar to the systematic bar of light experiment, with no relation to the angular position or speed of the stimulus. Manipulations of stimulus color, pattern, movement predictability and linearly moving stimulus were performed in a pseudo-random order in the same VR apparatus. Real world two-dimensional random foraging experiments and stimulus angle experiments were performed in a pseudo-random order, with an intermittent baseline of 25-40 minutes.

Surgery

All rats were implanted with 25-30g custom-built hyperdrives containing up to 22 independently adjustable tetrodes (13μm nichrome wires) positioned bilaterally over dorsal CA1 (-3.2 to -

4.0mm A.P., ±1.75 to ±3.1mm M.L. relative to Bregma). Surgery was performed under isoflurane anesthesia and heart rate, breathing rate, and body temperature were continuously monitored. Two ~2 mm-diameter craniotomies were drilled using custom software and a CNC device with a precision of 25μm in all 3 dimensions. Dura mater was manually removed and the hyperdrive was lowered until the cannulas were ~100 μm above the surface of the neocortex. The implant was anchored to the skull with 7-9 skull screws and dental cement. The occipital skull screws were used as ground for recording. Rats were administered ~5mg/kg carprofen (Rimadyl bacon-flavored pellets) one day prior to surgery and for at least 10 days during recovery.

Electrophysiology

The tetrodes were lowered gradually after surgery into the CA1 hippocampal sub region. Positioning of the electrodes in CA1 was confirmed through the presence of sharp-wave ripples during recordings. Signals from each tetrode were acquired by one of three 36-channel head stages, digitized at 40 kHz, band pass-filtered between 0.1Hz and 9 kHz, and recorded continuously.

Spike sorting

Spikes were detected offline using a nonlinear energy operator threshold, after application of a non-causal fourth order Butterworth band pass filter (600-6000Hz). After detection, 1.5ms spike waveforms were extracted. Spike sorting was performed manually using an in-house clustering algorithm written in Python.

Tuning curves and *z*-score calculation

Procedures similar to that described previously were used[29]. We binned the angular occupancy of the vertical bar and spikes in $N=120$ bins of width 3^o each and smoothed it with a Gaussian of $\sigma = 12^o$. Clockwise and counterclockwise movement directions were treated separately. To quantify the degree of modulation we computed sparsity s of an angular rate map where r_n is the firing rate in the n^{th} angular bin:

$$s = 1 - \frac{1}{N}\frac{(\sum_n r_n)^2}{(\sum_n {r_n}^2)}$$

To assess the statistical significance of sparsity, we used a bootstrapping procedure, which does not assume a normal distribution. Briefly, for each cell, in each movement direction, spike trains as a function of the vertical bar from each block of trials were circularly shifted by different angles and the sparsity of the randomized data computed. This procedure was repeated 250 times with different sets of random value shifts. The mean value and standard deviation of the sparsity of randomized data was used to compute the z-scored sparsity of actual data using the function *zscore* in MATLAB. The observed sparsity was considered statistically significant if the z-scored sparsity of the observed spike train was greater 2, which corresponds to $p < 0.0228$ in a one tailed t-test.

Similar procedure was employed for testing the significance angular tuning in the random bar of light condition. To keep the analysis comparable to systematic condition, spike trains were circularly shifted with respect to behavioral data by different random amounts for each block of 40 seconds, which is comparable to the time taken by the systematic visual cue to undergo four revolutions.

In addition to sparsity, we quantified SAC using several other measures.

Angle Selectivity index $ASI = {A_2}/{A_2 + A_0}$

where A_2 is the second harmonic component from the Fourier transform of the binned SAC response and $A_0$is the DC level. This formulation of ASI is analogous to Orientation selectivity index (OSI), which is widely used in visual cortical selectivity quantification[57–59]

Mean resultant length $(MVL) = \sum_n r_n . \left(e^{i\theta_n}\right)$

Where r_n is the firing rate in the n^{th} angular bin θ_n is the angular position corresponding to this bin and n is summed over 120 bins.

Coherence(CH) = correlation coefficient$(\{r_{n,raw}\}, \{r_{n,smoothed}\})$

Mutual information $(MI) = \sum_C p(C|\theta_n) . \log_2 \frac{p(C|\theta_n)}{p(C)}$

Where $p(C) = \sum_n p(\theta_n) . p(C|\theta_n)$

and C is the average spike count in 0.083 second window which corresponds to 1 angular bin that is 3^o wide. Statistical significance of these alternative measures of selectivity was computed similar to that for sparsity and is detailed in Extended Data Fig. 2.1.

Tuning curve width quantification

Full width at quarter maxima of the SAC rate map was computed around the maxima of the firing rate, i.e., the preferred angle, as the width at which the tuning curve first crossed 0.25 times the peak value. We chose 0.25 of maximum and not 0.5, i.e. FWHM as commonly done, because the tuning curves are often very broad with nonzero activity at nearly all angles, which is missed by FWHM.

Modulation Index calculation

Firing rate modulation index of stimulus angle tuning (used in Fig. 2.1g) was quantified as $(FR_{within} - FR_{outside}) / (FR_{within} + FR_{outside})$, where FR_{within} and $FR_{outside}$ are average firing rates in their respective zones. Similar definition of FR modulation index was used in Fig. 2.2g, to quantify the effect of uni-directional tuning inside and outside of the preferred zone, as $(FR_{tuned} - FR_{untuned}) / (FR_{tuned} + FR_{untuned})$, where FR_{tuned} and $FR_{unturned}$ are the average firing rates in the respective directions. Similarly in Fig. 4k, to quantify the effect of stimulus speed, as $(FR_{fast} – FR_{slow}) / (FR_{fast} + FR_{slow})$, where FR_{fast} and FR_{slow} are the average firing rates during stationary epochs of respective stimulus movement speeds.

Spike Train thinning

Neurons with larger number of spikes, e.g., due to longer experiments, have greater sparsity than when the number of spikes is less. To remove this artifact and compare the degree of SAC across all neurons and conditions, we employed a spike thinning procedure. Randomly chosen spikes were removed such that that the effective firing rate became 0.5 Hz for all neurons and then computed the sparsity of this thinned spike train (Extended Data Fig. 2.8). This procedure was

used separately for CW and CCW directions to allow comparison of the degree of tuning in both directions, independent of the firing rate changes.

Stability Analysis

Stability of neural angular tuning was quantified for CW and CCW directions separately. All the trials were split into two randomly chosen equal and non-overlapping groups (~30 trials each) and separate tuning curves computed for each half, with 120 equally spaced, non-overlapping angular bins. The correlation coefficient was computed between these two groups (C_{actual}), which is a measure of stability. To compute the significance of stability, this procedure was repeated 30 times, with different random grouping of trials, and correlation coefficient computed between the two groups computed each time. This provided a distribution of thirty values of stability C_{actual}. Same procedure was used for rate maps computed using random data (see z-score methods above) and correlation computed between two groups to obtain thirty different values of C_{random}. A cell's SAC was considered significantly stable if the following conditions were met: the nonparametric rank-sum test comparing the thirty C_{actual} with thirty C_{random} was significant at $p<0.05$ and $C_{actual} > C_{random}$. Untuned-stable responses were identified as responses with significant stability, but non-significant tuning (sparsity (z) < 2) and treated as a separate population in Fig. 2.2.

Population Vector Overlap

To evaluate the properties of a population of cells, sessions were divided into trials in the CCW and CW movement directions of the visual bar. Population vector overlap between CCW and CW movement direction at angles (Θ_r , Θ_m) for N single units was defined as the Pearson correlation coefficient between vectors $(\mu_{1,r}, \mu_{2,r}, \ldots \mu_{N,r})$ & $(\mu_{1,m}, \mu_{2,m}, \ldots \mu_{N,m})$ where $\mu_{i,p}$ is the normalized firing rate of the i^{th} neuron at p^{th} angular bin. Correlation coefficient of these sub-populations taken across angles indicates the existence of retrospective coding (Fig. 3h, k and Fig. 2.5j.). Similarly, for computing coherence in either direction, population vector overlap between two groups of trials of the same bar movement direction (as defined above, stability analysis methods) was computed separately for CCW and CW trials (Extended Data Fig. 2.9). Populations of tuned, untuned but stable and untuned-unstable cells were treated separately.

Decoding analysis

Using the stability labels as obtained from above, recorded cells were divided into three populations: tuned (sparsity $z>2$), untuned (sparsity $z<2$) and stable, untuned and unstable. All the trials across all the cells within each population were separated into two groups: ten, randomly chosen trials were treated as the 'observed trials' and these data were decoded using the firing rate maps obtained from the remaining trials or the 'lookup trials'. Commonly used population vector overlap method was used between the lookup and observed trials using a window of 250ms. Briefly, at each 250ms time point in the 'observed data', the correlation was computed between the observed population vector and the lookup population vectors at all angles. The circularly weighted average of angles, weighted by the (non-negative) correlations provided the decoded angle. The entire procedure was repeated 30 times for different sets of 10 trials. The error was computed as the circular difference between the decoded and actual angle at the observed time. Decoding of the stimulus distance (Extended data Fig. 2.15) was done similarly but by finding the distance corresponding to maximum correlation between 'lookup' and 'observed' data, since circular averaging is unavailable for linear distance close and away from the rat.

Same cell identification

Spike sorting was performed separately for each session using custom software[29]. Identified single units were algorithmically matched between sessions to enable same cell analysis (Fig 2.4&2.5). All the isolated cells in one session were compared with all the isolated cells in another session under investigation. Each putative unit pair was assigned a dissimilarity metric based on the Mahalanobis distance between their spike amplitudes, normalized by their mean amplitude. Dissimilarity numbers ranged from 2.5×10^{-5} to 17.2 across all combinations of units between two sessions. Putative matches were iteratively identified in an increasing order of dissimilarity, until this metric exceeded 0.04. These putative matches were further vetted, using an error index defined on their average spike waveforms.

Estimating the independent contribution of head position, running speed and stimulus angle using GLM

To compute the independent contributions of head position, running speed and stimulus angle, we employed an GLM based estimation of firing, using the *glmfit* function in MATLAB, as described recently[21] . Head position and running speed were decoded in GLM using basis functions consisting of sinusoids. The log of running speed was used to ensure similar amount of data in each bin, and bins with zero speed were assigned an arbitrary, small value, which was on average equal to half the minimum non-zero running speed. Spike train and behavior data were downsampled to 100ms bins. The extreme one percentile of head position data and top one percentile of running speed data was excluded to remove the effects of outliers and ensure a good fit. CCW and CW tuning curves for stimulus angle were computed seperately. The statistical significance of the resulting tuning curves was estimated by computing sparsity and a bootstrapping method described above and used recently[21].

Quantification of population remapping

To compute the amount of remapping of firing rate, strength of tuning, preferred angle of firing and similarity between CCW and CW SAC, we used the responses of the same cells recorded from different experimental conditions and defined remapping metrices as firing rate modulation index, difference between z-scored sparsity, circular distance between the angles corresponding to maximal firing, correlation coefficient between the firing rate responses and the peak value and angular latency corresponding to the cross correlation between their tuning curves in the two conditions. This calculation was repeated 100 times using a random permutation to break the same cell pairing, to obtain a null distribution. The mean and standard deviation of this distribution was plotted in Fig. 2.4e-g and Extended Data Fig. 2.14 and compared with the actual value of the corresponding remapping metric.

Quantification of trial to trial variability of SAC

Angular movement of the visual stimulus was separated into different trials starting and ending at 0^o, which is the angular position in front of the rat. Mean firing rate in each trial was obtained by binning the spikes in that trial into 120 angular bins (3 degrees wide), and finding the average value of firing rates in each bin. Similarly, mean vector angle and mean vector length were

obtained using *circ_r* and *circ_mean* functions of the Circular Statistics toolbox in MATLAB[59] either by using all trials or only those trials when atleast 5 spikes were recorded (each trial was 10s long, yeilding 0.5Hz lowerbound on mean firing rate).

To determine if the varibility was correlated across simultaneously recorded tuned cells, a co-fluctuation index for firing rate was defined for all cell pairs as the Spearman correlation between the trial-wise firing rate vectors of both cells. $Co\text{-}Fluctuation_{FR} = spearman(\{F_{1,k}\},\{F_{2,k}\})$ where $F_{i,k}$ denotes the mean firing rate of i^{th} cell on the k^{th} trial. Bootstrapping procedure to access significance of this index was employed by obtaining 100 shuffled indices when the order of trials was randomly reassigned. Similarly, to estimate the co-fluctation of SAC, we defined a similarity metric for each trial as $S_{i,k} = crcf(r_{n,k}, R_n)$ where n denotes the angular bins, R_n overall tuning curve, and $r_{n,k}$ is the firing rate in the n^{th} bin for the k^{th} trial and *crcf* is the correlation coefficient function. Co-fluctuation of tuning was defined analogously as $\text{Co-Fluctuation}_{SAC} = spearman(\{S_{1,k}\},\{S_{2,k}\})$, and bootstrapped similarly as the firing rate co-fluctuation index.

Extended Data Figures

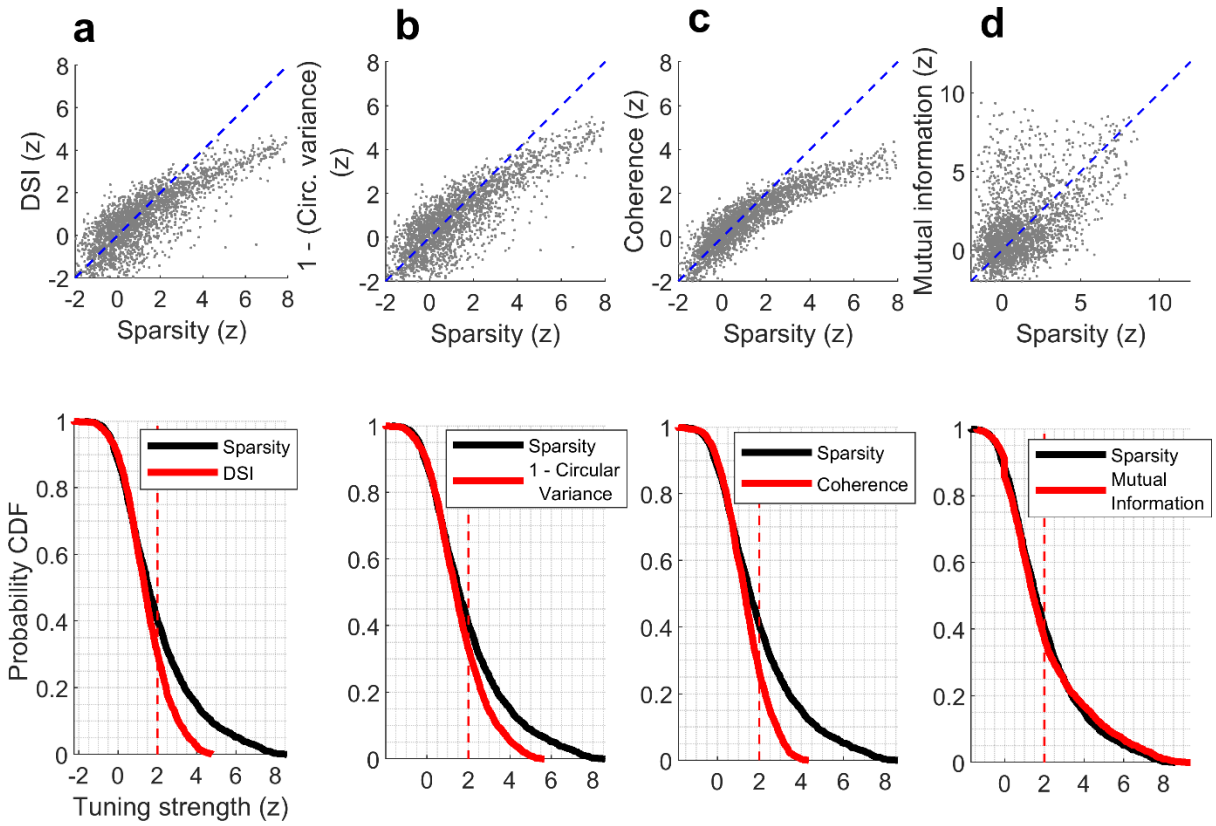

Extended Data Fig. 2.1 | Relationship between different properties of SAC (a) (top) SAC quantified by z-scored sparsity is significantly correlated (r=0.82, p<10^{-150}) with, but significantly greater than the z-scored direction selectivity index (DSI) (41% z>2 for sparsity vs. 31% for DSI, KS-test p=9.3×10^{-10}). (Bottom) Cumulative histogram (cdf) of z-scored metric of sparsity and DSI. **(b)** Similar as (a), (1- (circular variance)) is significantly correlated (r=0.84, p<10^{-150}) but significantly weaker (33% z>2 for (1-circular variance)) than sparsity. (KS-test p=7×10^{-6}). **(c)** Similar to (a) coherence is significantly correlated (r=0.89 p<10^{-150}) but significantly weaker (26% z>2 for coherence KS-test p=6.3×10^{-16}) than sparsity. **(d)** Similar to (a), but mutual information is significantly correlated (r=0.47 p=8.6×10^{-132}) but significantly smaller than sparsity (37% z>2 for mutual information, KS-test p=7.2×10^{-5})

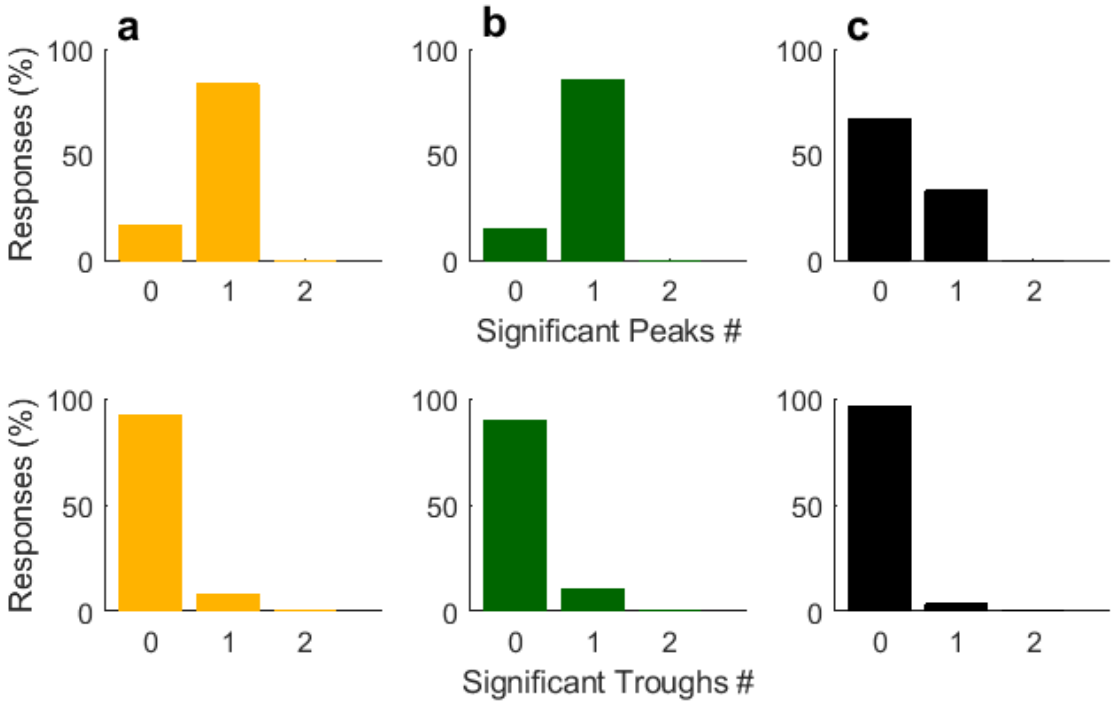

Extended Data Fig. 2.2 | Unimodality of SAC. Majority of (**a**) uni-directional as well as (**b**)bi-directional tuning curves were unimodal with only one significant peak (top row), whereas (**c**) untuned responses did not have significant peaks, as expected. Both tuned responses were used for the bi-directional cells, and only the tuned response was used for the uni-directional cells. Significant troughs, i.e. off-responses were not found for unidirectional or bidirectional cells (bottom row). Significance of a peak (or trough) was determined with the spike train shuffling analysis, similar to that performed to compute the z-scored sparsity. A peak (trough) was determined to be significant if it was larger (smaller) than the median value of peaks in all shuffles and had a height of at least 20% of the range of firing rate variation in the shuffle data. These criteria resulted in zero significant peaks for some tuned responses.

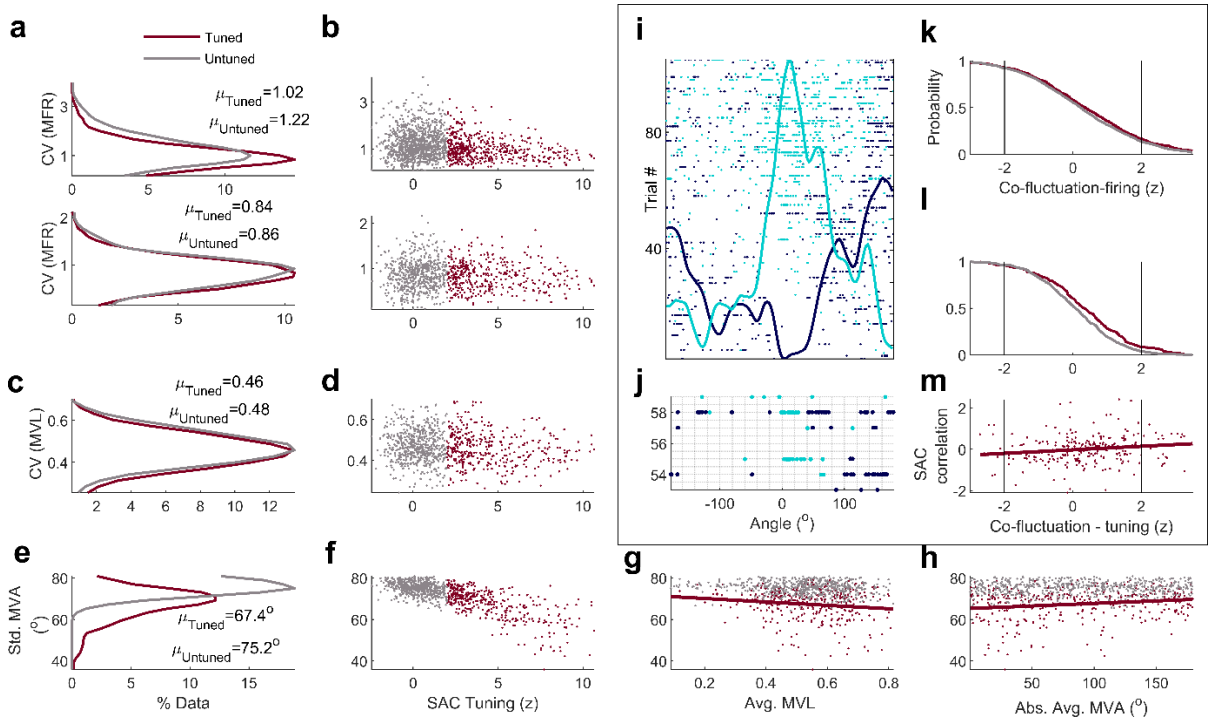

Extended Data Fig. 2.3 | Trial-to-trial variability and co-fluctuation of simultaneously recorded cells. For each cell, in each trial, we computed the mean firing rate (MFR), mean vector length (MVL) and mean vector angle (MVA) of SAC (see methods). **(a) (Top)** Trial to trial variation of firing rate was significantly (T-test p=3.4x10^{-12}) higher for untuned cells (gray, mean coefficient of variation (CV)=1.22), compared to tuned cells (maroon, mean CV=1.02), when using all trials. **(b) (Top)** The difference in variability was not significantly correlated with SAC tuning strength (after factoring out firing rate, partial correlation r=-0.04, p=0.14). **(a) (Bottom)** The rate-variability was qualitatively similar between tuned and untuned cells when using only the responsive trials (firing rate above 0.5Hz, T-test p=0.2), and **(b) (Bottom)** uncorrelated (partial correlation after factoring out mean firing rate p=0.85) with the degree of SAC. **(c)** The variance of mean vector length, which is a measure of the non-uniformity of spiking as a function of the stimulus angle, was significantly greater for untuned cells (T-test p=0.002) than tuned cells and **(d)** was inversely related to SAC tuning strength (r=-0.19, p=7.3x10^{-10}). **(e)** The circular standard deviation of MVA, which signifies the instability of SAC tuning from trial to trial, was significantly (p=4.1x10^{-94}) smaller (11%) for tuned than untuned cells and **(f)** strongly anti-correlated with SAC (r=-0.77 p=7.4x10^{-192}). **(g)** This standard deviation of MVA was

inversely correlated with MVL for tuned (r= -0.15 p=0.004), and for untuned cells (r= -0.12 p=0.003). **(h)** It was also positively correlated with the location of tuning (r=0.18 p=3.5 x 10^{-4}), with lower variation for cells tuned to the front angles (abs. avg. MVA around 0^{o}) than behind ($\pm 180^{o}$). Standard deviation of MVA was uncorrelated with location of tuning for untuned cells (p=0.64). (**i)** Two simultaneously recorded cells showing SAC in the CCW direction, **(j)** and zoomed in for trial numbers 53 to 59, showing mostly uncorrelated rate variability. **(k)** Only 17% of tuned cell-pairs showed significant (z>2) co-fluctuation of mean firing rates across trials, while 7% cell pairs had significantly opposing fluctuations (z<2). (see methods). **(l)** Only 9% of cell pairs showed significant co-fluctuation of SAC. SAC and firing rate co-fluctuations were computed between simultaneously recorded cell-pairs of tuned or untuned cells in only trials when the rat was stationary (see methods). CCW and CW tuning curves were treated as separate responses throughout these analyses. **(m)** The strength of rate co-fluctuation was positively correlated with overlap between the two tuning curves, quantified as the correlation coefficient between their SAC (r=0.178 p=0.004).

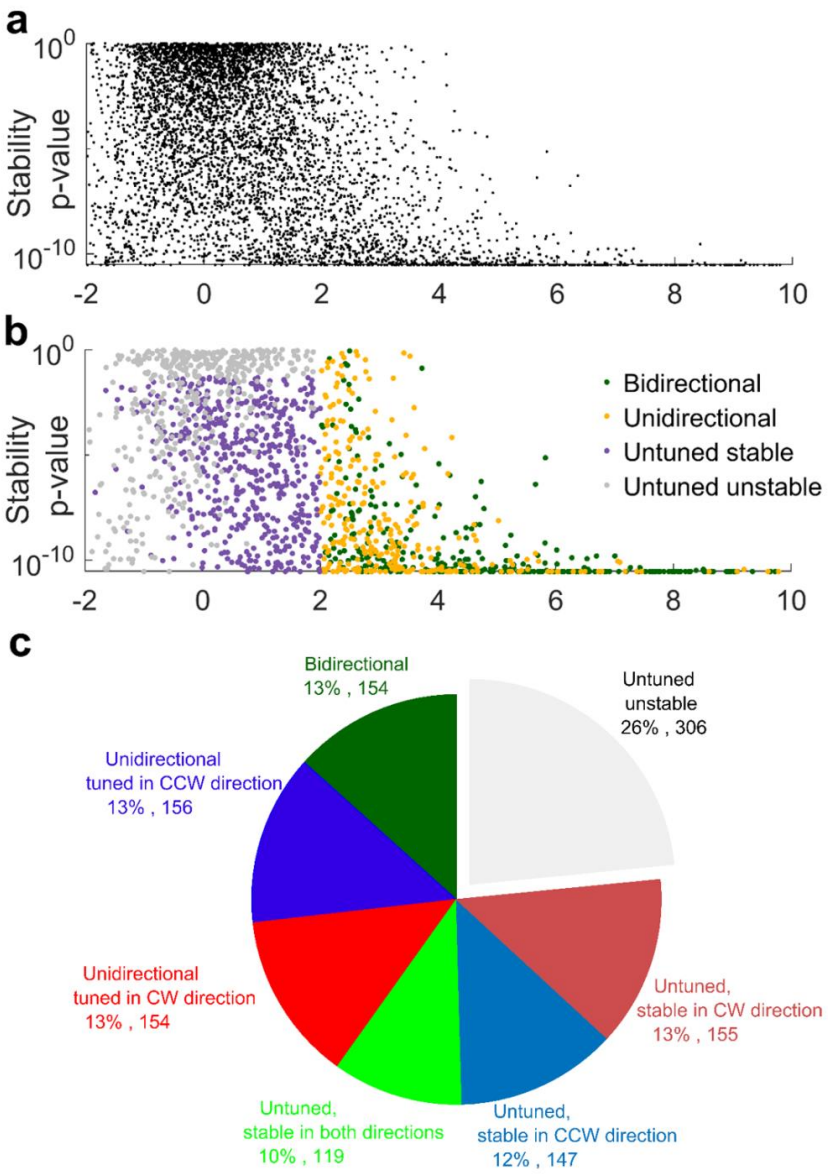

Extended Data Fig. 2.4 | Continuity of stability and sparsity measures. (**a**) across all neurons, the z-scored sparsity, i.e., degree of tuning, and stability varied continuously, with no clear boundary between tuned and untuned neurons. (**b**) Same distribution as (a), with color-coding of stable and tuned responses separated. (**c**) Detailed breakdown of SAC properties that had significant sparsity (i.e., tuned) or significant stability and whether these were observed in both directions (e.g., bidirectional stable) or only one direction (e.g., unidirectional tuned). If unidirectional, whether CW or CCW direction was significant. Nearly all cells that were significantly tuned in a given direction were also stable in that direction.

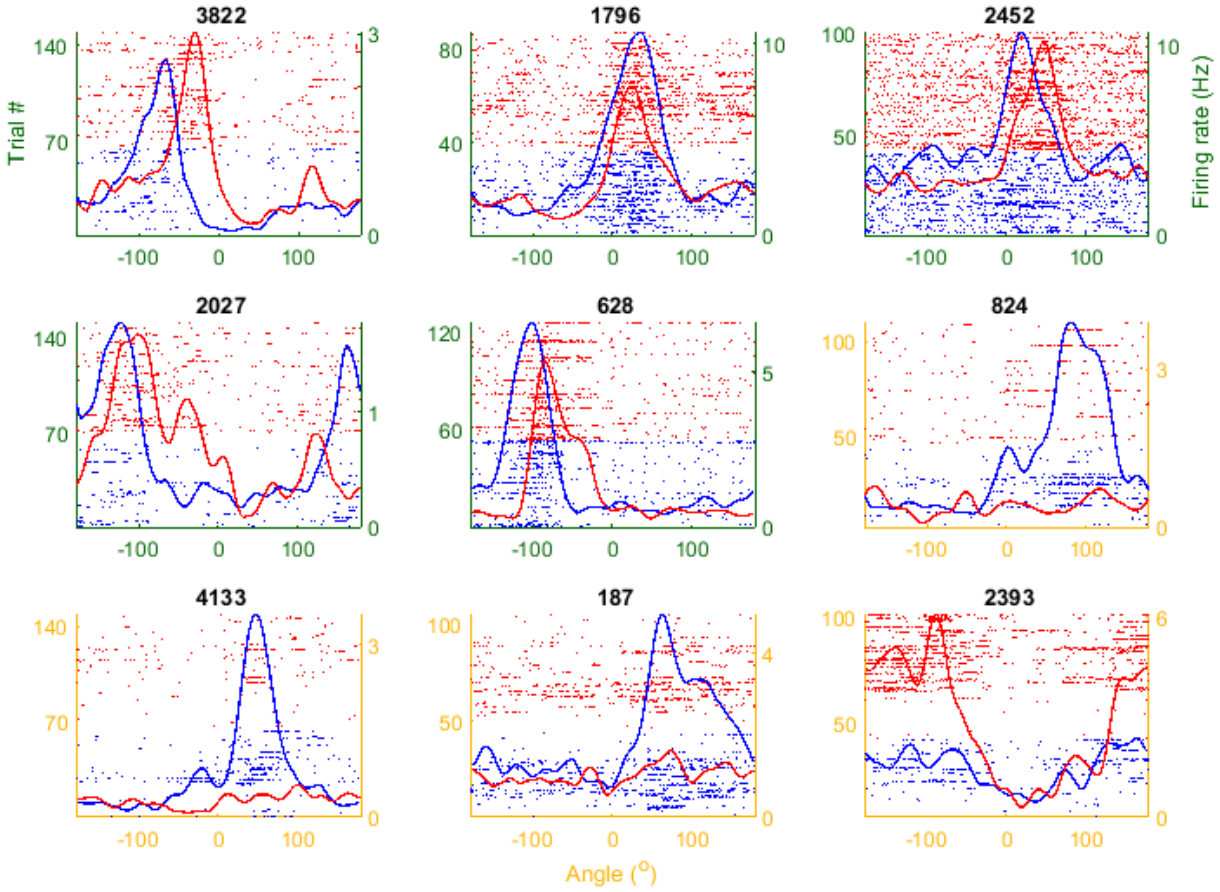

Extended Data Fig. 2.5 | Additional Examples of SAC tuned cells. For clarity, the CCW (blue) and CW (red) trials are stacked separately in all raster plot figures, even though these alternated every four trials. First five examples are of bi-directionally tuned cells (green y-axis); next four examples are of uni-directionally tuned cells (orange-yellow y-axis).

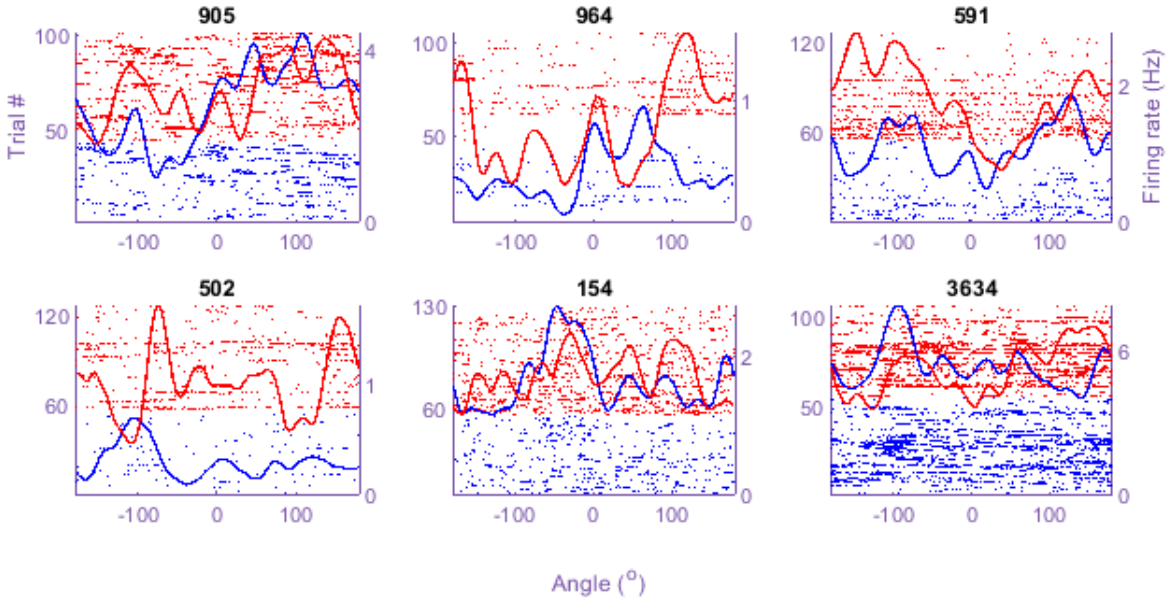

Extended Data Fig. 2.6 | Additional Examples of bi-directionally stable but untuned cells. These cells did not have significant sparsity (z<2) in either direction but had significant stability.

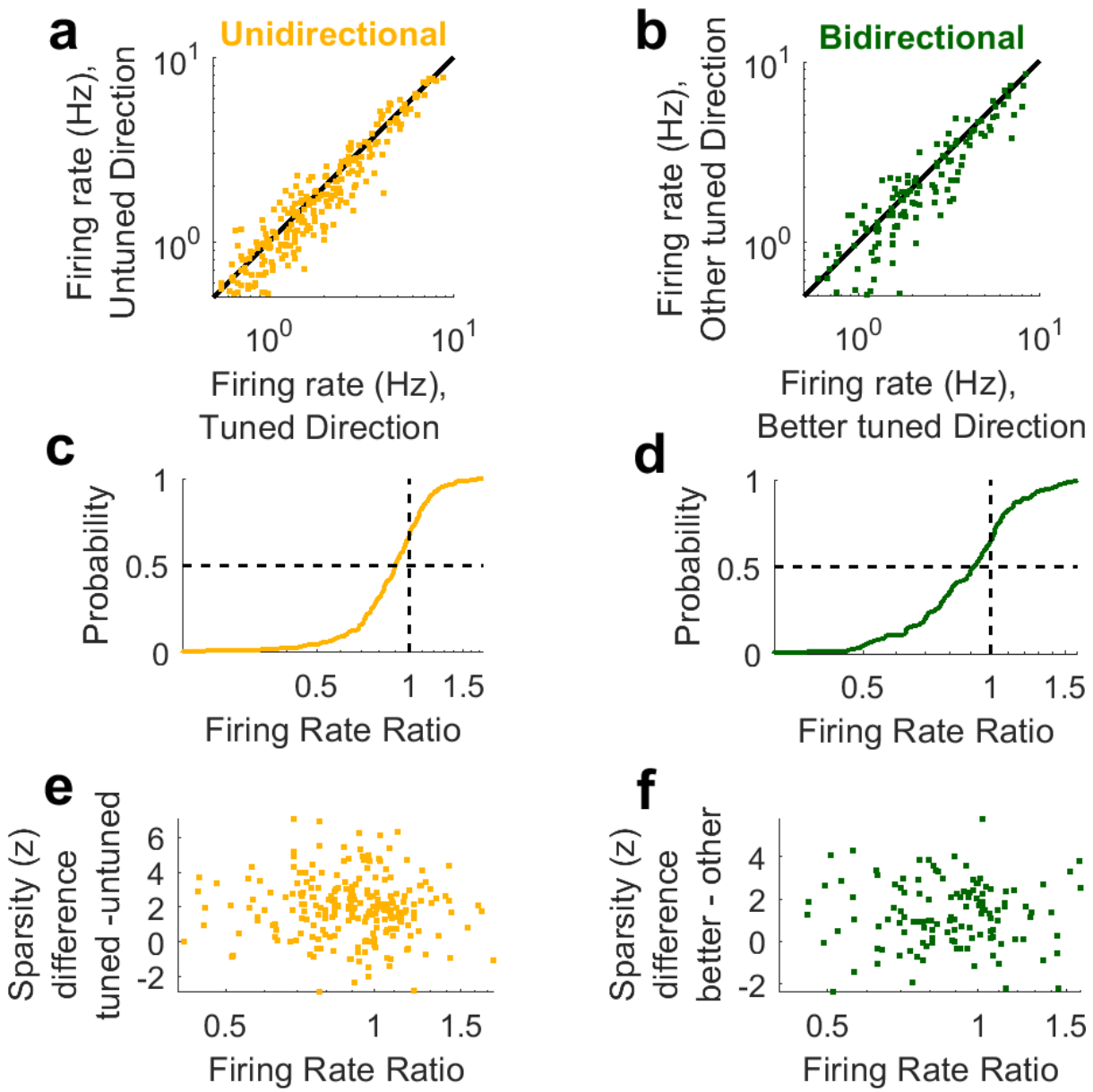

Extended Data Fig. 2.7 | Firing rate differences between CW and CCW revolution direction. Firing rate of (**a**) unidirectional cells in tuned versus untuned directions shows significantly higher (paired t-test p=4.5x10^{-10}) firing rates in the tuned direction (**b**) Same as (a), for bidirectional cells showing higher firing rate (paired t-test, p=2.0x10^{-6}) in the revolution direction with better tuning. (**c**) Cumulative histogram of ratio between firing rate in untuned to tuned direction was less than one for 67% (65%) of cells. **(d)** Same as

(c), but for bidirectional cells (other/better since both directions are tuned) showing 65% of firing rate ratios were less than one. (**e**) To remove the contribution of firing rate to sparsity, the strength of tuning (z-score sparsity) difference was computed with spike thinning procedures (similar to Extended Data Fig. 2.8, see methods) ensuring equal firing rate in both directions. The difference in tuning strength (z-scored sparsity) was not significantly correlated with firing rate ratio for unidirectional (r=-0.09 p=0.16) as well as (**f**) bidirectional (r=0.005 p=0.95) populations. For bi-directionally tuned cells, SAC with higher z-scored sparsity was labeled as the 'better' response, and the SAC with lower z-scored sparsity was called 'other' response.

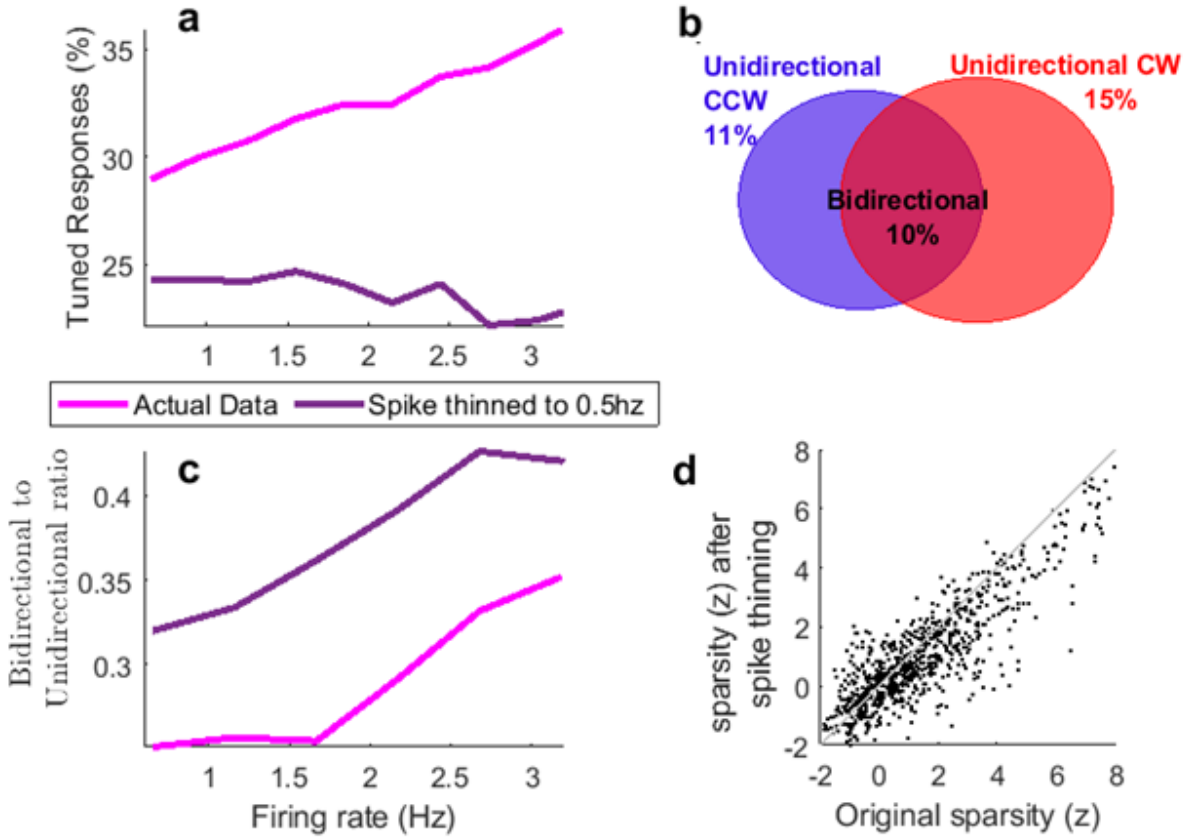

Extended Data Fig. 2.8 | The relative number of bidirectional cells increases with mean firing rate, but not the fraction of tuned cells. To remove the effect of firing rate on z-scored sparsity computation, we randomly subsampled spike trains to have a firing rate of 0.5 Hz (see methods). (**a**) The fraction of cells with significant sparsity, i.e., fraction tuned, increased with the firing rate for the actual data (r=0.11 p=2.2x10^{-6}), but after spike thinning, there was no correlation (r=0.01, p=0.77). Thus, the true probability of being tuned was independent of the firing rate of neurons. (**b**) Proportion of bidirectional and uni-directional tuned neurons is comparable (10% vs 13%) with and without spike thinning. (**c**) Fraction of bi-directional cells compared to uni-directional cells increases with original firing rate, even after spike train thinning. (**d**) Spike thinning procedure reduces the sparsity of the tuning curves, as expected, due to loss of signal. After spike thinning, sparsity was significantly correlated in both directions of revolution (r=0.39, p=3.8x10^{-31}) and this was not due to the rate changes because sparsity was uncorrelated with firing rates (r=0.01, p=0.72 for CCW sparsity and firing rate, r=0.02, p=0.54 for CW sparsity and firing rate).

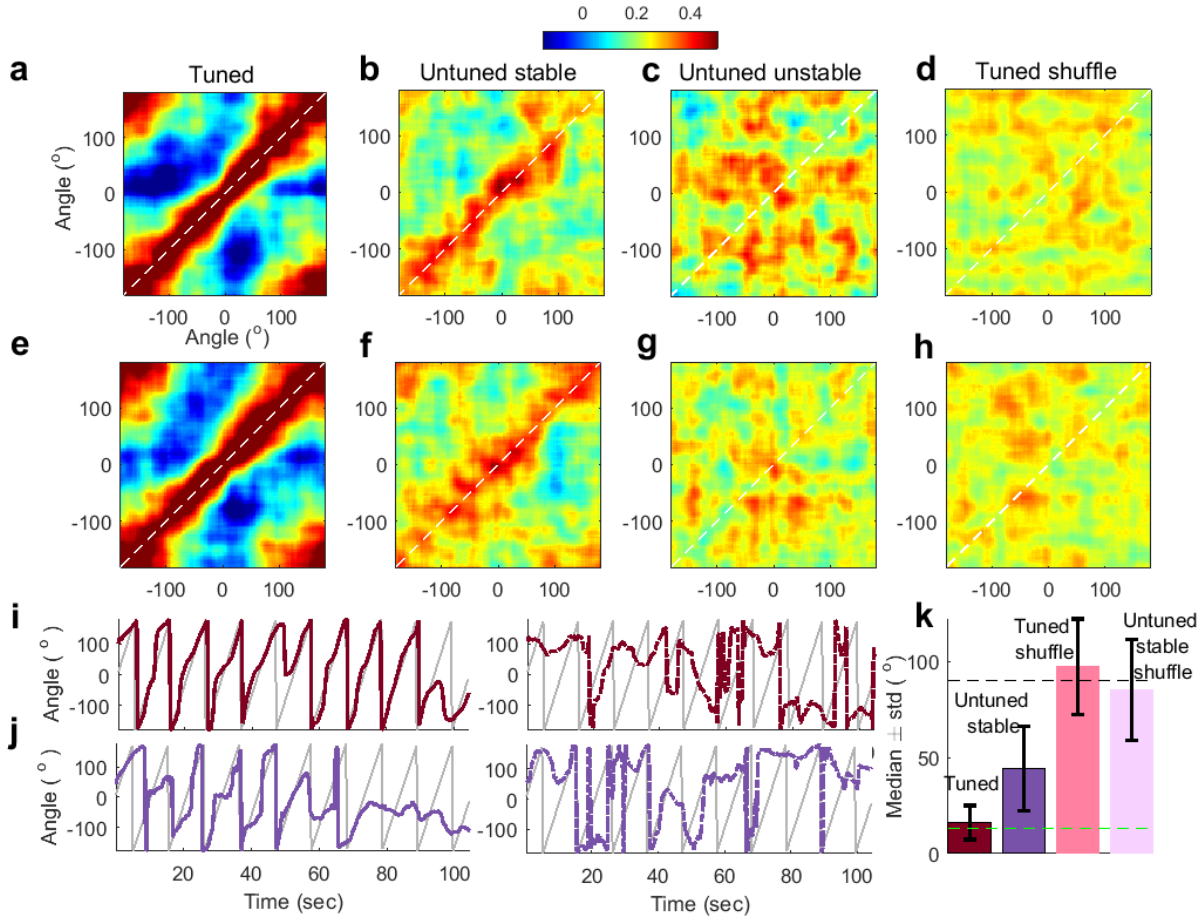

Extended Data Fig. 2.9 | Population vector stability and decoding of stimulus angle. (**a**) Stability for CCW tuned responses (n=310). Color indicates correlation coefficient between two non-overlapping groups of trials' population responses (see methods). The maximum correlation values were pre-dominantly along the diagonal. Maxima along x-axis and y-axis were significantly correlated (Circular correlation coefficient r=0.97, $p<10^{-150}$) (**b**) Same as (a) but using untuned stable cells (n=266) showed significant ensemble stability (r=0.91, $p<10^{-150}$). (**c**) Same as (a) but using untuned and unstable cells (n=306). This was not significantly different than chance (r= -0.16, p=0.09). (**d**) Same as (a), using tuned cells with their spike trains circularly shifted in blocks of four trials, showed no significant stability (r=1.1x10^{-3}, p=0.99). **(e)- (h)** Same as (a)-(d), but for CW data. **(i)** Decoding CW direction shows similar results as in CCW direction (shown earlier in Figure 2). Similar analysis as shown in Fig 2 for the stimulus movement in CW direction. (**Left**) Decoding cue angle in 10 trials of CW cue movement, using all other CW trials to build a population-encoding matrix. Gray trace indices

movement of visual bar, colored trace is the decoded angle. **(Right)** Same as left, for shuffle data. (**j**) Same as (i) but using the untuned-stable cells in CW movement direction. (**k**) Median error between stimulus angle and decoded angle over 10 instantiations of decoding 10 trials each for actual and cell ID shuffle data. Green dashed line indicates width of the visual cue; black dashed line indicates median error expected by chance.

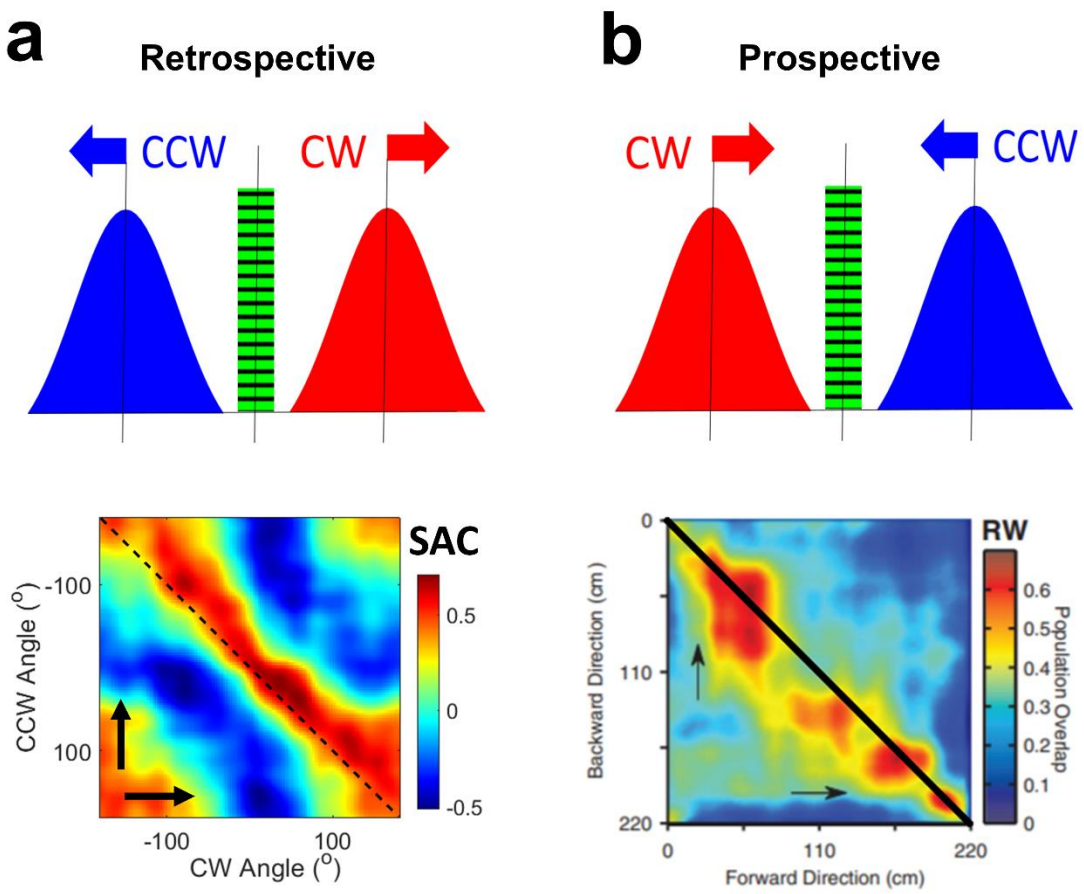

Extended Data Fig. 2.10 | Retrospective coding of SAC cells versus prospective coding in place cells. (a) Top- A bidirectional cell responds with a latency after the stimulus goes past the angular position of the bar of light depicted by the green stripped bar. **Bottom**- Population overlap is above the 45º line, indicating retrospective response. **(b)** Same as (a) but for a prospective response, where the neuron responds before the stimulus arrives in the receptive field. Such prospective responses are seen in place fields during navigation in the real world, where the population overlap is maximal below the 45º line (adapted from earlier work[29]). Prospective coding was seen in purely visual virtual reality, but those cells encoded prospective distance, not position.

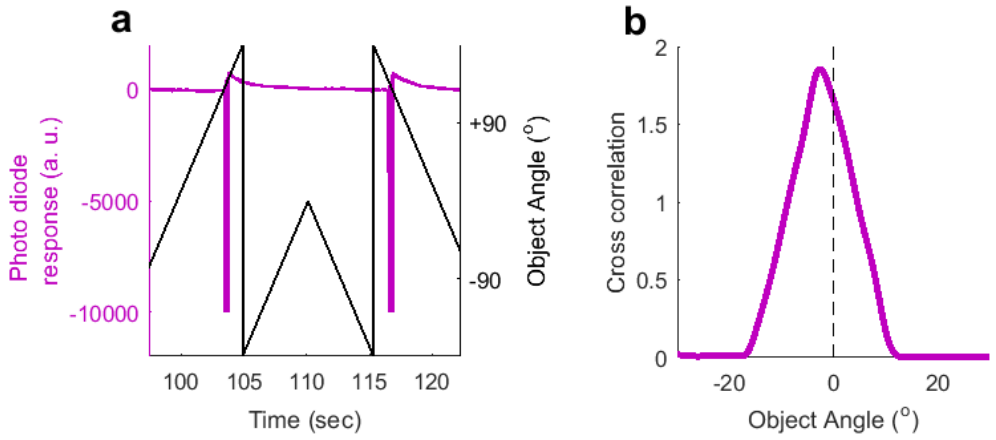

Extended Data Fig. 2.11 | Photodiode experiment to measure the latency introduced by the equipment. Instead of a rat, we placed a photodiode where the rat sat. (**a**) The signal from the photodiode (purple trace) synchronized with bar position (black) was extracted and (**b**) cross correlation computed between the CW and CCW tuning curves of photodiode response. The cross correlation had maxima at a latency of -2.8º, which corresponds to a temporal lag of 38.9ms. This was much smaller than the latency between neural spike trains (median latency 22.7º, corresponding to a temporal latency of 315.3ms before accounting for the recording apparatus latency). For all the latency numbers reported in the main text, this small latency introduced by the recording apparatus was removed.

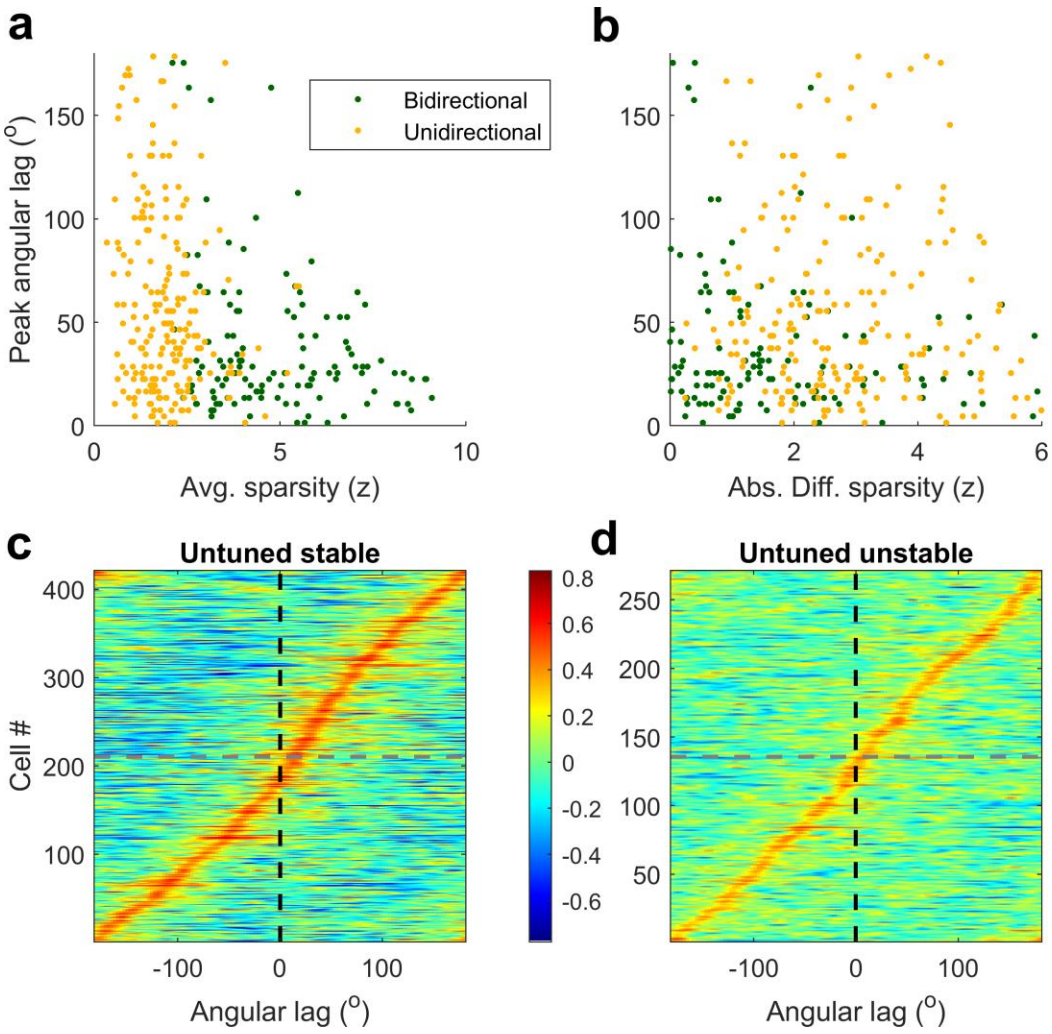

Extended Data Fig. 2.12 | Significant retrospective SAC in the untuned stable cells but not unstable cells. (a) Average strength of tuning in CCW and CW direction is inversely related to the peak angular lag between the two SAC for bidirectional (r=-0.19 p=0.04) as well as unidirectional cells (r=-0.16 p=0.02). **(b)** Absolute difference between strengths of tuning between CCW and CW directions was not significantly correlated with the peak angular lag in their cross correlation for bidirectional (r=0.13 p=0.14) or unidirectional cells (r=0.03 p=0.64). This analysis was restricted to cells with retrospective lags, which were in majority. (**c**) Untuned stable cells too show significant retrospective bias, quantified using the cross correlation between the tuning curves in CCW and CW directions (median lag =13.6° circular t-test p=0.02). (**d**) This is not seen for the untuned unstable population (median =4.6°, circular t-test p=0.39).

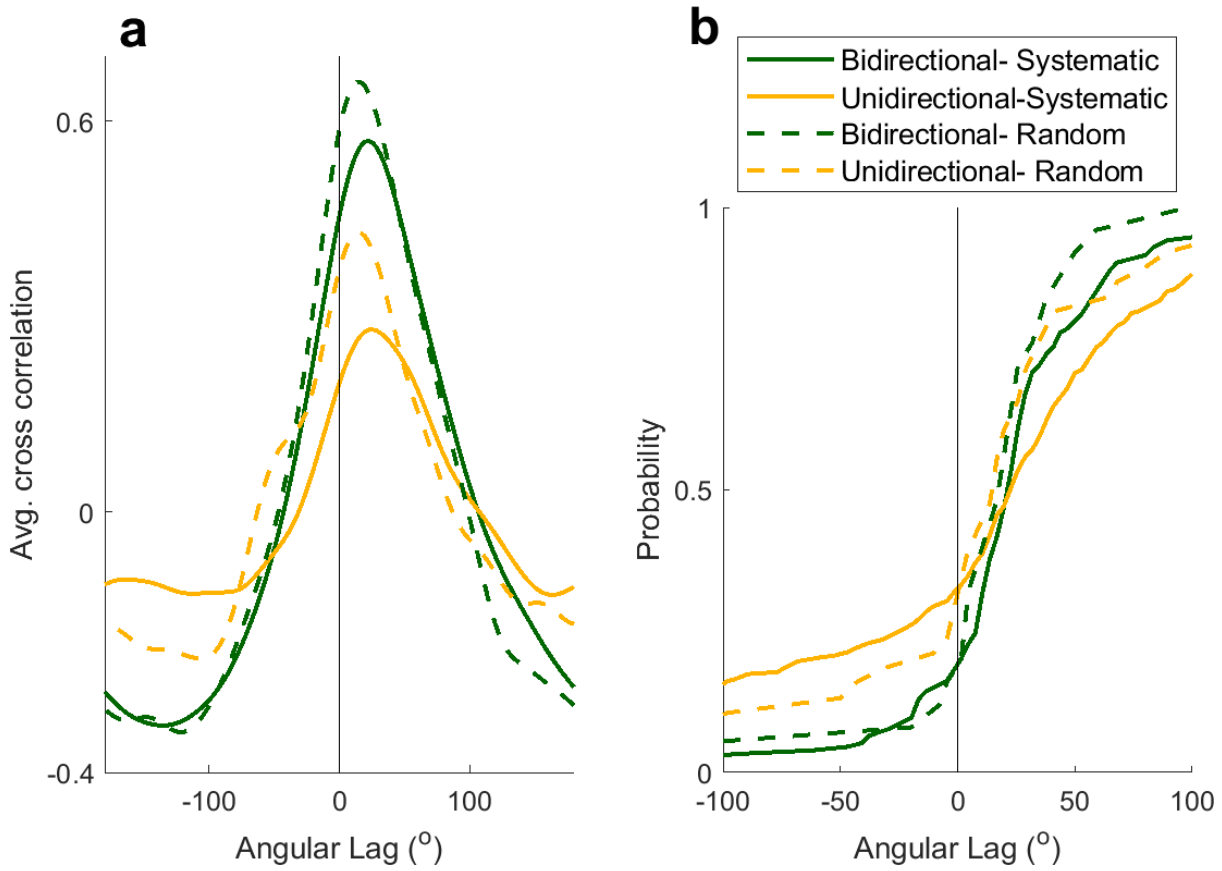

Extended Data Fig. 2.13 | Comparable retrospective coding in systematic and randomly revolving bar experiments. (**a**) Cross-correlations between CCW and CW tuning curves were averaged across all the bidirectional cells (green curves) for the systematic (latency for peak=25.7º) and random (16.7º) condition and showed a similar pattern of retrospective coding. (two sample KS-Test to ascertain if the distribution of latencies was significantly different, p=0.75). Unidirectional cells showed similar pattern for systematic (19.7º) and random (31.8º) conditions, but correlations were weaker than bidirectional cells. (**b**) Cumulative distributions show that under systematic and random conditions comparable number of cells had positive latency (80% each) for bidirectional cells, and (67% and 68%) unidirectional cells, respectively.

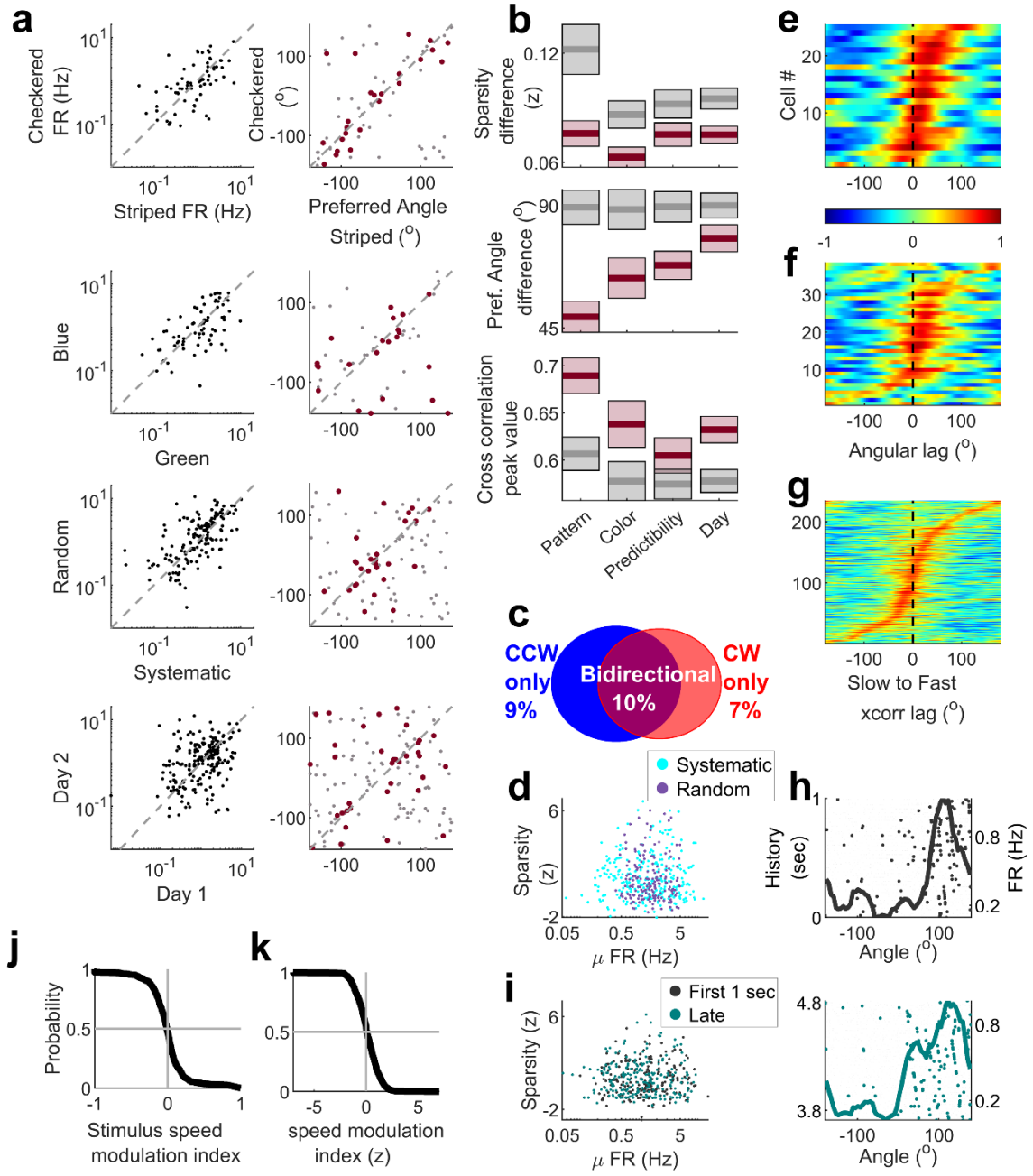

Extended Data Fig. 2.14 | Additional properties of SAC invariance. (**a**) **(Row 1**) For same cells recorded in response to the movement of a green striped and green checkered bars of light, mean firing rate during stationary epochs (running speed< 5cm/sec), was significantly correlated (r=0.48 p= 2 x 10^{-5}). Preferred angles of SAC between the two stimulus patterns were also significantly correlated (circular correlation r=0.32 p= 5 x 10^{-3}). Solid red dots denote preferred angles of cells tuned (sparsity (z) > 2) in both conditions; gray dots are for cells with significant tuning in one of the

conditions. **(Row 2)** Same as (a-Row 1), but for responses to changes of stimulus color, green and blue. Firing rate (r=0.45 p= 1 x 10^{-4}) & preferred angle (r=0.36 p= 0.01) were correlated. **(Row 3)** Same as (a-Row 1), but for changes to predictability of the stimulus, also called 'random' vs. 'systematic'. Firing rate (r=0.55 p= 2 x 10^{-13}) & preferred angle (r=0.27 p= 0.01) were significantly correlated between systematic and random stimuli movement. **(Row 4)** Same as (a-Row 1), but for responses recorded across 2 days. Firing rate (r=0.28 p=3.2 x 10^{-5}) & preferred angle (r=0.22 p=0.006) were correlated. **(b)** Similar to Fig 2.4, we computed the population remapping indices based on sparsity difference, preferred angle difference and peak value of cross correlation. The sparsity difference did not show a systematic pattern, but the other two metrics showed increasing remapping going from pattern (r=0.69, angle difference=49.1^o) to color (r =0.64, angle difference=63.3^o) to predictability (r =0.60, angle difference=68^o) and across days (angle difference=77.9^o). **(c)** Percentage of tuned responses in the random stimulus experiments, showing, comparable bidirectionality (10% here vs 13% for systematically moving bar). **(d)** For same cells recorded in random and systematic stimulus experiments, the distributions of firing rates and SAC, quantified by z-scored sparsity, were not significantly different (cyan-systematic, purple-random, KS-test for z-scored sparsity p=0.14, for firing rate p=0.27). **(e)** Cross correlation between CCW and CW tuning curves showing lagged response for the majority of bidirectional cells in the random condition. **(f)** Same as (e), but for unidirectional cells. **(g)** Cross correlation of tuning curves (for tuned cells in the random stimulus experiment) between fast- and slow-moving stimulus was calculated from the subsample of data for a particular speed in CW and CCW direction separately and stacked together after flipping the CCW data, and was not significantly biased from zero (Circular median test at 0^o, p=0.56). **(h)** Example cell showing similar SAC for data within 1 second of stimulus direction change(left), or an equivalent, late subsample(right). **(i)** Firing rate (KS-test p=0.73) and sparsity (KS-test p=0.87) were not significantly different for these two subsamples of experimental recordings. **(j)** In the randomly moving stimulus experiments, stimulus speed modulation index (see methods) was not significantly biased away from zero. **(k)** This modulation index was z-scored (see methods), and only 5.2% of cells had significant firing rate modulation beyond z of ±2.

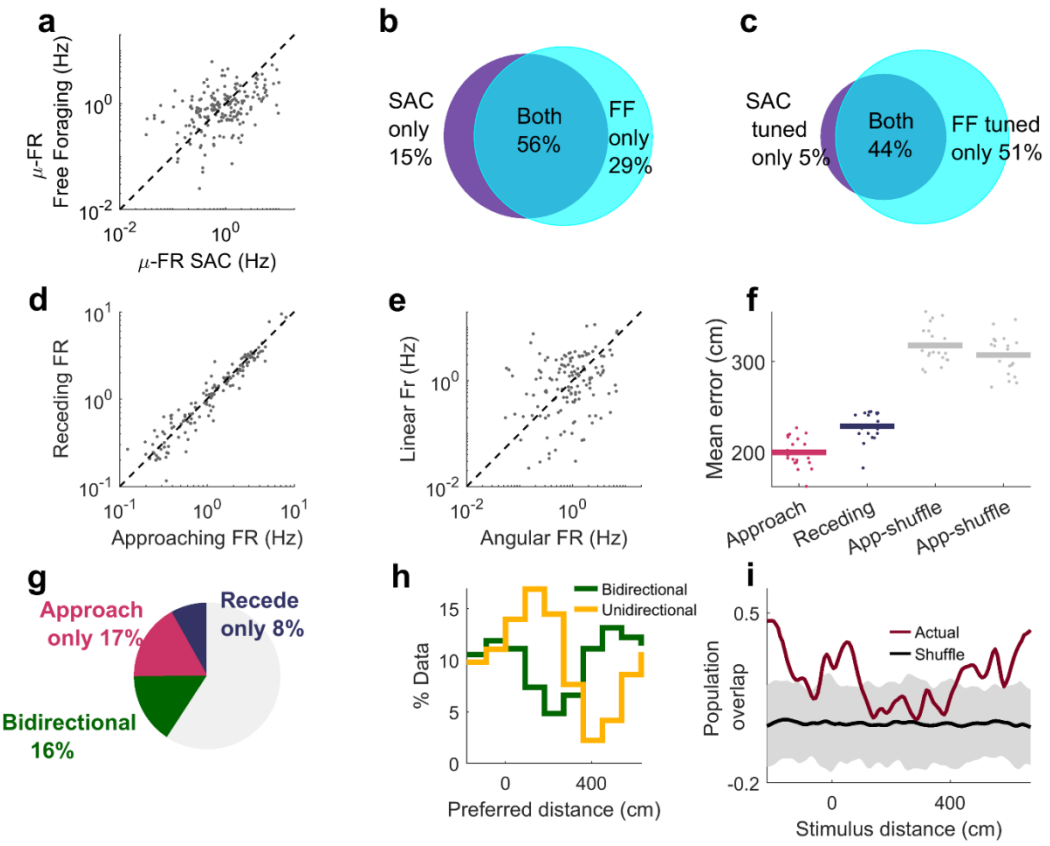

Extended Data Fig. 2.15 | Relationship between SAC cells place cells and stimulus distance tuned cells. (a) The mean firing rates of cells was significantly correlated (r =0.43 p=4.5x10^{-10}) between the SAC and spatial exploration experiments. **(b)** Majority of cells active during the SAC experiments were also active during random foraging in real world. **(c)** Almost all of the SAC cells were also spatially selective during spatial exploration. **(d)** Between the approaching and receding directions, the mean firing rates, computed when the rats were immobile, were highly correlated (r=0.96 p=4x10^{-81}) and not significantly different (t-test p=0.93). **(e)** Firing rates, computed when rats were stationary, during the stimulus angle and stimulus distance experiments were significantly correlated (r=0.22 p=0.008). **(f)** Population vector decoding of the stimulus distance (similar to stimulus angle decoding, Fig 2), was significantly better than chance. (KS-test p=5.5x10^{-10} for approaching and p=4.7x10^{-9} for receding data). Approaching stimulus decoding error (mean=204cm) was significantly lesser than that for receding (mean=231cm) (KS-test p=4.2x10^{-5}). These errors were 63% and 74% of the error expected from shuffled data, which was greater than that for SAC decoding,

where the error was 33% of the shuffles, when controlling for the number of cells. **(g)** More than twice as many cells were unidirectional tuned for approaching (coming closer) movement direction, as compared to receding (moving away). **(h)** For bidirectional cells, location of peak firing in the approaching and receding direction shows bimodal response, with most cells preferring either the locations close to the rat, i.e., 0 cm or far away, ~500cm. Unidirectional cells preferred locations close to the rat. **(i)** Population vector overlap, (Fig. 5h), was further quantified by comparing the values along the diagonal for actual tuning curves, with the spike train shuffles. The actual overlap was significantly above two standard deviations of the shuffles for distances close to the rat (around 0) and far away (beyond 400cm).

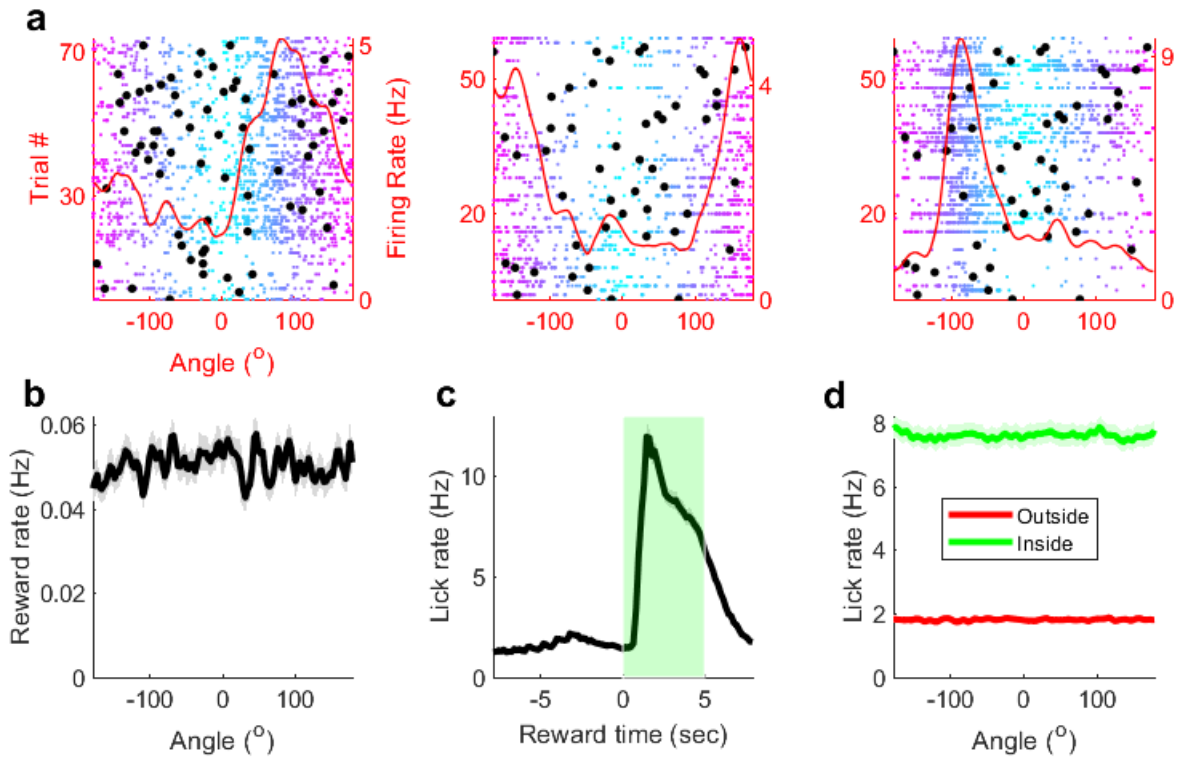

Extended Data Fig. 2.16 | Rewards and reward related licking are uncorrelated with SAC. (a) Example cells showing SAC from Figure 1, with reward times overlaid (black dots), showing random reward dispensing at all stimulus angles. **(b)** The average rate of rewards was uncorrelated with visual stimulus angle (circular test for uniformity p=0.99) **(c)** Rat's consumption of rewards, estimated by the reward tube lick rate, was measured by an infrared detector attached to the reward tube[28]. As expected, lick rate increased after reward delivery by ~4 fold and remained high for about five seconds (green shaded area). This duration is termed the 'reward zone'. **(d)** Lick rate inside the reward zone (green) was significantly larger than that outside (red, KS-test p= 2.3 x 10^{-54}). Inside as well as outside reward-zone lick rates were uncorrelated with visual stimulus angle (circular test for uniformity p=0.99 for both).

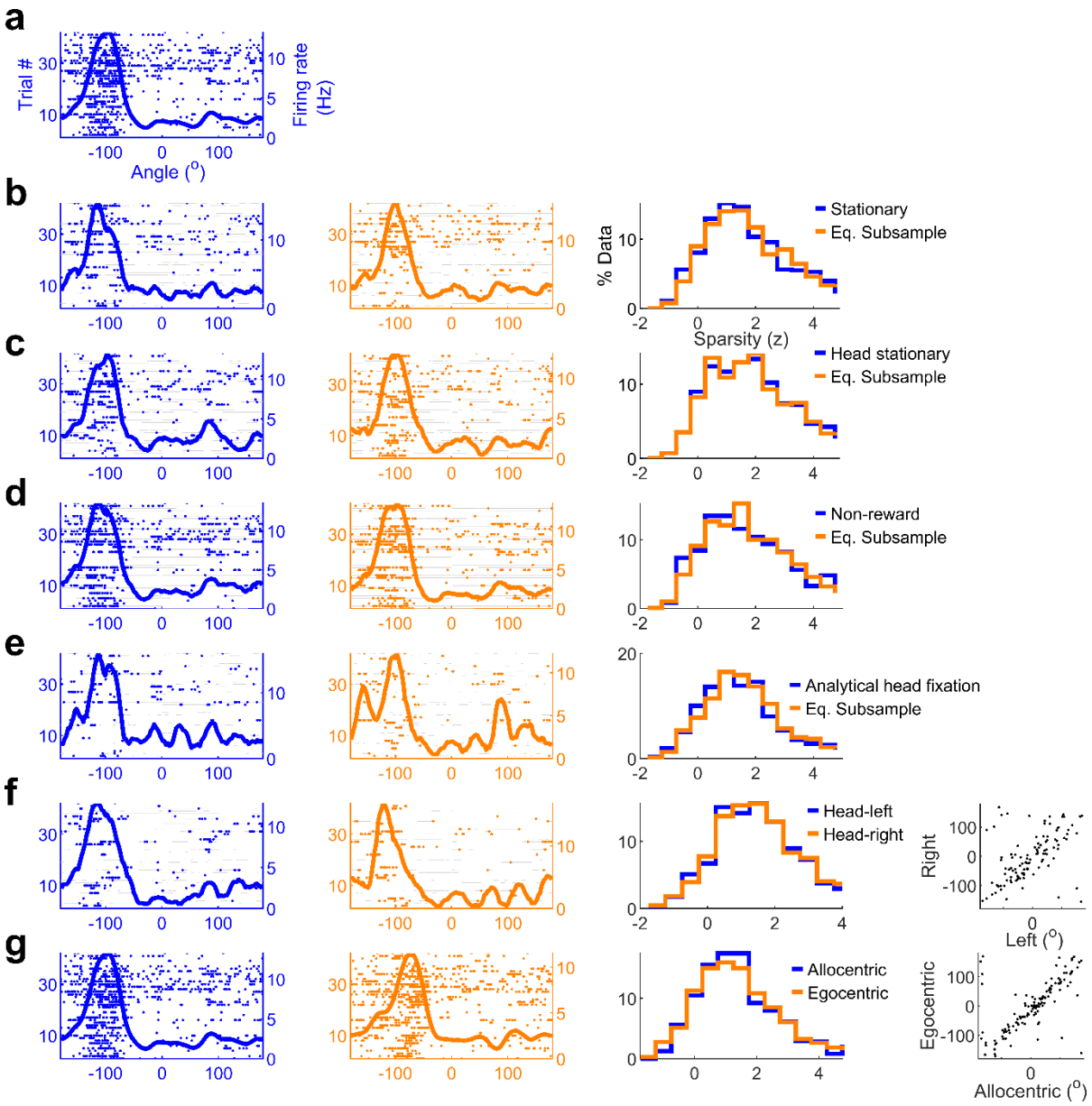

Extended Data Fig. 2.17 | Behavioral controls of SAC. To ascertain whether systematic changes in behavior caused SAC, we employed a 'behavioral clamp' approach and estimated tuning strength using only the subset of data where the hypothesized behavioral variable was held constant. **(a)** Example SAC tuned cells maintained its tuning even if we used only the data when the rat was **(b)** stationary (running speed <5cm/sec, blue, left). This was comparable to a random subsample of behavior, obtained by shuffling the indices of spikes and behavior when the animal was stationary (orange, middle) (see methods). 38% of cells were SAC tuned (sparsity *z*>2) when using only the stationary data which is substantially greater than chance, whereas

42% were significantly tuned in the equivalent, random subsample and this difference was significant (KS-test p=0.02). **(c)** Similar to (b) but using only the data when the rat's head was immobile (head movement velocity < 10mm/sec). 43% and 42% of cells were significant tuned in actual behavioral clamp and equivalent subsample, and these were not significantly different (KS-test p=0.93) **(d)** Similar to (b) but using only the data beyond 5 seconds after reward dispensing, called non-reward. 43% SAC were tuned for non-reward, 43% for equivalent subsample, KS-test p=0.56. **(e)** Using a subsample of data, from when the rat's head was within the central 20 percentile of head positions (typically $<10^{o}$), rat was stationary and there were no rewards in the last 5 seconds. This condition was called 'analytical head fixation'. 28% of cells were SAC tuned under this behavioral clamp, which was lesser than that in an equivalent subsample (31%, KS-test p=0.05) **(f)** Tuning curves for head positions to the leftmost 20 percentile and rightmost 20 percentile were correlated (circular correlation r=0.67 $p=1.3\text{x}10^{-11}$, with 31% and 32% cells tuned in the two conditions (KS-test p=0.67). The preferred angles of tuning were highly correlated and did not have significantly different concentration (circular t-test p=0.86). **(g)** SAC tuning was recomputed in the head centric frame, by accounting for the rat's head movements (obtained by tracking overhead LEDs attached to the cranial implant) and obtaining a relative stimulus angle, with respect to the body centric head angle. Overall tuning levels were comparable, between allocentric and this head centric estimation. First panel of (g) is the same as that in (a) since all SAC tuning reported earlier was in the allocentric or body centric frame. Using a subset of data when both overhead LEDs were reliably detected, 25% and 26% of cells were significantly tuned for the stimulus angle in the allocentric and egocentric frames (KS-test p=0.9). Preferred angle of SAC tuning for tuned cells was highly correlated (r=0.81 $p=1.8\text{x}10^{-15}$) and not significantly different between the two frames (circular t-test p=0.82).

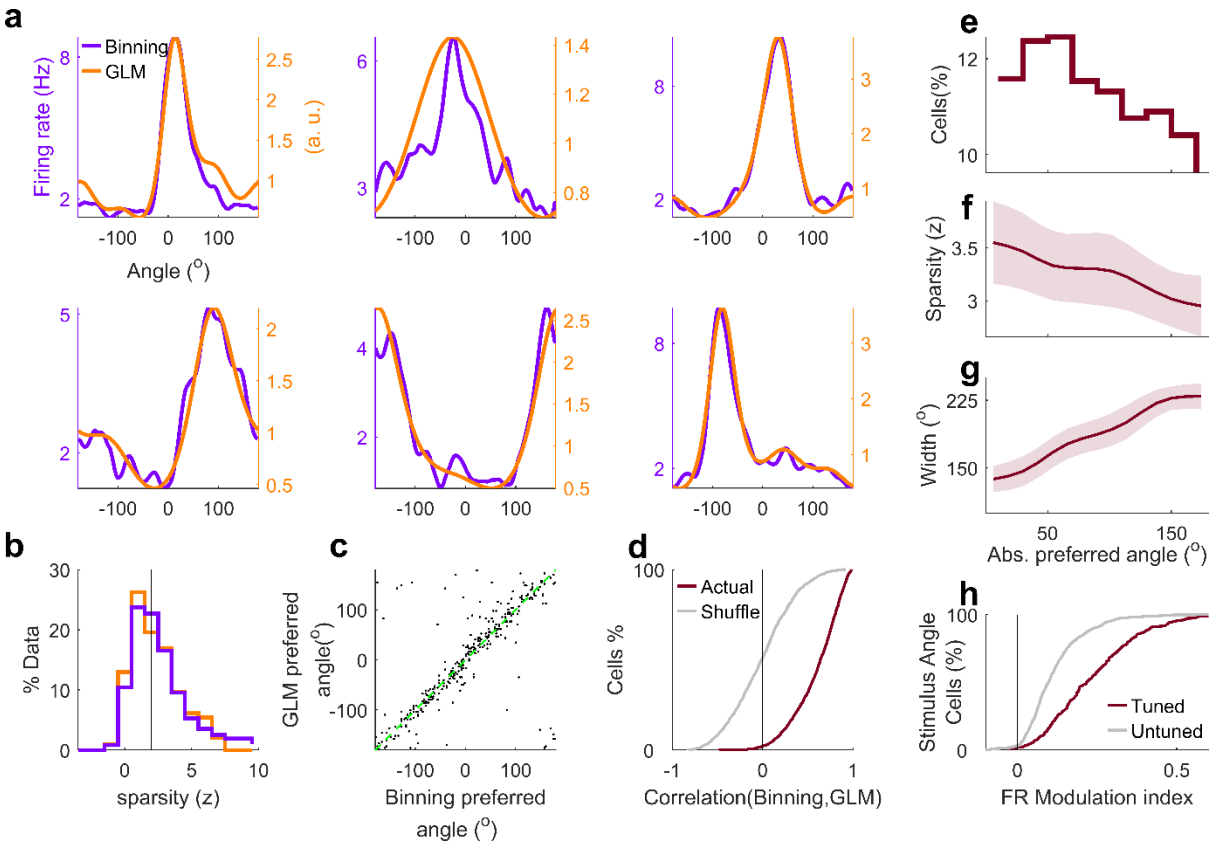

Extended Data Fig. 2.18 | GLM estimate of SAC tuning. To estimates the independent contribution of stimulus angle to neural activity, while factoring out the contribution of head position and running speed, we used the generalized linear model (GLM) technique (see methods)[21]. **(a)** Tuning curves obtained by binning methods were comparable with those from GLM estimation, for the same cells as used in Fig. 2.1. **(b)** Sparsity levels were comparable (KS-test p=0.07) and 40% of cells were found to be significantly tuned for stimulus angle using GLM based estimated, compared to 43% from binning in this subset of data (n=991). **(c)** Preferred angle of firing between GLM and binning based estimates of SAC were highly correlated (circular correlation test r=0.86 $p<10^{-150}$) **(d)** Correlation between the SAC tuning curves from the two methods was significantly greater than that expected by chance, computed by randomly shuffling the pairing of cell ID across binning and GLM (KS-test $p<10^{-150}$). **(e-h)** Properties of SAC tuning responses based on GLM estimates were similar to those based on binning method, as shown in Fig. 2.1. (**e**) Distribution of tuned cells as a function of the preferred angle (angle of maximal firing). There were more tuned cells at forward angles

than behind. (**f**) Median z-scored sparsity and its variability (SEM, shaded area, here and subsequently) of tuned cells as a function of their preferred angle. (Correlation coefficient r=-0.17 p=0.004). (**g**) Median value of the full width at quarter maxima across the ensemble of tuned responses increased as a function of preferred angle of tuning. (r=+0.33 $p<10^{-150}$). (**h**) CDF of firing rate modulation index within versus outside the preferred zone (see methods) for tuned cells were significantly different (Two-sample KS test $p=2.9\text{x}10^{-37}$).

CHAPTER 3: HIPPOCAMPAL REPRESENTATIONS FOR REAL WORLD SPACE DURING VIRTUAL ENVIRONMENT NAVIGATION

Introduction

Body fixed virtual reality (VR) introduces a dissociation between distal visual cues, and other sensory cues, raising the question of whether hippocampal neurons would encode the virtual visual space, or the real world, room space. Here we show that, CA1 neurons of rats performing VR navigation have small, highly precise, $2cm^2$ place fields in the real-world space explored by head movements. These results imply that multisensory association present in the real world plays a stronger role in hippocampal firing than navigational demands tied to virtual navigation.

Rodent hippocampal neurons are believed to support cognitive mapping, with spatially selective responses observed in the CA1 region, called place fields[23]. This selectivity is posited to be governed by distal visual cues[6], although other sensory-motor cues also contribute[60,61]. Prior report of body-fixed rodents exploring a two-dimensional virtual reality (Fig. 3.1a) showed markedly reduced spatial selectivity to the virtual space[14]. This was true even while the subject was performing successful navigation in that space, indicated by edge avoidance and reward guided movements. On the other hand, VR systems allowing 360^o rotation of the subject found significantly larger fraction of cells showing spatial selectivity[13], similar to free foraging in open arenas.

Simultaneous exploration of constrained real world (c-RW) and virtual reality (VR) spaces

Owing to the body fixation, the range of head movements in our VR setup was substantially smaller than real world (RW) experiments. Head movements typically spanned positions around a semi-circular arc (Fig. 3.1b-c). We called this space explored by head movements as the constrained real world (c-RW) space. In 35 sessions from 4 rats performing random foraging in a 2-meter diameter virtual reality (VR) environment, the range of exploration of the c-RW space was 4 orders of magnitude smaller than the virtual space (Fig. 3.1d-e). On the other hand, the incremental exploration with time for both the VR and the c-RW spaces was comparable with a faster time course for the c-RW space (Fig. 3.1f), suggesting that the lack of exploration of the c-RW space was not due to short experiment durations.

Do hippocampal neurons have spatial selectivity to this c-RW space? We recorded extracellular spiking activity of 626 putative pyramidal neurons from the dorsal CA1 region of the hippocampus using tetrodes (see *Methods*). c-RW tuning curves were obtained by spatial binning of spikes and occupancy (see *Methods*). Multiple neurons showed elevated firing in limited regions of the c-RW space, with almost no firing outside (Fig. 3.2a, Extended Data Fig. 3.1, 3.2). Often, neurons had a gradient in their firing response along the X-axis as well, suggesting encoding of the two-dimensional c-RW space, rather than merely a response to the angle of head with respect to the fixed body. After using partial correlations to factor out neuronal firing rates, strength of tuning in the c-RW was found to be uncorrelated with the tuning in the VR space (Fig. 3.2b). Out of the population of pyramidal cells recorded, 212 (or 33.9%) were deemed spatially selective to c-RW space, based on the z-scored sparsity of their tuning curves (see *Methods*). This fraction was significantly greater than that expected by chance (z=2 corresponding to p=0.0228) as well as compared to the degree of spatial selectivity to the VR space (19%, Fig. 3.2c).

Small place fields in the c-RW space

The size of these c-RW place fields was quantified using full-width at half maxima (FWHM, see *Methods*). Median FWHM was 17.3% of the total space explored, which is comparable to typical place fields in free foraging[29,56] (Fig. 3.2d). The small size of the c-RW space resulted in exceedingly small place fields, with a median value of 2.1cm^2. To the best of our knowledge, these are the smallest place fields reported from the CA1 region, and at least an order of magnitude smaller than the other place fields reported in other constrained spaces[17]. In contrast to those experiments, as well as other experiments in VR[13], rats in our experiments were not able to completely turn around. Hence, these highly precise place fields in our experiments arise even without the complete range of rotational movements and accompanying vestibular cues. Neurons with higher firing rates had better c-RW tuning (Fig. 3.2f) and larger place fields (Fig. 3.2g).

Majority of neurons were non-directional (Extended Data Fig. 3.3), showing similar c-RW tuning in responses computed separately for up and downward head movements (corresponding to increasing and decreasing c-RW Y-position, respectively).

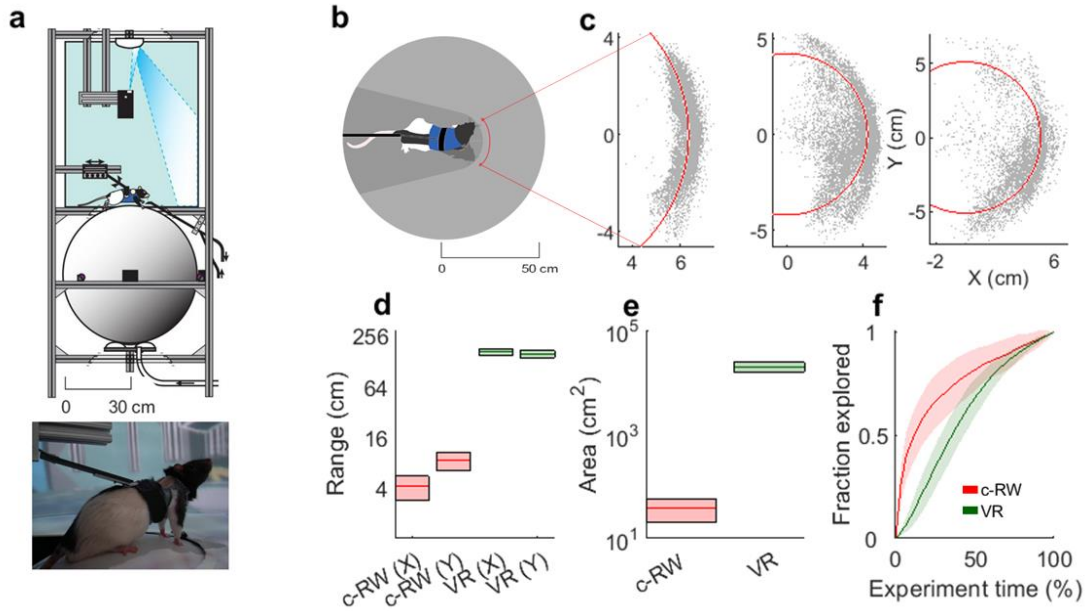

Fig. 3.1 | Simultaneous exploration of constrained real world (c-RW) and virtual reality (VR) spaces (a) Top- Experimental apparatus depicting the body-fixed rat running on an air levitated spherical treadmill. Bottom- Image of the rat, which is free to move its head, but not body, while the VR is immersive and projected all around the animal, as well as on the floor. **(b)**Illustration of the top view in the constrained RW space, showing head movements around a semi-circular arc. **(c)** Three example sessions showing head position occupancy in gray, and best fit circle in red. **(d)** The range of movements was defined as extent of pixels explored along X or Y direction, after excluding the bottom and top 1 percentile values of occupancy. c-RW range (mean=4.14cm and 8.42cm along X and Y directions) was 40 times smaller than for VR space (166.3 and 156.7cm X and Y respectively).**(e)** The area explored by head movements (mean=38.7 cm^2) was more than 500 times smaller than the area explored by leg movements, in the virtual space. (mean=20005cm^2) **(f)** Fraction of the total area explored increased with time, as expected and this increase was similar for c-RW and VR space.

Rats explored the c-RW space using head movements, which may or may not be accompanied by leg movements. Less prevalent but significantly greater than chance c-RW tuning was observed during non-running epochs, compared to epochs when head movements were accompanied by running. (Extended Data Fig. 3.4)

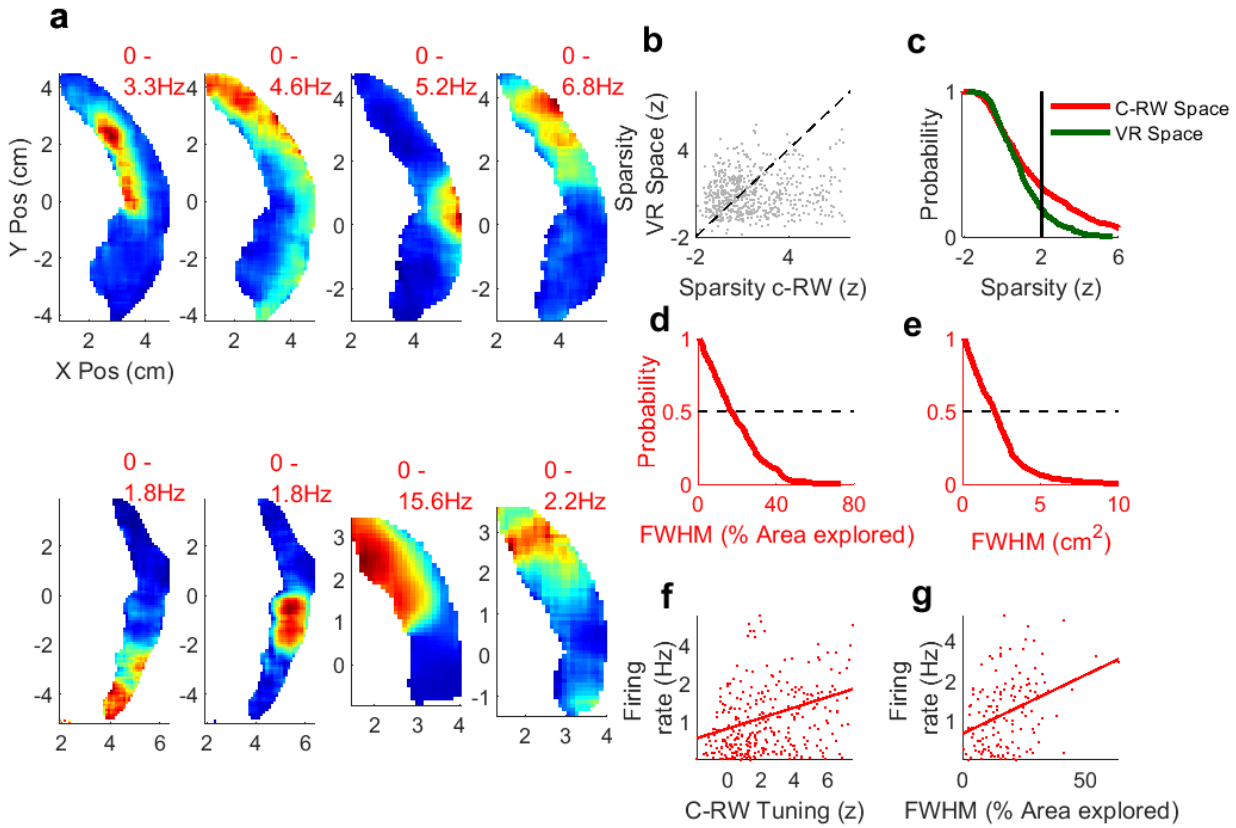

Fig. 3.2 | Small place fields in the c-RW space (a) Eight example cells showing c-RW place fields spanning different positions and have a gradient along the X-direction. Color corresponds to firing rates, whose range is denoted at the top. **(b)** c-RW tuning, quantified by z-scored sparsity was not significantly correlated with the VR space tuning **(c)** Significantly higher sparsity for c-RW space (33%), compared to the VR space (18%). **(d)** c-RW place fields were extremely small with a median value of 2.3cm^2 but covered 20% of the region explored by the head movements, on average. **(e)** More c-RW tuned cells were recorded for positions away from the center, along the y direction. **(f)** c-RW tuning was recomputed after 'spike thinning', to an effective firing rate of 0.5Hz. c-RW tuning thus obtained was positively correlated (r=0.3 p=9.8x10^{-8}) with the

actual firing rate. **(g)** Firing rate was also positively correlated with the size of place fields (r=0.332 p=3.5x10^{-5})

Independent contributions of head and leg movements on theta oscillations

In free foraging experiments, navigation from one location to other is driven by self-generated running epochs. This changes the constellation of distal visual as well as proximal cues, which are consistently paired together. In our body fixed apparatus, leg movements control the changes in distal visual cues, whereas head movements enable a rotated sampling of the same visual cues along with other, uncorrelated, proximal, non-VR cues. Head movements could be initiated at different positions in the virtual space leading to inconsistent pairing between distal visual cues and proximal cues. What is the relation between the speeds of these head and leg movements? We found epochs of behavior when the two movements speeds were either correlated or inversely related. (Fig. 3.3a). To quantify their relation, we computed the correlation coefficient between leg and head movement speeds. Majority (91%) of movement bouts had positive instantaneous correlation between leg and head speeds, compared to the null distribution (Fig. 3.3b, see *Methods*). Cross correlation between these speeds revealed that head movements typically preceded leg movements in vast majority (89%) of movement bouts with a median latency of 0.9 seconds (Fig. 3.3c). Such initiation of head movements prior to running is presumably to enable scanning of the virtual environment and locate the next virtual location of reward. Rats spent 25% and 23% of the non-reward time being stationary and engaging in head movements without running, respectively (Fig. 3.3d-e).

Individual neurons as well as theta band oscillation of hippocampal ensemble is known to be affected by running speed[29,62,63] and head movements are expected to have smaller effects[64]. Hence, we quantified the independent contributions of head and leg speeds to the excitation (*Exc*) and inhibition (*Inh*) ensemble activity (see *Methods*). *Exc* as well as *Inh* ensembles showed increased firing at higher leg speeds, as expected, but *Inh* showed stronger modulation than *Exc* (Fig. 3.3f). Modulation by head movements was weaker as evidenced by smaller partial correlation values, but majority of correlations were positive. Theta (6-12Hz, see *Methods*) power had a positive relation with leg as well as head movement speeds, but theta frequency had a negative correlation with both (Fig. 3.4g, Extended Data Fig. 3.5). This report of negative correlation between running and theta frequency is in apparent conflict with prior reports[29] in the

same apparatus during one-dimensional VR track foraging, where no significant correlation was reported. Unlike those analyses which excluded stationary and low (v<10 cm/sec) speed epochs, we used all behavioral data, binned on a logarithmic scale of speeds. This led to results similar to recent report[65] as well as the reported negative correlation between running speed and theta frequency by others[66]. Hence, leg movements exerted greater control over theta oscillations ensemble firing and head speed showed similar but weaker effect. But spatial selectivity was found in the space explored with head movements and not leg movements.

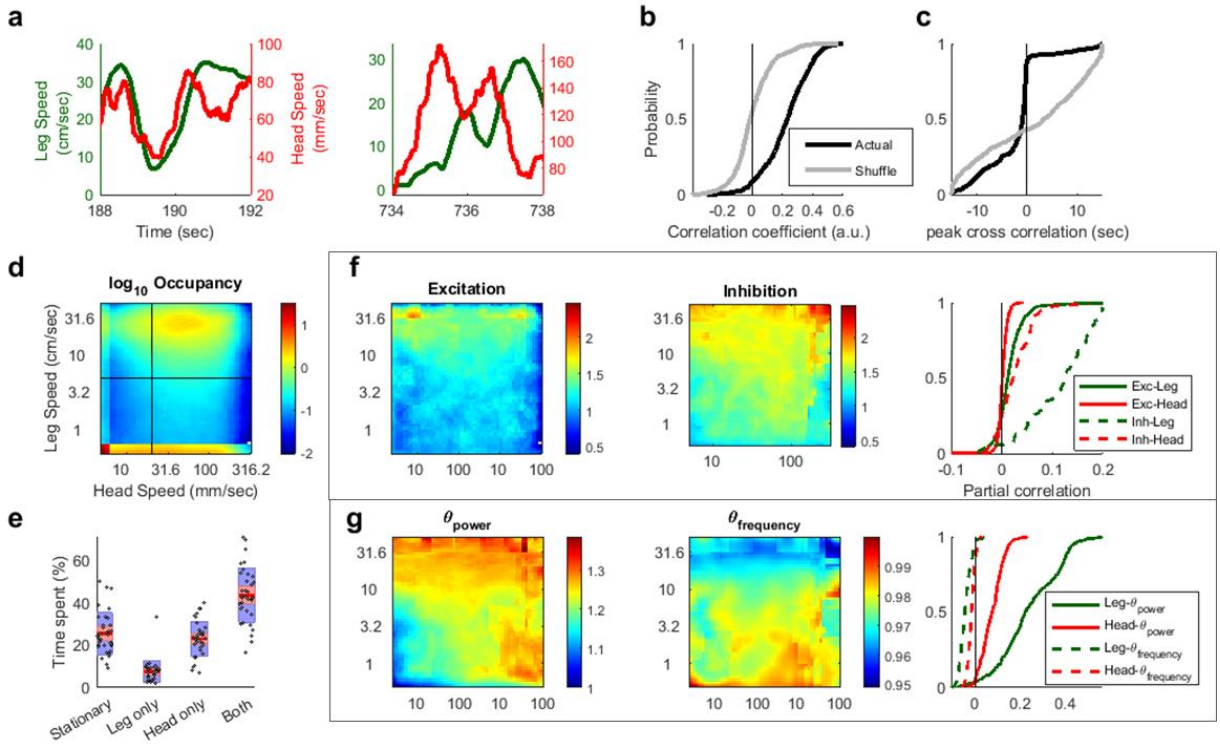

Fig. 3.3 | Firing and theta oscillation dependence on leg and head movements. **(a)** Instances of leg and head movement across 2 second windows showing similar (left) responses, and head movement signal(red) preceding the leg movements in green(right). **(b)** Cumulative histogram showing majority of bouts having positive instantaneous correlation between leg and head movements, **(c)** but peak cross correlation at negative latency for 88% of actual data. **(d)** 2-D histogram on log scale of behavior, binned using logarithmically spaced bins for leg and head speeds. Vertical line indicated the cutoff for head movement vs stationary 20mm/sec and horizontal line denotes the cutoff on leg speed for running vs stationary 5cm/sec **(e)** Average

percentage of time spent in different behavioral epochs. **(f)** 2D histograms, averaged over excitatory or inhibitory neurons of firing, after normalizing by the 1st bin, corresponding to lowest leg and head speeds. **(g)** Similar as (f) but for theta power and frequency, computed from the local field potential (see *Methods*).

Place cells firing during free foraging is modulated by the phase of the theta-cycle[67,68] and this relation between phase and position transforms the firing rate code into a temporal code[69]. Hence, we analyzed the populations of c-RW spatially tuned as well as untuned cells for theta phase modulation (see *Methods*). Population average responses of phase modulation were comparable (Extended Data Fig. 3.6) for tuned and untuned cells. Further, we classified the spikes of a tuned cell to be inside and outside its c-RW place field, defined as the region within its FWHM. Again, theta phase modulation was comparable for the spikes inside and outside the c-RW field suggesting that the theta phase modulation was independent of c-RW space tuning. No significant difference was found between autocorrelation theta periods, both for inside vs. outside the c-RW place field, as well as for cells tuned and untuned for the c-RW space. Theta phase precession was also seen for firing in the c-RW place fields, but this effect was only significant in 31% of the c-RW tuned cells. Hence, theta phase modulation is independent of the c-RW tuning, and phase precession in c-RW is only seen in a subset of tuned neurons. Burst spiking was more common inside the place field than outside, even after accounting for the differential firing rates inside and outside the c-RW place field, but theta-range frequency of firing was unaffected (Extended Data Fig. 3.7).

Hippocampal neurons have previously been shown to encode spatial information in multiple frames of reference[70]. Abrupt changes of the environment drive bi-stable flickering between past and present representations[71]. Although spatial selectivity was impaired, directional selectivity has been reported in the VR setup used in these recordings[21]. We wondered if spiking corresponding to the VR-angle, determined by distal visual cues is sequestered with respect to the c-RW spiking. Fraction of neurons tuned for both angles was comparable to that expected by chance due to independent processes. We also did not find evidence of c-RW tuned and VR-angle tuned units occupying separate theta neither cycles nor different phases of the theta cycle (Extended Data Fig. 3.8). The VR-angle selectivity was causally governed by distal visual cues, but c-RW tuning was found in VR environments with blank as well as rich distal visual cues.

Further, c-RW tuning found during passive presentation of a moving bar of light was inversely related to hippocampus representation to the angle of the bar of light[72]. (Extended Data Fig. 3.9)

Although distal visual cues in the VR suffice to guide navigation, they are insufficient to create spatial selectivity. In spite of cognitive and navigational demands of the visual VR, spatial selectivity is found for the c-RW space, where multisensory cues are consistently paired together (for example, self-motion and olfactory). c-RW tuning is non-directional and present during epochs of immobility when the distal visual cues, controlled by running do not change. These results can be explained by the hypothesis that multisensory association drives hippocampal firing more strongly than cognitive mapping. This hypothesis also bridges the gap between our experiments and others[13] where the animals were afforded 360^{o} rotation. The pairing of self-motion cues with visual cue changes in VR in those experiments lead to spatial selectivity for the VR space.

Methods

Electrophysiology:

Data previously reported[14,21] from VR experiments was reused in these analyses. The virtual environment was a 200-cm diameter circular platform at the center of a 300 cm × 300 cm room with rich set of distal visual cues. There were either two or three fixed reward locations. Electrophysiological data from the dorsal CA1 were obtained using hyperdrives with 22 independently adjustable tetrodes. Spike extraction and sorting were done offline using custom software.

Head position and leg movement tracking:

Rats were body restricted with a fabric harnesses as they ran on an air-levitated spherical treadmill of 30cm radius. The rat was placed at the center of a cylindrical screen of radius 50cm and 74 cm high. Body restriction allowed the rat to scan his surroundings with neck movements. Running speed was measured by optical mice recording rotations of the spherical treadmill at 60Hz with an accuracy of 0.1mm. Head movement with respect to the harnessed and fixed body was recorded at 55Hz using an overhead camera tracking two red LEDs attached to the cranial implant using the methods described above. (Chapter 2, Methods)

Rate map, *z*-score and FWHM calculation:

c-RW rate maps were obtained by binning the head position and spikes in a square grid of 300 x 300 mm, where the actual range of the head positions was limited to a smaller region of this grid. Firing rate responses were computed by excluding bins with less than 0.3 seconds of occupancy as well as excluding data within 3 seconds after reward dispensing. Resultant rate responses were smoothed by applying a 6 mm^2 Gaussian smoothing window on the occupancy and spike responses. To quantify the degree of modulation, we computed sparsity s of rate map. First, we restricted the analysis to only those bins where sufficient occupancy of head position was observed, and these bins were linearized, leading to r_n as the firing rate in the n^{th} bin and sparsity as:

$$s = 1 - \frac{1}{N}\frac{(\sum_n r_n)^2}{(\sum_n {r_n}^2)}$$

To assess the statistical significance of sparsity, we used a bootstrapping procedure, which does not assume a normal distribution. Briefly, for each cell, spike trains were circularly shifted by different random amounts of time and the sparsity of the randomized data computed. This procedure was repeated 100 times with different sets of random value shifts. The mean value and standard deviation of the sparsity of randomized data was used to compute the z-scored sparsity of actual data using the function *zscore* in MATLAB. The observed sparsity was considered statistically significant if the z-scored sparsity of the observed spike train was greater 2, which corresponds to $p < 0.0228$ in a one tailed t-test. Full width at half maxima (FWHM) was computed as the bins in which the response was above 50% of the range of C-RW firing rate response.

Head and leg movement analysis:

Head and leg movement speeds were obtained by taking the temporal derivative of the head position measured through LED-tracking (see above) and leg movements from the optic sensors. Entire session was divided into different behavioral bouts, which were demarcated by instances of reward dispensing. Cross correlation between leg speed and head-movement speed was computed using the *xcorr* function in MATLAB. Analysis was restricted to bouts which were at least 30 seconds long. The corresponding null distribution was obtained by circular shifting of the head speed, with respect to leg speed. Correlation between the two speeds was computed by using the *corrcoef* function.

Excitation and Inhibition firing dependence on speed:

Single units of excitation and inhibition were labeled based on their mean firing rates (MFR) and complex spiking index (CSI) which is the fraction of burst spiking instances with second spike having smaller amplitude than the first one. Excitatory units were identified as having a CSI above 15 and MFR between 0.2 and 8Hz. Inhibitory units were identified as those having CSI below 10 and MFR above 10Hz. These populations of cells were treated separately in Fig. 3.3.

Theta band power, frequency, and phase calculations:

Signals from each tetrode were acquired by one of three 36-channel head stages, digitized at 40 kHz, band pass-filtered between 0.1Hz and 9 kHz, and recorded continuously. To obtain theta-band properties from this local field potential (LFP), this signal was first band passed between 6-12Hz. Theta power was computed by applying the Hilbert transform on the band passed signal and taking its magnitude. Theta phase was computed as the corresponding phase of the band passed signal. Instantaneous frequency was calculated from the zero crossings of theta phase. Phase modulation of spiking was computed by assigning theta phase from the same tetrode and then binning the corresponding phases into 30 bins.

Extended Data Figures

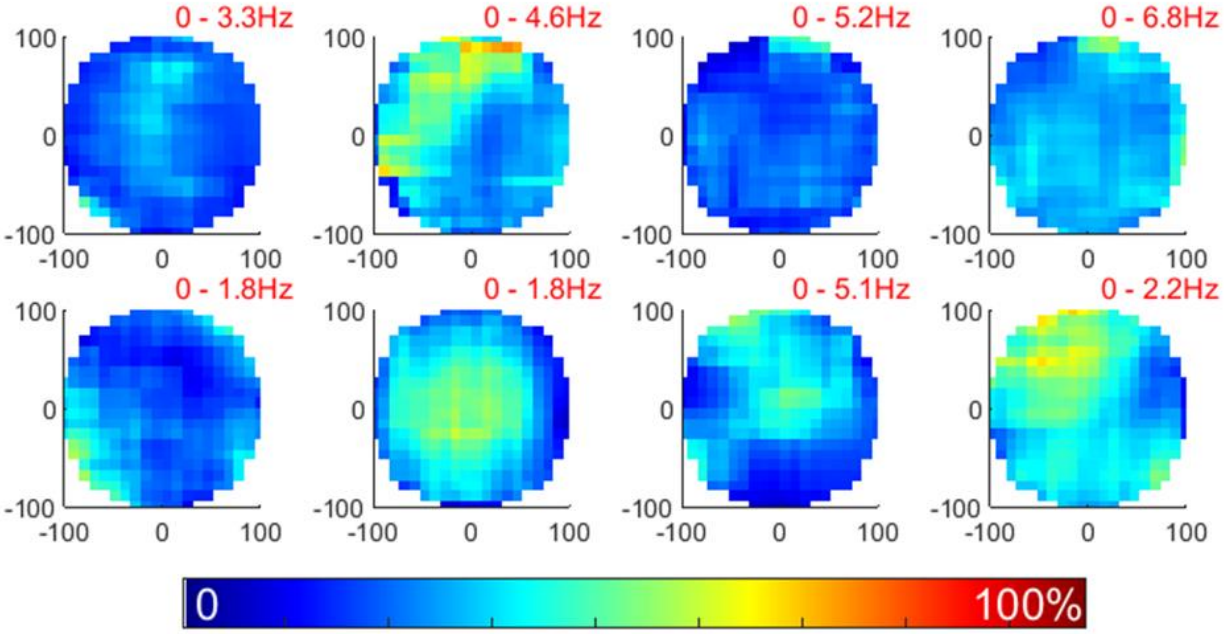

Extended Data Fig. 3.1 | Response of the eight cells in Fig. 3.1, shown here for the VR space, depicted with the same color scale.

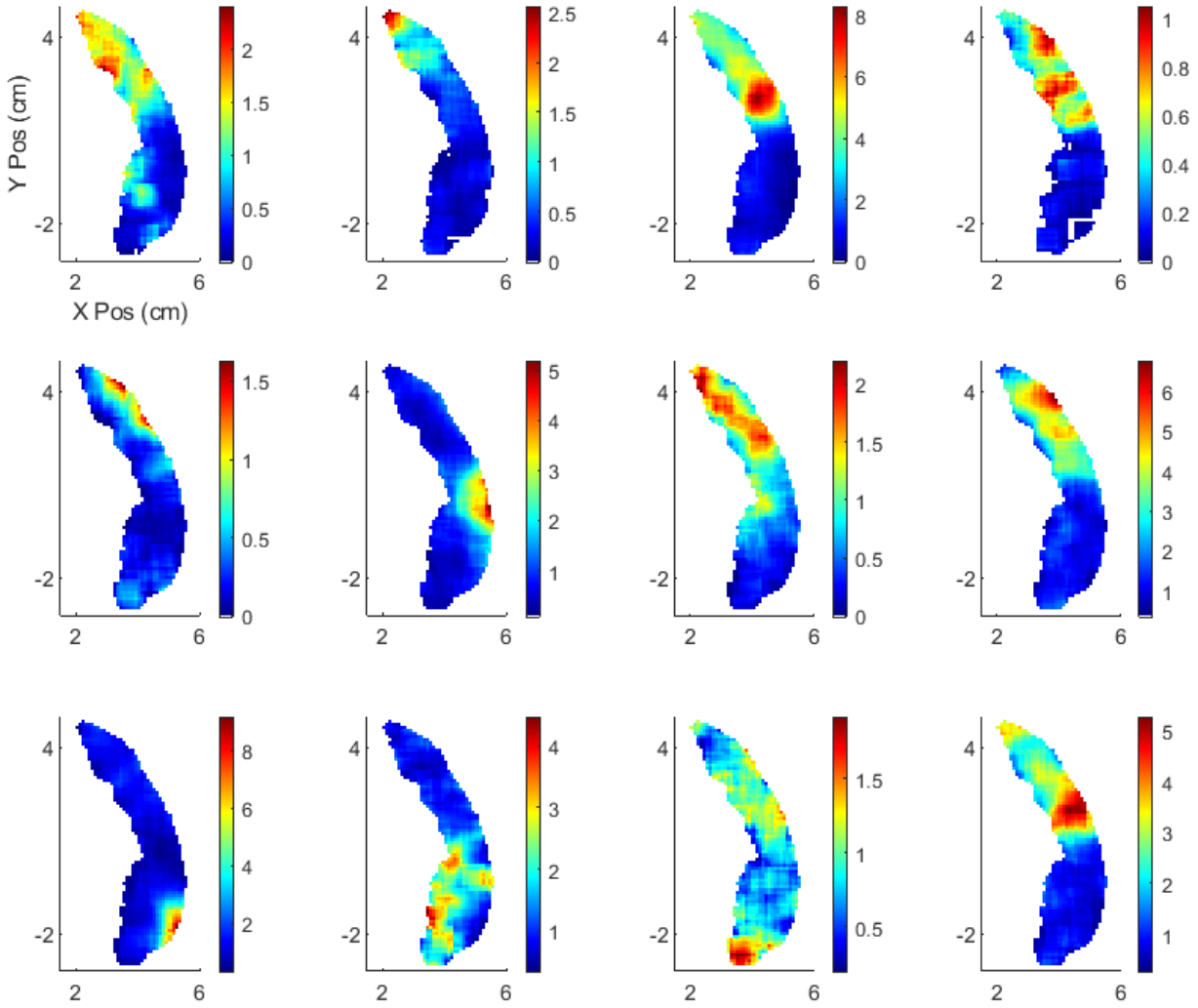

Extended Data Fig. 3.2 | 12 simultaneously recorded cells showing different c-RW tuning curves.

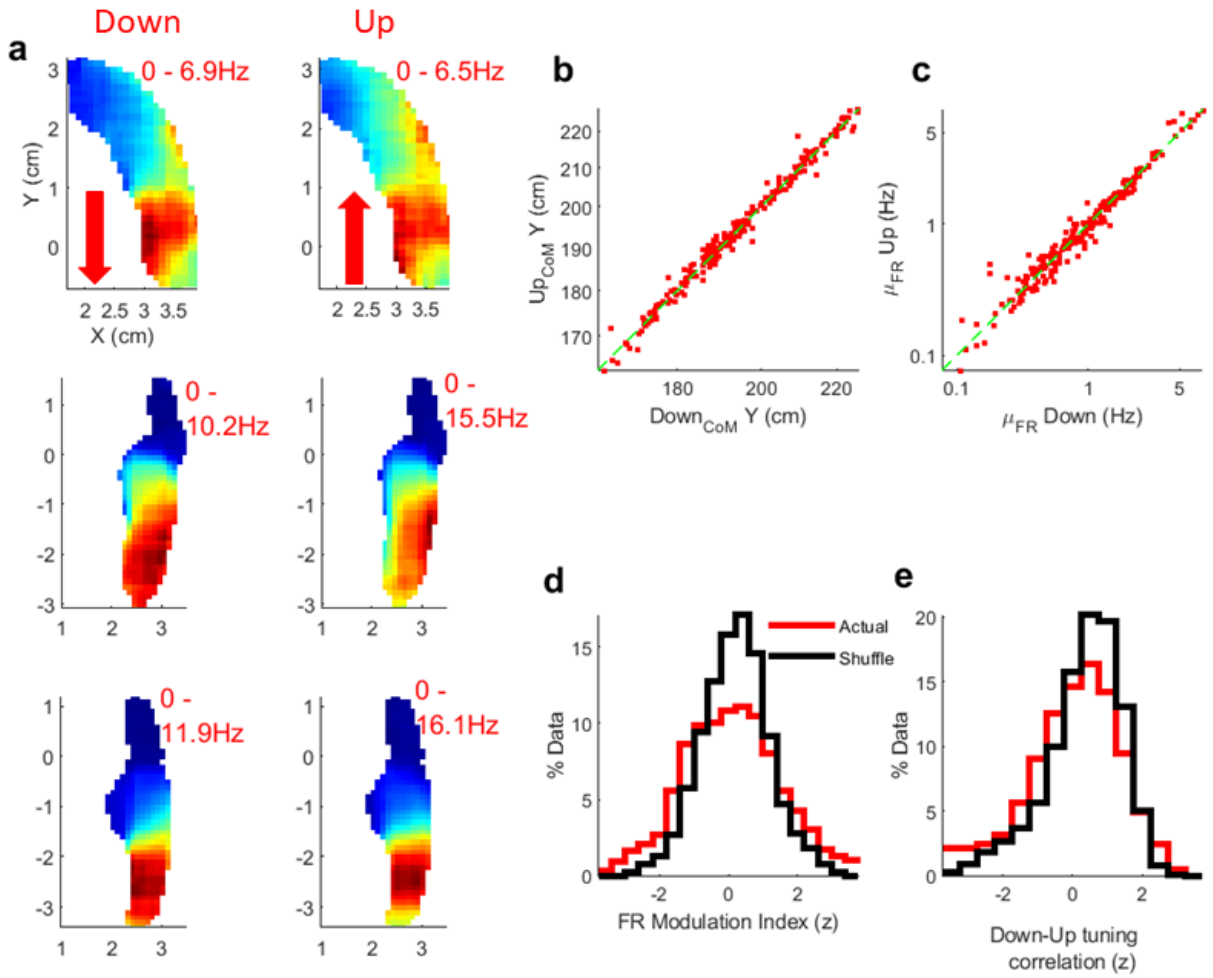

Extended Data Fig. 3.3 | c-RW place fields are not directional. (a) 3 example cells showing similar c-RW tuning during downwards head movement (decreasing Y position values, left) and upwards (increasing Y position values, right). **(b)** Center of mass (CoM) of place fields using the data in upward or downward only head movement was highly correlated. **(c)** Similarly, the mean firing rate in the two movement directions was unbiased and highly correlated (r=0.98 $p<10^{-100}$). **(d)** We further quantified this by computing a Firing rate modulation index as $(FR_{Down} – FR_{Up})/ (FR_{Down} + FR_{Up})$. This index was bootstrapped by randomly shuffling the head movement direction IDs. The indices for actual data were not significantly different from shuffle. **(d)** Similar to the firing rate modulation index we also bootstrapped the correlation between the tuning curves in two directions. These were also not significantly different from chance levels.

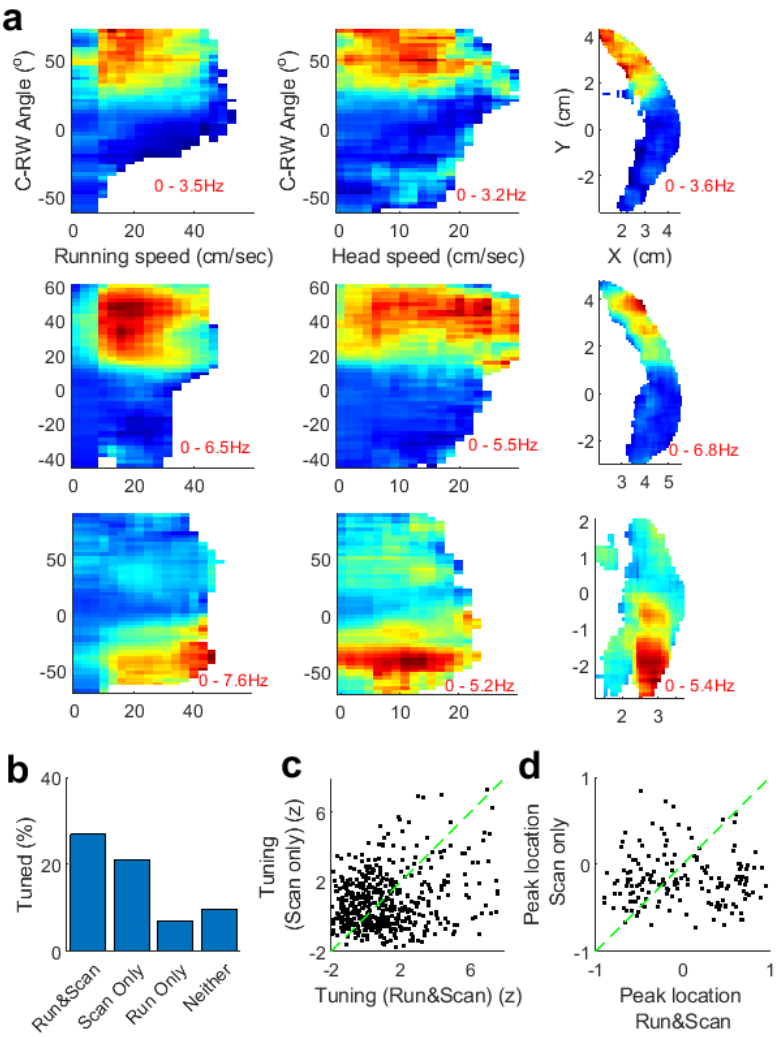

Extended Data Fig. 3.4 | Effect of movements on c-RW tuning. (a) Three example cells showing c-RW tuning. These cells showed higher firing rates at higher running speeds (first column), but head speed did not have a similar effect (middle column). c-RW position was converted to an angle estimate, by fitting a circle to obtain c-RW Angles. **(b)** Sessions were bifurcated into 4 epochs, based on the leg speed (Run= leg speed>5cm/sec) and head movement speed (Scan=head speed>2cm/sec). Maximum c-RW tuning is seen for epochs with running and head movements (27%), followed by those epochs with only head scanning (21%). Epochs without head movements had low c-RW selectivity (7 and 10%). Only epochs which had 300 seconds of data or more were used herein. **(c)** Strength of c-RW tuning was positively correlated (r=0.131 *p*=0.003) during head scanning epochs with and without running. **(d)** Peak location of tuning was not significantly correlated between these two epochs.

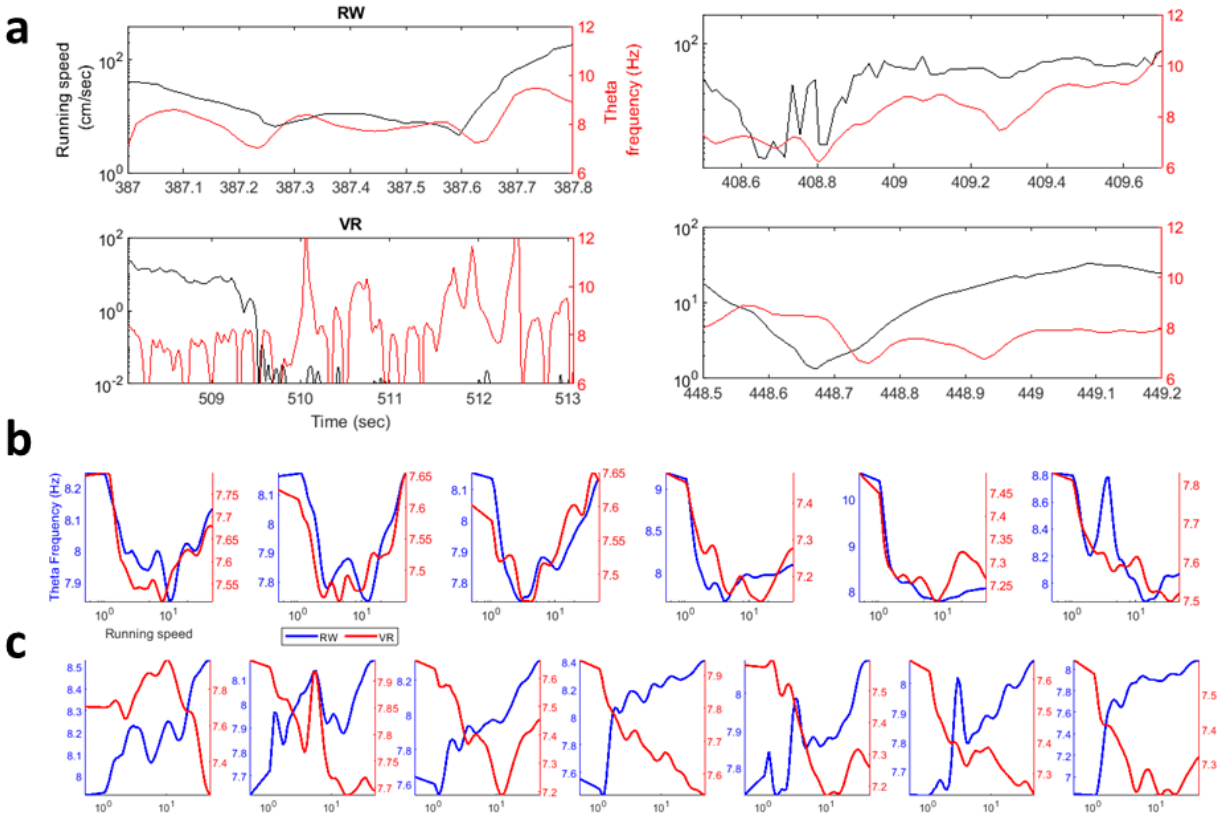

Extended Data Fig. 3.5 | Same tetrode comparison in RW and VR. (a) 2 examples of tetrodes recorded on the same day in RW and VR, showing different relationship between theta frequency (red traces) and running speed (shown on $\log_{10}$ scale). **(b)** 6 tetrodes showing similar response of theta frequency to running speed in VR and RW environments. **(c)** 7 tetrodes showing opposite effects of running speed on theta frequency with decreasing theta frequency in VR (red) but increasing theta frequency in RW (blue).

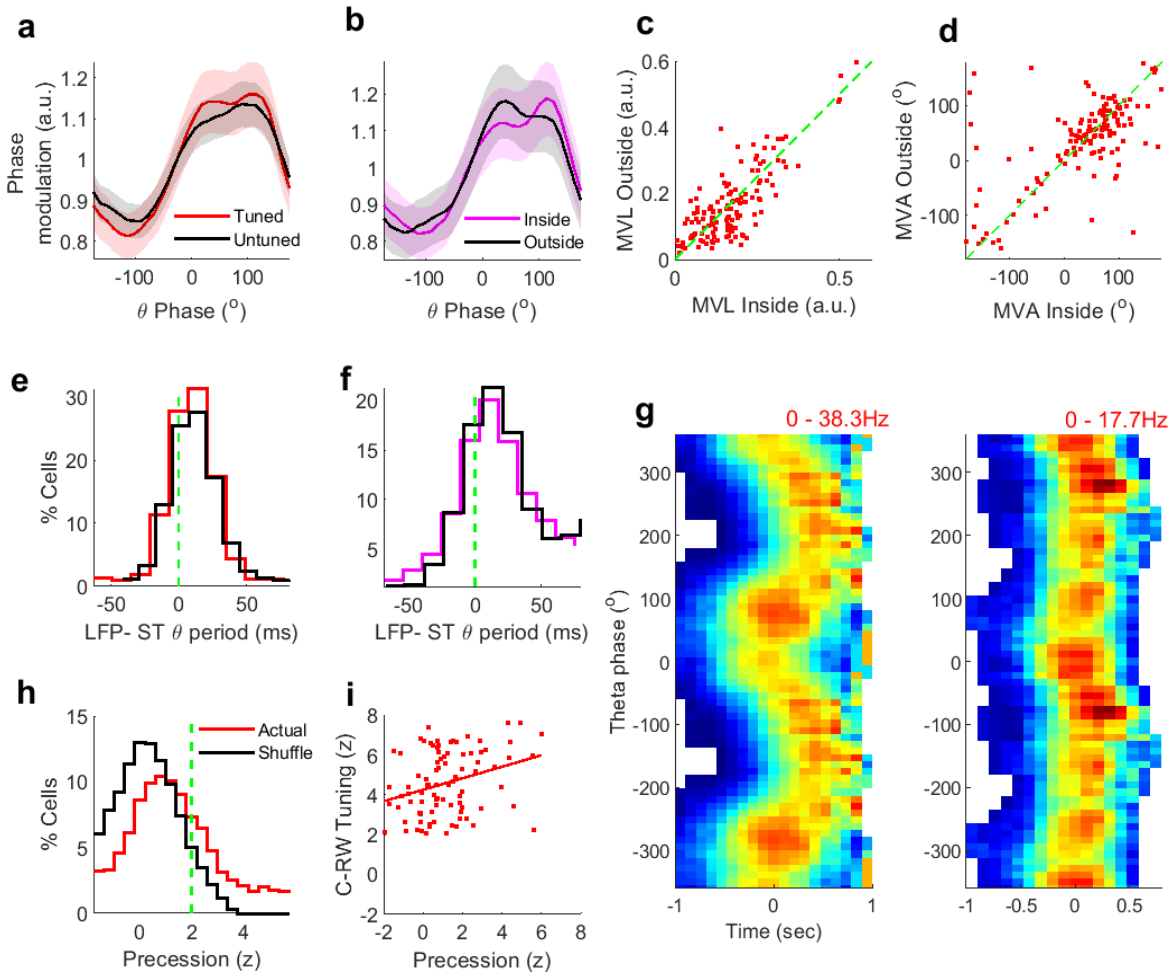

Extended Data Fig. 3.6 | Precession in c-RW space. (a) Average theta phase modulation for tuned as well as untuned cells had comparable profiles during running and non-reward epochs (mean ± std = 68.4° ± 77.2° tuned, 72.4° ± 78.0° untuned). **(b)** Theta phase modulation was similar for spikes inside and outside the c-RW place field (mean ± std = 73.8° ± 77.4° inside, 62.6° ± 77.2° outside), using only the tuned cells with at least 100 spikes inside as well as outside the c-RW tuning zone. **(c)** Phase modulation was further quantified by the mean vector length (MVL) and angle (MVA). MVL values were highly correlated (r=0.68 $p<10^{-100}$) but not significantly different for spiking inside vs outside the c-RW place field (T-test p=0.81). **(d)** MVA were biased to values between 50 ° to 100° but correlated for spiking inside and outside c-RW place fields (Circular correlation test r=0.5 $p=1.7\text{x}10^{-7}$). **(e)** Majority of tuned as well as untuned units had larger local field potential (LFP) period than spiking period obtained from the peak in autocorrelation in the 50-200ms range[14]. LFP-ST θ period differences were not significantly different between tuned and untuned cells (KS-test p=0.25 μ_{tuned}= +4.1ms and $\mu_{untuned}$= +6.5ms). **(f)** Autocorrelation peak differences were also not

significantly different for spiking inside vs. outside the c-RW place fields (KS-test p=0.28 μ_{inside}= +9.7ms and $\mu_{outside}$= +15.1ms). **(g)** Two c-RW tuned example cells showing negative correlation between the epochs of time spent inside the c-RW place field and theta phases. An epoch of entry and exit of the animal's head in and out of the c-RW place field was considered valid if it lasted at least 500ms, had more than 1 spike and running speed>5cm/sec throughout. Time spent inside each epoch was mean adjusted, by the average spike time of spikes in the current epoch. **(h)** Circulo-linear correlation between 'time inside c-RW field' and theta phase was bootstrapped by obtained different circularly shifted theta phases in each epoch. This correlation, called 'precession' was significant for 31% of neurons at a z-score level of 2. **(i)** Strength of c-RW tuning was positively correlated with precession, after factoring out the mean firing rates (partial correlation r=0.25 p=0.02)

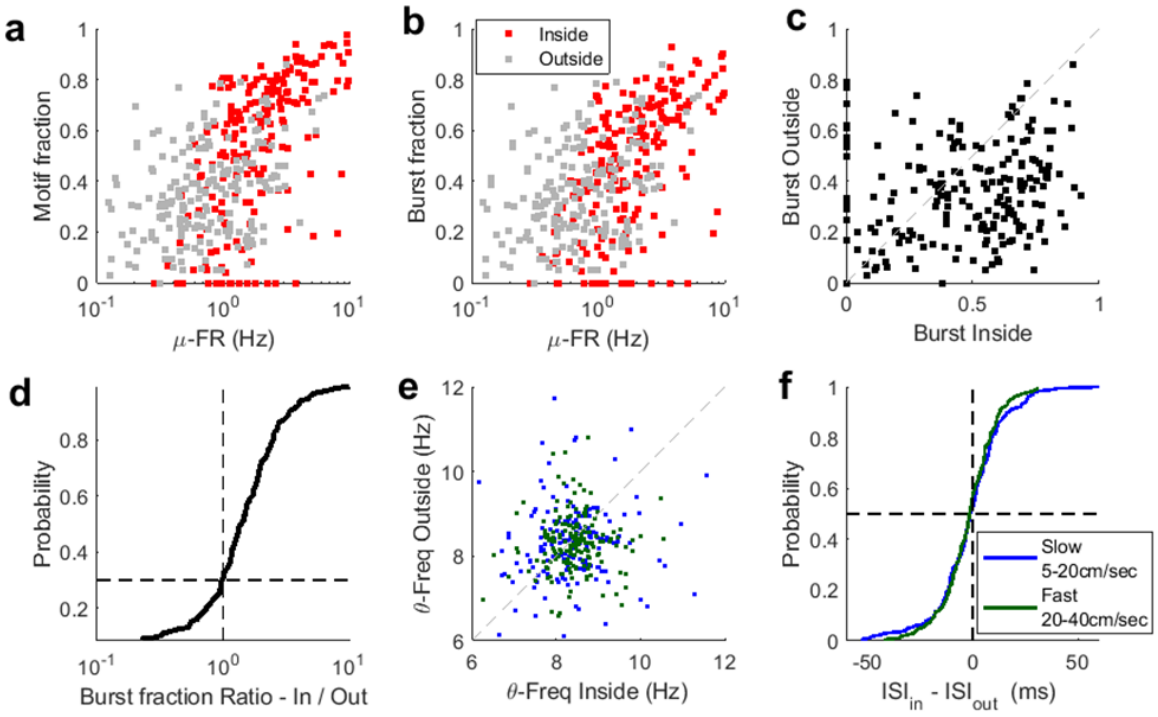

Extended Data Fig. 3.7 | Burst-firing properties of c-RW cells. (a) Similar to free foraging experiments, spiking in the body constrained VR was also observed to have transient bursts of spiking, earlier called 'Motifs'[14]. Fraction of spikes inside the Motif was higher for cells with higher firing rates, but this could occur because the Motif threshold was fixed at 5Hz. **(b)** We recomputed the fraction of spikes inside a burst, using an adaptive threshold, which accounted for the number of spikes inside or outside the c-RW zone, to find similar trend as (a). **(c)** Fraction of spikes emitted inside of bursts was significantly higher inside than outside the c-RW place field for majority of cells, such that **(d)** the ratio was above unity for 70% of cells. **(e)** The theta frequency of spiking, computed by finding the median of the ISIs in the theta range (6-12Hz and hence 83-166ms range in ISI time). This was not significantly biased for spikes inside or outside the c-RW fields or by **(f)** slow or fast running epochs.

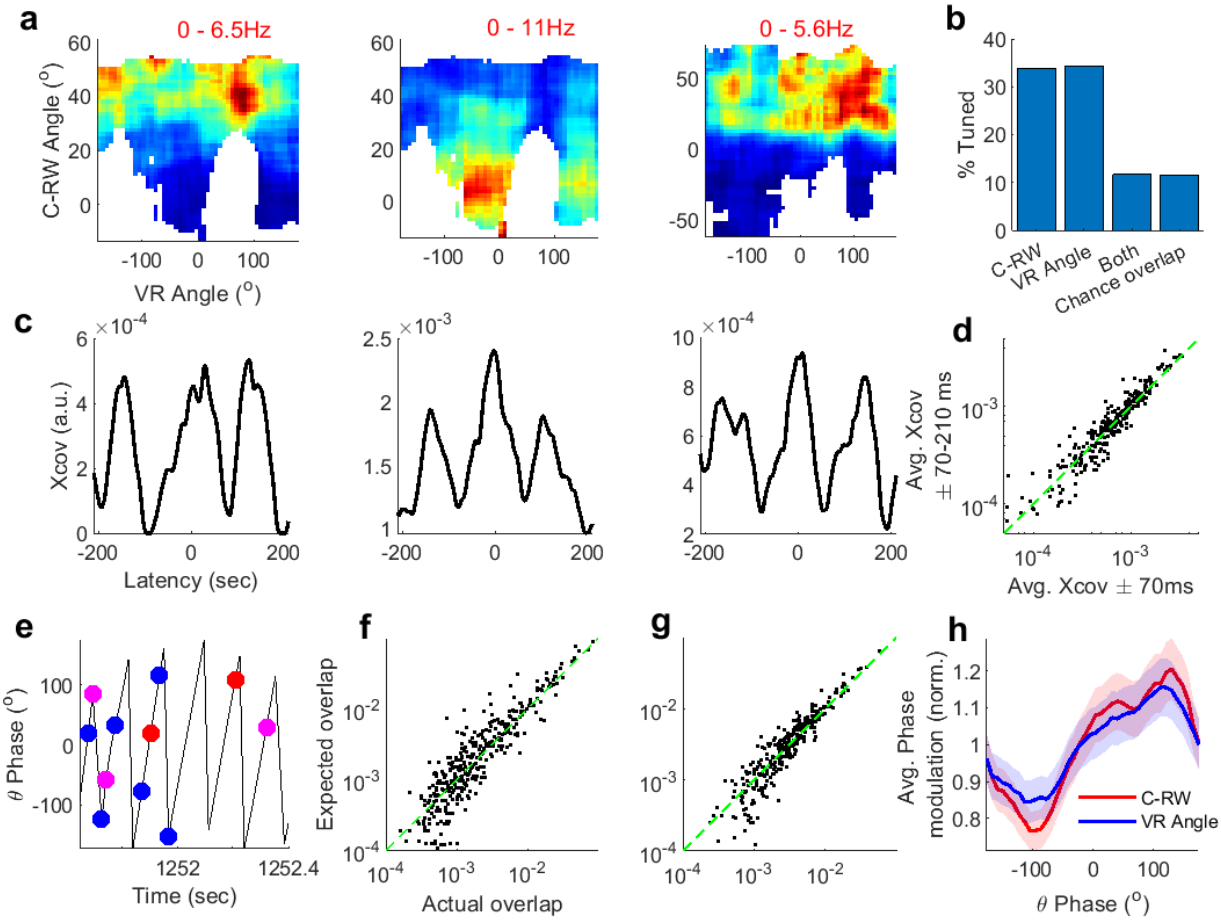

Extended Data Figure 3.8 | Conjunctive representations of c-RW angle and VR-angle. (a) 3 example cells showing elevated firing at specific c-RW angles but all VR-angles resulting in horizontal tuning curves. **(b)** 33.2 and 34.3% of all cells were tuned for c-RW angle and VR angle, resulting in an expected overlap of 11.4%. This was comparable to the actual fraction of cells having VR angle as well as c-RW tuning (12.8%). **(c)** Three examples of cross correlation between spikes of c-RW and VR-angle tuned cell pairs, showing comparable central correlation of spiking for small latencies(±70ms) and first harmonic of theta period range latencies (+70 to +210ms and -210 to -70ms). **(d)** Spike train correlation within the same theta cycle (±70ms) were correlated (r=0.95 $p<10^{-100}$) and not significantly different from those in a preceding (-210 to -70ms) or succeeding theta cycle (+70 to +210ms) (KS-test p=0.68). **(e)** Example of spiking from one VR-angle tuned cell (blue) and two c-RW tuned cells (red and magenta) showing no evidence of theta cycle sequestering. **(f)** Co-spiking in theta cycles was further quantified by computing the fraction of theta cycles shared by tuned

cell pairs of the same category (c-RW pair or VR-angle) and comparing the overlap with that expected by chance. These were not significantly different (T-test p=0.14). **(g)** Similar to (f), for cell pairs of C-RW and VR-Angle tuned cells (T-test p=0.21). **(h)** C-RW tuned cells and VR-Angle tuned cells had comparable and highly overlapping theta phase modulation profiles.

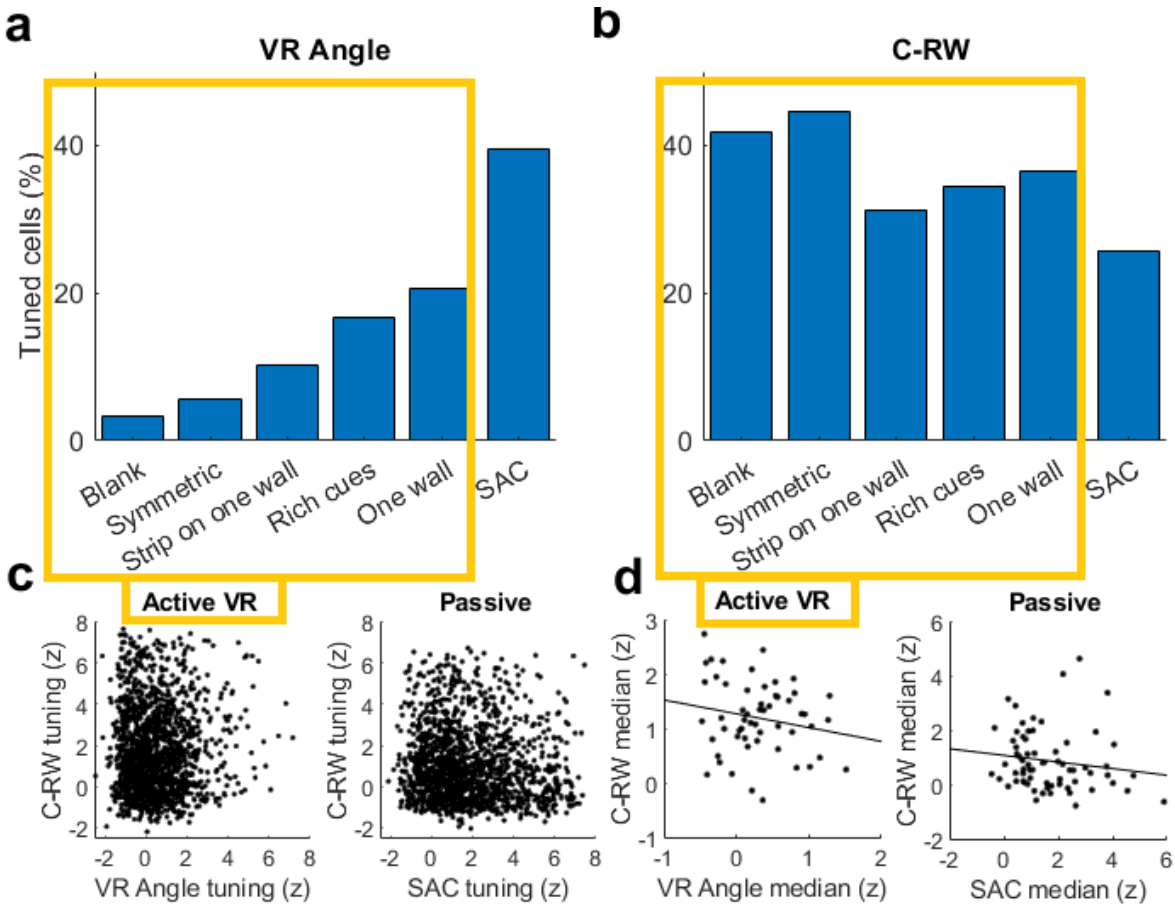

Extended Data Figure 3.9 | c-RW tuning persists in VR environments with and without distal visual cues. (a) Using GLM framework to estimate independent contributions of VR-angle, VR-Space, running speed and C-RW position (converted to one dimensional c-RW angle estimate using best-fit circle) to single unit firing, we replicated prior results that VR angle tuning is at chance levels when distal visual cues are either absent or 'symmetric' i.e., similar on all 4 virtual walls. Maximal tuning to VR-angle was obtained in a 'passive VR/SAC' experiment where a bar of light rotated around the animal, independent of their movements[72] (See Chapter 2 above). VR-angle in this experiment corresponded to the angular position of the bar of light. **(b)** Significant c-RW tuning was observed in all types of VR environments. **(c)** VR angle and c-RW tuning of single units was not correlated in the active VR experiments (r=0.004 *p*=0.87), but significantly anti-correlated for the passive VR experiments (r=-0.06 *p*=0.01). **(d)** The relation between VR-angle tuning and c-RW tuning was re-computed on a per-session basis, by computing the median sparsity (z-scored) in sessions with at least 10

units. This correlation was negative but not significant for active VR experiments (r=-0.11 p=0.4) but significantly anti-correlated for the passive VR sessions (r=-0.254 p=0.04).

CHAPTER 4: STREAMING VISUAL STIMULI ELICIT SELECTIVE RESPONSES IN RODENT HIPPOCAMPUS

Introduction

Primate hippocampus is believed to be involved in object place association[3], whereas in humans, the hippocampus is believed to be the centrally involved in formation of short-term memories[1]. In rodents, on the other hand, hippocampus is primarily studied in the context of spatial memories, and the seat of a cognitive map of space[23]. This cognitive map is believed to be abstract and allocentric, creating a distinction between the hippocampus and cortical regions, which respond to sensory stimuli in the retinotopic frame. Recent work has shown selectivity in hippocampal regions to non-spatial variables, but this selectivity goes away upon removal of task[18] or memory[41] demands.

We recently reported that neurons from hippocampal subregion CA1 can encode the distance, angle and movement direction of a simple visual stimulus – a vertical bar of light, without active movement, rewards or memory requirements[72]. This reinstates hippocampus at the apex of the visual processing hierarchy[46] and suggests that it shows selective responses to simple sensory stimuli, akin to the cortical areas. But hippocampus does not show selective responses to other simple visual stimuli like Gabor patches and drifting gratings[73], which are traditionally used to study visual cortical responses. However, these artificial stimuli lack the spatial or temporal characteristics of natural visual stimuli and might not be predictive of neural responses to complex visual scenes. Hence it is necessary to ascertain the response and selectivity of hippocampal neurons to complex visual scenes, having naturalistic spatio-temporal associations, to understand the hierarchical processing of visual information from lateral geniculate nucleus to the hippocampus.

Rodent hippocampus shows selective responses to streaming visual stimuli.

To answer these questions, we investigated single neuron responses in hippocampal as well as visual cortical areas to the presentation of a 30 second clip from the movie *Touch of Evil* (Welles, 1958) from a publicly available dataset[73]. Awake, head fixed mice were shown 60 repetitions of the movie split in 2 blocks of 30 trials each. Movie presentation was part of an experimental protocol where a battery of other, simple visual stimuli were also presented. The

animals were head-fixed but free to run on a circular disk throughout the visual stimulus presentations. Movie was contrast and luminance normalized (see Extended Data Fig. 4.1 for snippets and details). 4-6 *Neuropixels* probes simultaneously recorded single unit spiking from contralateral hemisphere to the visual stimulus. Similar results were seen in wild-type as well as mutant genetic lines, and data from all mice was combined (17 rats, 4 female, 11 wild type, 6 from transgenic *Cre* lines (3- Sst IRES-Cre, 2- Vip-IRES-Cre, and 1- Pvalb-IRES-Cre lines)). A total of 12010 broad spiking neurons were analyzed, which were identified by an automated clustering algorithm (see *Methods*), in 17 sessions, each from a separate subject. Running affects the neural firing in visual[74] as well as hippocampal[75,76] areas. To avoid confounding effects of running on neural spiking, we only used data from the stationary epochs (see *Methods*) and only from sessions with at least 50% of data obtained in stationary behavior.

Mean tuning responses were obtained by averaging firing responses to different movie frames across all stationary epochs and significance of the response was obtained by bootstrapping procedures (see *Methods*). As expected and reported earlier[33,77–79], large fraction of visual cortical neurons showed selective responses to different movie frames (Extended Data Fig. 4.2). Highest prevalence of selectivity at p=0.0228 level was seen in antero-median and posterior-medial higher visual areas (95.6%), which is quite higher than that reported earlier[33] (~40%). This higher selectivity could be because of our strict criteria of excluding running epochs as well as using extra-cellular spiking instead of the calcium transients, as done previously. More surprisingly, we found single unit responses in hippocampal regions showing succinct, bar code like firing rate responses (Fig. 4.1a), similar to that in visual areas reported in anesthetized cats[77,78,80]. We call this streaming movie selectivity (SMS) or tuning. Largest prevalence of tuning was seen in subiculum (23.1%) followed closely by dentate gyrus (21.6%). Selectivity was lower but still greater than that expected by chance in CA3 (10.1%) (Fig. 4.1b). During free foraging, hippocampal firing responses typically have a single peak called its place field[81]. Similarly, bar of light selective neurons in CA1 were also unimodal[72]. To further characterize SMS, we computed the full width at half maxima (FWHM, see *Methods*) for the hippocampal as well as cortical tuned neurons. Since we observed many SMS neurons to have multiple peaks as well as troughs, we did not require FWHM to be contiguous. In all regions, peak-FWHM (elevated mean firing frames) was narrower than troughs (dips in mean firing) and hence the

better FWHM was predominantly of the peak type (Extended Data Fig. 4.3). For all regions, median FWHM was < 60 frames, or <7% total length of each clip (30 seconds, 900 frames). Hence SMS tuning was sharper than place cells whose fields typically cover a third of the experimental arena on one-dimensional tracks[32].

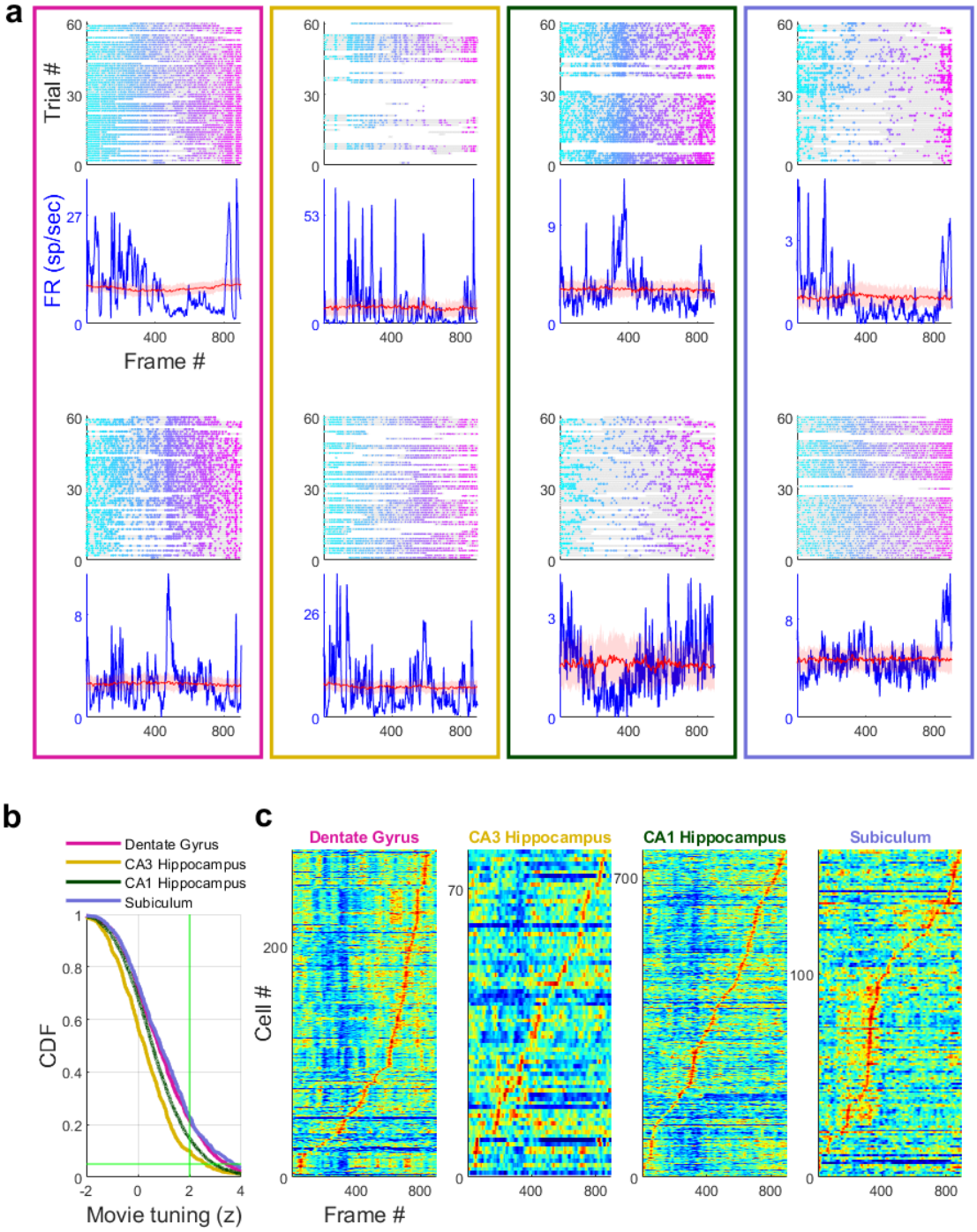

Fig. 4.1 | Hippocampal neurons show selective responses to movie frames. (a) Example raster plots (top) and mean rate responses (blue, bottom) as a function of the frame number of movie presented. Gray background in raster signifies the stationary epochs used in analysis to compute mean rate responses. White gaps represent epochs when the animal was moving, and hence that occupancy as well as spiking was excluded from analysis. Red line and shaded area signify mean and standard deviation of firing rate response expected by chance obtained by bootstrapping procedures (see *Methods*). 2 example cells each from 4 hippocampal regions shown, with increased spiking responses to different frames in the movie. **(b)** Largest prevalence of selectivity in broad spiking neurons was seen in subiculum (23.1%, 161 out of 696) followed closely by dentate gyrus (21.6%, 283 out of 1310) then CA1 (14.9%, 764 out of 5142) and least by CA3 (10.1%, 79 out of 783). Green vertical line indicates threshold of z>2 (see *Methods*) and the green horizontal line indicates chance level of 5%. **(c)** Stack plots of all tuned cells, arranged in the increasing order the frame corresponding to highest firing rates. Response of each cell was normalized to ±1 and smoothed with a moving Gaussian window of 300ms.

How do the visual features of the movie affect SMS? For each neuron, we identified frames with a 'significant response', where the actual SMS response was outside the mean±2std range obtained from the bootstrap data. Peaks and troughs of response were quantified from this significant response (see *Methods*). Unlike visual cortical areas, the distribution of maximal firing was more biased in hippocampal regions. DG and CA1 had greater prevalence of minima in firing between frames 100 to 400, when the view was panning rightwards following the person running in the same direction in the movie (Extended Data Fig. 4.4). This effect was also observed in the stack plots of tuned cells (Fig. 4.1c), where a large fraction of dentate and CA1 neurons showed reduced firing in that range of frames. Subiculum neurons showed the opposite effect with larger concentration of peaks in this range of frames.

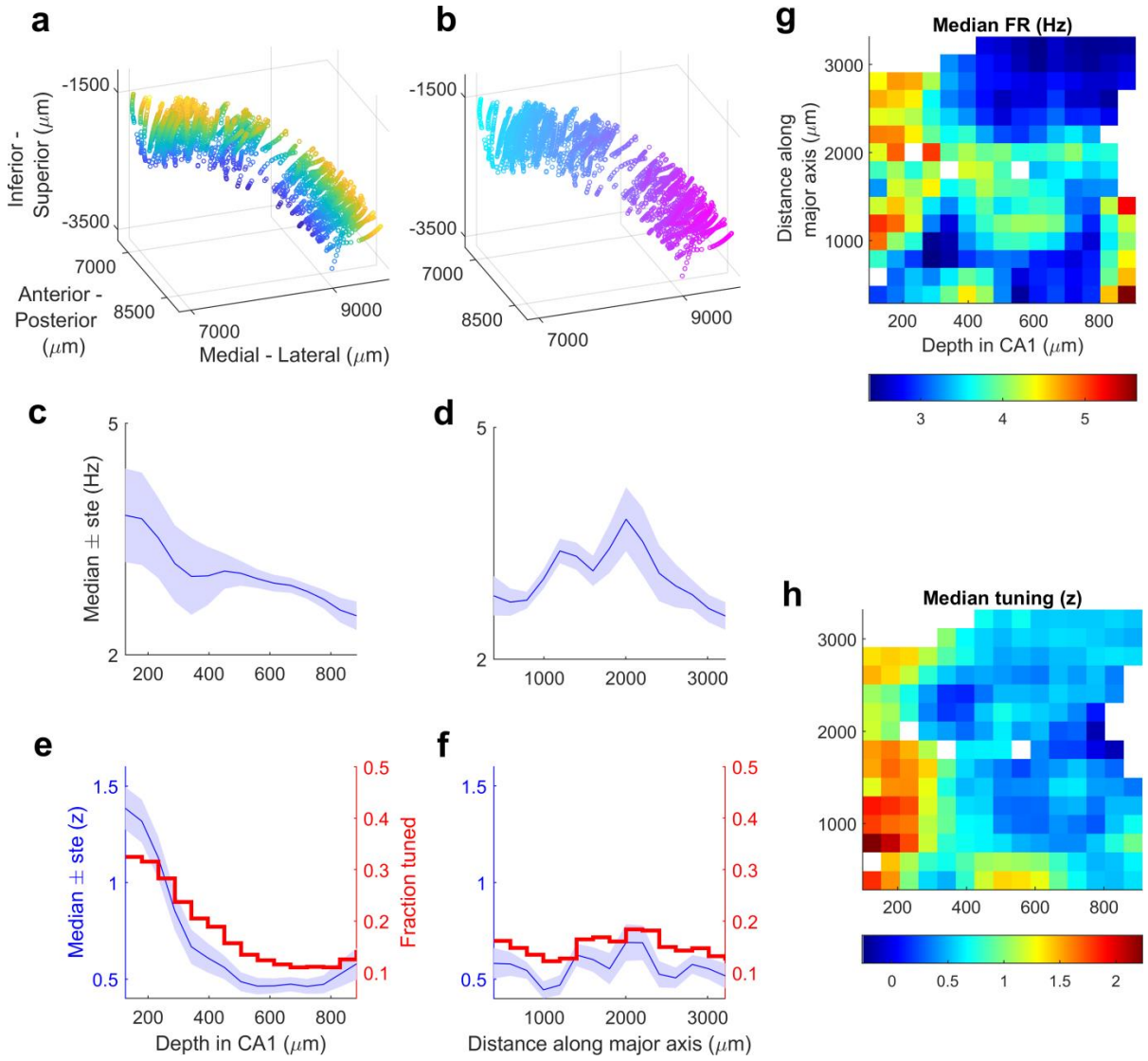

Fig. 4.2 | Deeper layers of CA1 have larger mean firing rates as well as streaming movie selectivity (SMS) (a) Location of all broad spiking neurons from CA1 region were assigned to a Neuropixel recording site corresponding to the channel with largest spike amplitude. These were fitted with a circular arc in the medio-lateral and inferior-superior plane, to obtain depth values; blue deepest (0), yellow superficial. **(b)** Similar to (a), fitting in 3D yielded distance along the major axis, cyan anterior-medial, pink posterior-lateral. **(c)** Mean firing rate, averaged over all frames from the stationary epochs was inversely related to the depth (Spearman correlation r=-0.1 p=1.27x10^{-13}) **(d)** Mean firing rate, was also weakly inversely related to the distance along the major axis (Spearman correlation r=-0.03 p=0.02) **(e)** SMS was inversely correlated to depth, even after factoring out the effect of firing rate by partial correlation (r=-0.14 p=1.76x10-

[23]) **(f)** SMS was uncorrelated with distance along the major axis (partial correlation with firing rate r=-0.004 p=0.77) **(g)** Joint distribution of firing rate with depth and distance along major axis. **(h)** Same as (g), for SMS.

Deeper layers of CA1 have higher mean firing rates as well as streaming movie selectivity (SMS)

In primates and other higher mammals, cortical areas show feature maps in general and cortical columns in particular, where preference of cells for stimulus parameters is topographically mapped[22,82]. In rodents, the preference of neurons is arranged randomly, albeit with some weak spatial clustering[83]. On the other hand, spatial encoding in hippocampus is non-topographic since a local cluster of neurons can cover the entire testing environment[84]. But spatial encoding is more prevalent in dorsal, compared to ventral hippocampus[85]; the latter is believed to be involved in emotion and stress processing[86]. Also, neurons in deeper sub layers of CA1 show different firing properties and oscillation entrainment than superficial layers[87]. Hence we leveraged the high density recording capabilities of *Neuropixels* probes combined with registration of recording sites to a common coordinate framework[88], to investigate the neural firing and SMS dependence on depth (Fig. 4.2a) and along the major (longitudinal) axis of CA1 (Fig. 4.2b). Mean firing rates of broad spiking, putatively pyramidal neurons were higher in deeper sub-layers than superficial (Fig. 4.2c), showing continual increase with depth, similar to that shown for CA1 neurons during free foraging[87]. No clear pattern was seen along the major axis (Fig. 4.2d). Interestingly, neurons in deeper layers were also better tuned for SMS, with prevalence of ~40% (Fig. 4.2e), similar to better coupling of place cells to landmark cues in deeper than superficial layers[45]. No clear pattern was seen along the major axis (Fig. 4.2f) suggesting that visual information is equally encoded by dorsal as well as ventral CA1 neurons, in contrast to spatial information. Hence mean firing rate responses (Fig. 4.2g) as well as SMS (Fig. 4.2h) distribution was non-uniform in CA1 neurons.

Sub-Poisson variability of streaming movie selectivity (SMS)

Neural responses in cortical as well as hippocampal regions are typically noisy, with the presentation of same stimulus causing varied responses, even in tuned cells, which is not necessarily driven by membrane potential variability[89,90]. It has been reported that the onset of preferred stimulus (one which causes selective responses) leads to reduction of spiking

variability across multiple cortical regions[91]. Hence, we quantified the trial-to-trial variability of SMS. For tuned cells with at least 30 trials where the animal was stationary throughout, we computed the coefficient of variation (*cov*) as the ratio of mean and standard deviation of the SMS response. *cov* calculations can be biased by different number of total spike count inside and outside the FWHM defined earlier. Hence, we divided all frames into 2 zones- inside (higher firing rates) and outside (lower) such that expected spikes in each group was approximately equal. *cov* was low in visual(Fig. 4.3a) as well as hippocampal (Fig. 4.3b) areas, and neurons were sub-Poisson (*cov*<1), unlike earlier reports[33,72,91] where *cov* was greater than or close to unity. SMS variability was comparable in visual as well as hippocampal regions (Fig. 4.3c), which, to the best of our knowledge, is the first direct comparison of variability in both brain regions in the same experiments and to the same stimulus. Stability of SMS was quantified for tuned cells as the correlation between movie tuning curves obtained from 2 non-overlapping sets of first and last 30 trials. In all brain regions, stability was greater than that expected by chance (see *Methods*), but lesser in hippocampal regions than cortical (Fig. 4.3d). Trial to trial variability was negatively related with strength of movie tuning (Fig. 4.3e) as well as the stability (Fig. 4.3f), as expected. Tuned cell pairs from dentate gyrus showed higher co-fluctuation of firing as well as SMS, compared to chance levels, and to other brain regions (Extended Data Fig. 4.5).

Population vector decoding reflects visual structure of movie presented.

Drifting gratings or Gabor patch are simple stimuli which lend high control of stimulus properties to ensure sampling over the entire stimulus space. These are typically presented in a pseudo-random order. On the other hand, a continuous streaming visual movie led to high correlations between consecutive frames, as well as between some non-contiguous frames (Fig. 4.4a, e). Ensemble of a few hundred tuned neurons is sufficient to decode the rat's position during free-foraging as well as to decode the position of a visual cue during passive viewing using population vector decoding[34,72]. Using similar methods, we decoded the movie frame using tuned responses from different brain regions (see *Methods*). Population vector decoding was near-perfect using cortical responses (Fig. 4.4b, d), as reported earlier[92]. Decoding of movie frames was less accurate but better than chance using hippocampal responses (Fig. 4.4c, d).

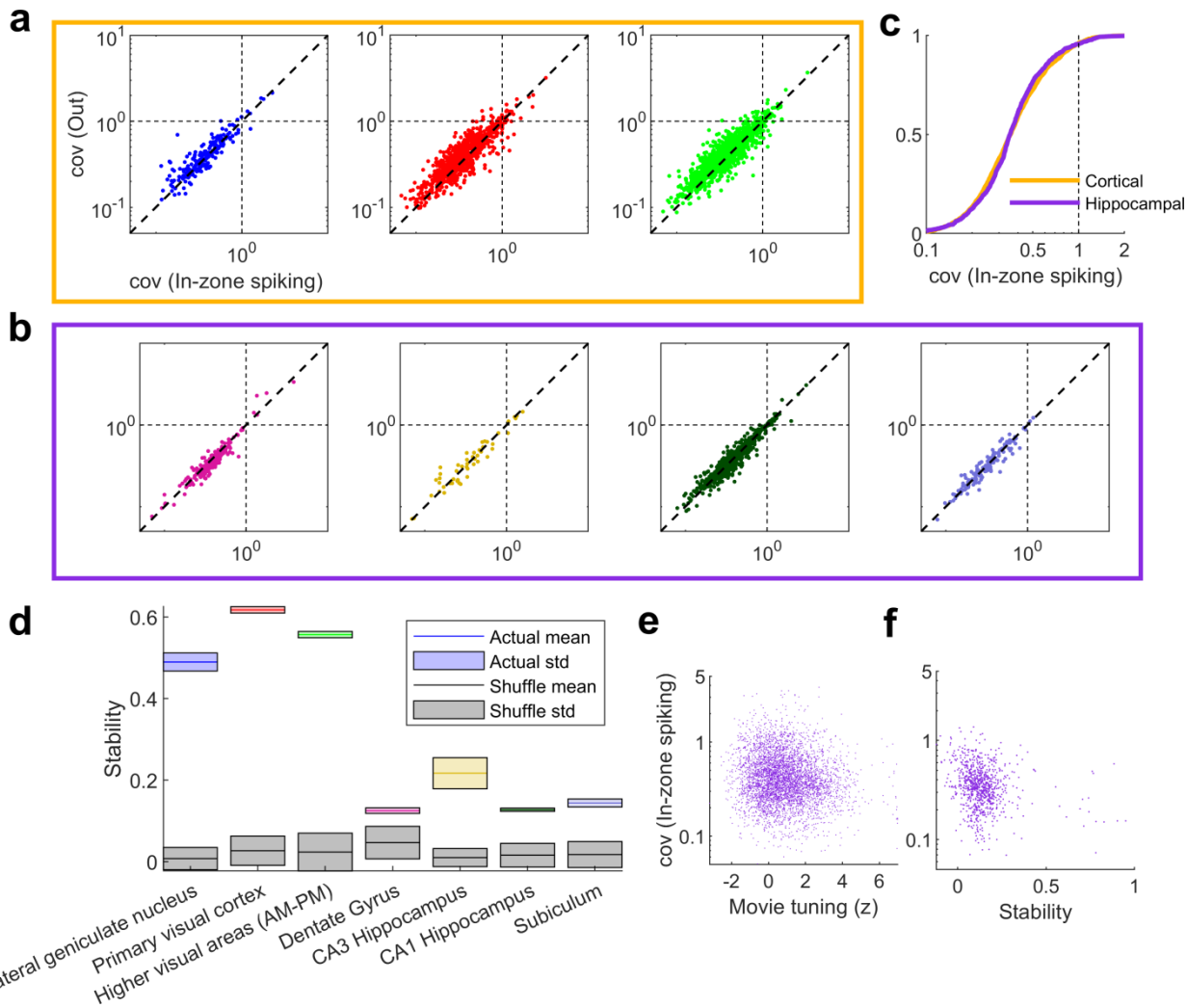

Fig. 4.3 | Sub-Poisson variability of Streaming Movie Selectivity (SMS) (a) Coefficient of variation of firing across trials in the 3 cortical regions was highly correlated (r>0.88 p<10^{-80}) for spikes inside and outside of 'tuning zone', defined based on a threshold to ensure comparable spikes in both said zones. **(b)** Similar to (a) for hippocampal variability (r>0.95 p<10^{-30}). **(c)** Across the population of broad spiking neurons, in-zone variability was not significantly different between cortical and hippocampal units (KS-Test, p=0.08). **(d)** Stability of SMS was greater than chance level for all brain regions (KS-test actual vs. shuffle p<10^{-12}), with average sparsity across all units in primary visual cortex being highest at 0.62 and lowest for dentate gyrus at 0.12. **(e)** *cov* of in-zone firing was inversely related to Movie tuning (SMS) (r=-0.1 p=5.4x10^{-12}). **(f)** For tuned cells, *cov* of in-zone firing was also inversely and significantly correlated with stability (r=-0.19 p=8.7x10^{-9}).

These differences cannot necessarily be accounted for by the difference in the number of tuned cells, since, for example, lateral geniculate nucleus and dentate gyrus had comparable number of cells (279 vs. 281), but their decoding errors were an order of magnitude different (0.34 vs. 6.3). To account for the correlated nature of frames, we computed a frame-to-frame correlation vector, as the correlation between 2 consecutive frames (one-off diagonal entries from Movie correlation matrix, 4.4a). Apart from the drop of correlation from the end of trial *n* to start of trial *n+1*, there were 3 other instances within the first 300 frames where the correlation drops considerably (Fig. 4.4e). Remarkably, decoding score in cortical regions (primary visual and higher visual areas AM-PM) reflected this structure of the stimulus presented (Fig. 4.4f). This effect was largely missing in the hippocampal regions (Fig. 4.4g) where decoding scores were lower than in cortical regions, but better than chance levels (Fig. 4.4h).

Small but systematic eye movements cannot fully explain SMS.

To avoid confounding effects of self-motion on firing, we restricted our analysis to the stationary epochs. But we wondered if the animals made systematic eye-movements in response to the movie, especially from frame #70 to 370 when the person in the movie runs across the screen. Such movements would be expected from the opto-kinetic reflex, which is seen is almost all mammals during monocular horizontal movement, and is believed to help stabilize the image on the retina[93]. The (99 percentile) range of horizontal as well as vertical eye-gaze was less than 10^o, which is an order of magnitude less than the dimensions of the movie presented on a 120^o x 95^o screen. More than half of the sessions had significant gaze bias with respect to different frames of the movie (Extended Data Fig. 4.6, see *Methods*), while around a third had biased pupil dilation, which is linked to arousal and altered cortical activity[94,95]. Eye-movement bias had little effect on SMS in the cortical areas but had significant and mixed effect on hippocampal SMS. Horizontal gaze bias reduced SMS, while vertical gaze and pupil dilation bias increased SMS (Extended Data Fig. 4.6). But movie frames had a stronger effect on firing when considered with gaze and pupil dilation, causing vertical bands of firing when considered in a 2D space of frame number (x-axis) and eye-movements(y-axis) (Extended Data Fig. 4.7). Further, firing response to gaze on screen or pupil dilation during gray-screen presentation was not predictive of SMS responses obtained during movie-presentation. (Extended Data Fig. 4.7).

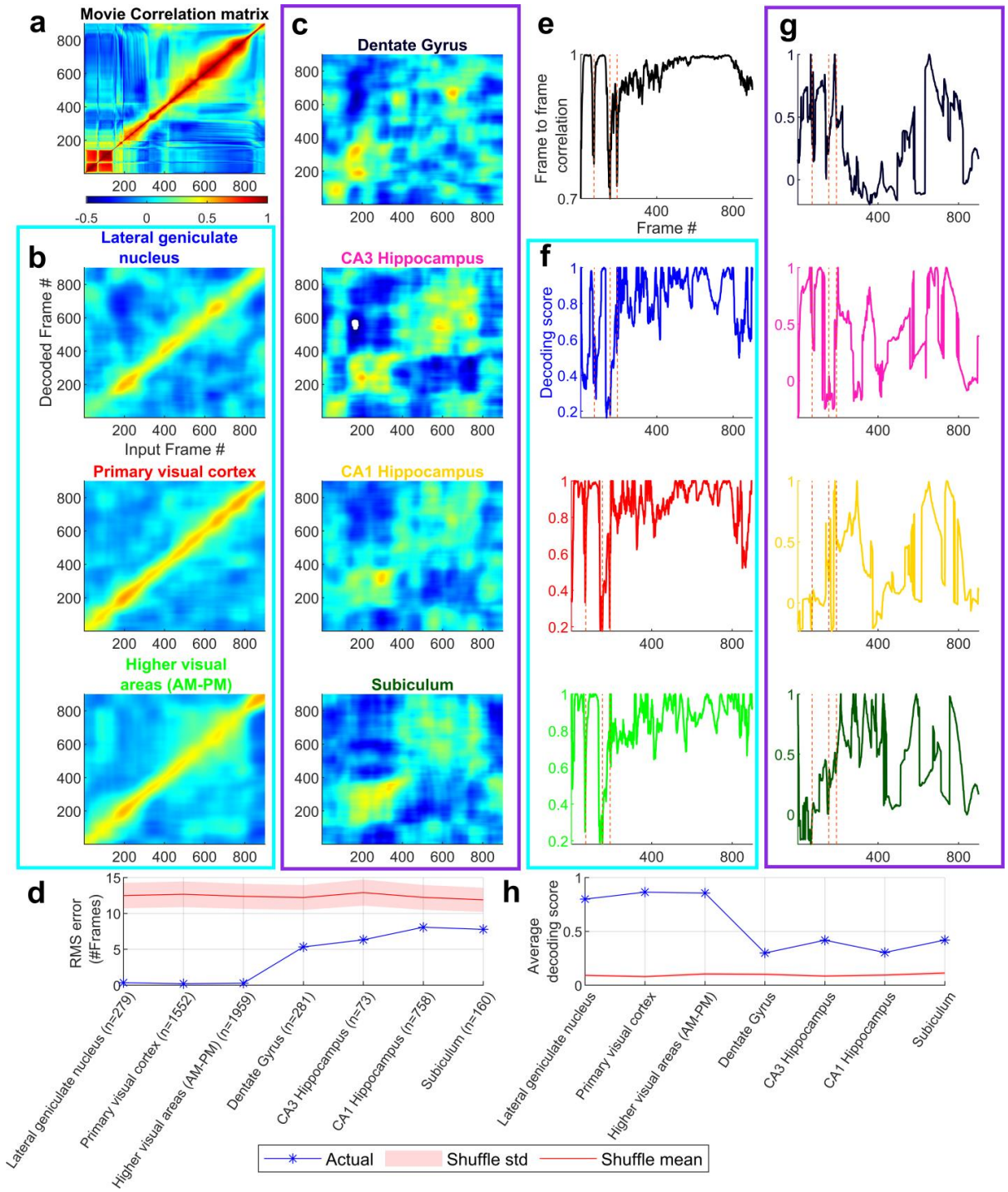

Fig. 4.4 | Population vector decoding reflects visual structure of movie presented **(a)** Correlation between all possible pairs from the 900 frames in the movie represented as a (symmetric) matrix, with unity values along the diagonal. Note higher correlation values away from the diagonal after frame 370 when the scene largely stabilizes. **(b)** Population vector decoding matrix for cortical regions, showing highest correlation along

diagonal. For each input frame, we compute a correlation coefficient for the spiking activity at that frame and the encoding vector corresponding to all frames. These correspond to each column in the matrix. Color scale is same as (a). See *Methods* for more details. **(c)** Same as (b), for hippocampal regions, showing weaker decoding. **(d)** Frame corresponding to the largest correlation in (c) and (d) was called the decoded frame and RMS error between input and decoded frames was computed. Shuffle values were obtained by a random permutation of the encoding matrix to break association with the decoding vector of the same cell. Decoding errors in visual areas were small (<1 frame, z-score compared to shuffles <-4) but larger in hippocampal regions (5.3 to 8.1 frames, z-score -1.9 to-3.7). **(e)** Correlation coefficient between consecutive frames, with large drops in correlations marked with orange dotted lines. **(f)** Decoding score variation with frame number for visual cortical areas**.** Decoding score was computed as the weighted average of the correlation between encoding and decoding values of any two frames weighted by the correlation between said frames. **(g)** Same as (f), for hippocampal neurons. **(h)** Average decoding score across all frames was significantly higher than shuffle for cortical (score>0.79, KS-test between actual and shuffle decoding scores, $p<10^{-140}$) as well as hippocampal neurons (score>0.29, KS-test between actual and shuffle decoding scores, $p<10^{-67}$)

Lack of selectivity to static visual scenes and reduced selectivity to scrambled movie presentation in hippocampus but not visual neurons.

Is the streaming nature of movies (where 2 consecutive frames are typically correlated) causal to SMS? Or do hippocampal neurons in rodents show selective responses to random presentation of static natural scenes? We investigated this question by analyzing the neural responses to 118 images of natural scenes, which were part of a complementary dataset. Analysis was again restricted to only the stationary epochs. We did not find selectivity beyond chance levels (5%) to natural scenes in hippocampal neurons (Fig. 4.5b). As a control, we found majority of neurons in the visual areas to be selective to these visual scenes (Fig. 4.5a), as reported earlier[96]. To better understand the effect of contiguous nature of the movie stimulus, we analyzed SMS to a scrambled presentation of the movie, where the same sequence of shuffled frames was presented in 20 trials. For a fair comparison, we re-analyzed SMS using only the first 20 trials of the regular, sequential movie presentation.

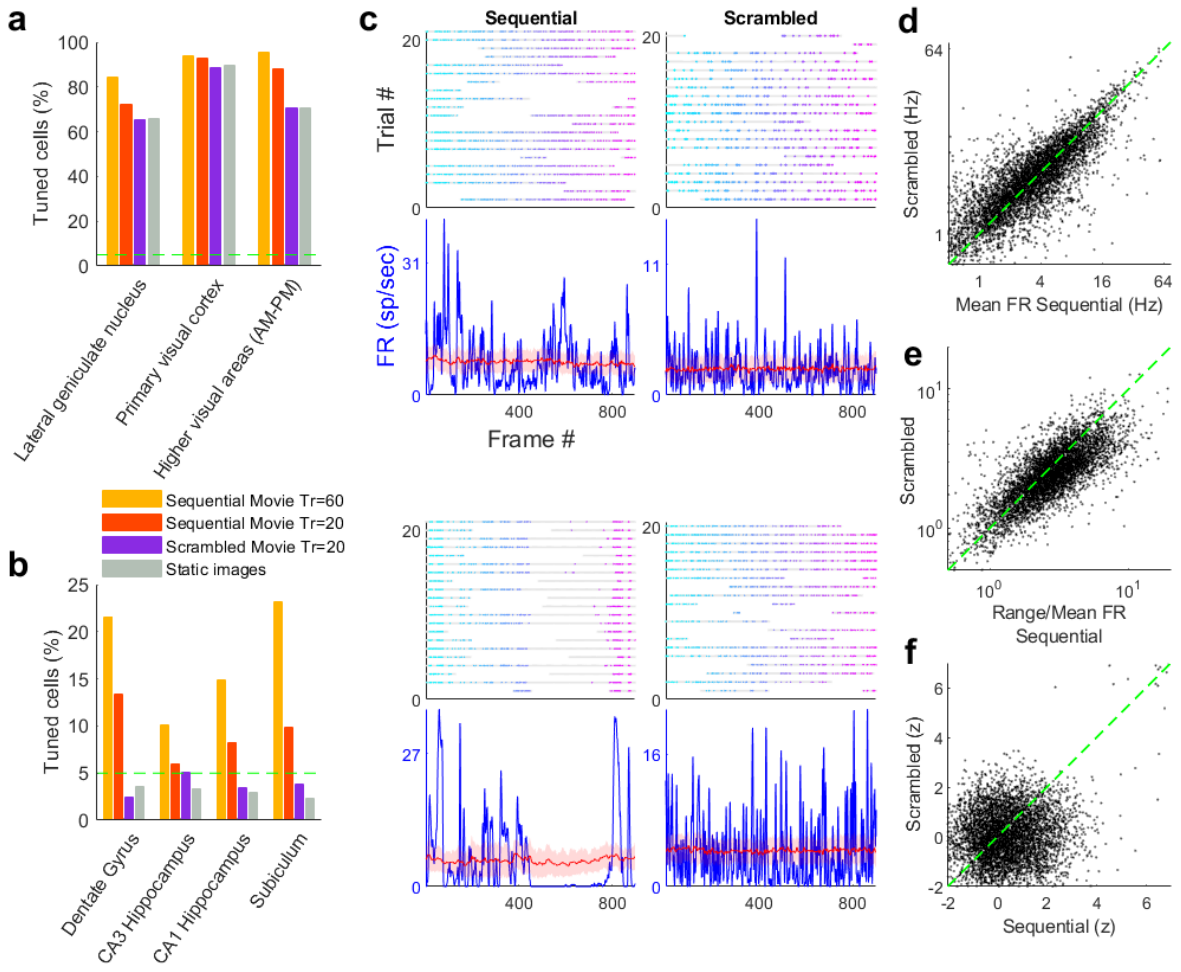

Fig. 4.5 | Lack of selectivity to static visual scenes and reduced selectivity to scrambled movie presentation in hippocampus but not visual neurons. (a) Fraction of tuned cells in visual areas was highest for movie presentations when calculated using all trials and significantly larger than the calculation based on first 20 trials (84.1% vs. 72.3% LGd, 93.9% vs. 92.8 V1, 95.6% vs. 87.8% AM-PM, KS-test $p<3.2x10^{-9}$). Tuning to scrambled movie presentation was not significantly different than sequential presentation for lateral geniculate nucleus neurons (KS-test p=0.22), but significantly lower in other cortical regions (92.8% vs. 88.4% V1, 87.9% vs. 70.5% AM-PM, KS-test $p<3x10^{-23}$). **(b)** Similar to (a), selectivity reduced upon using 20 instead of 60 trials (KS-test p<0.008). Static images (fraction tuned <3.7%, KS-test with sequential

movie, 60 trials $p<10^{-6}$) as well as scrambled movies (fraction tuned <5.2%, KS-test with sequential movie, 20 trials is not significantly different for CA3, but $p<0.002$ for other regions) elicit selectivity below chance level (green dashed line). **(c)** 2 example cells from hippocampal regions showing selective responses to sequential movies (left) and greater than chance variation leading to statistically significant response to scrambled movies (right). Raster and mean response format same as Fig. 4.1a. **(d)** Mean firing rate of hippocampal neurons in sequential and scrambled movie presentation for all cells is significantly correlated ($r=0.79$ $p<10^{-150}$) but not different (KS-test $p=0.002$). **(e)** Range normalized by mean of firing was correlated ($r=0.75$ $p<10^{-150}$) but higher for sequential than scrambled movie presentation (KS-test $p=2.1\text{x}10^{-24}$) **(f)** SMS tuning was correlated ($r=0.07$ $p=1.4\text{x}10^{-7}$) but higher for sequential than scrambled movie presentation (KS-test $p=9.2\text{x}10^{-37}$)

Selectivity for scrambled movies was slightly lower but significantly above chance levels in visual areas (Fig. 4.5a) but fell below the 5% chance level for the population of hippocampal neurons (Fig. 4.5b). Nevertheless, some of the hippocampal SMS neurons showed selective responses above chance levels to the scrambled movie presentation as well (Fig. 4.5c). Mean firing rates were highly correlated during sequential and scrambled movie presentations, suggesting that the lack of selectivity was not accompanied by shutting down of neural spiking (Fig. 4.5d). Mean rates were slightly but significantly higher in sequential than scrambled movie presentation. Movie tuning (Fig. 4.5f) as well as range/mean of firing (Fig. 4.5e) was lower but highly correlated in scrambled movie presentation suggesting reduction in firing modulation by movies when the streaming nature is lost, and the spatiotemporal structure of stimuli begins to resemble random presentation of static images.

Discussion

Here we show that similar to visual cortical areas, hippocampal broad spiking neurons also have selective responses to different frames of a movie. This selectivity is less prevalent than visual cortical areas and lateral geniculate nucleus neurons. Selectivity as well as firing rates vary through the depth of CA1 sub layers, similar to the dependence of place cell selectivity on landmarks[45,87], suggesting a common mechanism for processing of sensory cues in spatial navigation and passive viewing experiments. SMS drops to chance levels when the frames of the

movie are presented in a scrambled fashion, suggesting a causal role of sequential stimuli in hippocampal firing. This is consistent with the lack of selectivity to random presentation of images; furthering the view that hippocampus is involved in generation and processing of sequences[97–99].

These results have apparent similarities and important differences with the recently reported selectivity in CA1 to the position, angle and movement direction of a bar of light[72]. Both these experiments were performed in rodents, whose movements were decoupled from the visual cues. Those experiments demonstrated that a simple visual cue could elicit selective responses in CA1, whereas the current results pertain to complex streaming visual cues. In V1, response of neurons to simple stimuli, like drifting gratings, is not necessarily predictive of their response to natural (and hence complex) visual scenes[77]. Moreover, the bar of light in our prior work covered all angles, and hence was presented binocularly, whereas the movie presentation herein was monocular. Secondly, animals in current analyses were head fixed, whereas earlier they were only body fixed and afforded neck movements. Lastly, we report selective responses in all major sub regions of the hippocampus herein, whereas the prior work pertained only to CA1 region.

These as well as our previous[72] results support the hierarchical organization of visual processing, with hippocampus at the apex position[46], and hence showing sensory, non-abstract responses in hippocampal neurons. This complements the reports of visual cortical neurons having modulation by spatial position and coordinated activity with hippocampal neurons during navigation[53,100]. These results establish a singular experimental paradigm which can be used to probe selective responses in cortical as well as hippocampal regions. Evidence for visual responses without navigation demands can potentially bridge the gap between rodent and human studies[101,102], where natural movies can be decoded from fMRI signals[103].

Methods

Experimental and surgical procedures, spike sorting

We used neural data and correlated behavior signals recorded by the Allen Brain Institute and made publicly available at (https://portal.brain-map.org/explore/circuits/visual-coding-neuropixels). The details of the experimental pipeline are available at the above link as well as with related publications[96]. Prior to implantation with *Neuropixel* probes, mice passively viewed the entire dataset including drifting gratings, Gabor patches and the natural movies of interest here. Neural signal obtained from probes was split into 2 channels one for spiking, and other for local field potentials (LFP). Data from the spiking band, sampled at 30 kHz with a 500Hz high pass filter was used herein which was referenced to a ground wire inserted in the brain during surgery. Videos of the body and eye movements were obtained at 30Hz and synced to the neural data and stimulus presentation using a photodiode. Movies were presented monocularly on an LCD monitor with a refresh rate of 60Hz, positioned 15cm away from the mouse's right eye and spanned 120^{o}x95^{o} of viewing angle. Presentation of the movies was preceded by various sets of visual stimuli including Gabor patches, drifting gratings, and full field flashes. 30 trials of the sequential movie presentation were followed by 10 trials of the scrambled movie. There was a spontaneous running block of 30 minutes with gray screen of mean luminance, before the other block of sequential and scrambled movies was presented.

Prior to spike sorting, spikes were offset corrected and median adjusted to center the signal around zero. Spike sorting was automated using *Kilosort2*[94]. Output of *Kilosort2* was post-processed to remove noise units which are characterized by templates not possible due to current flows associated with action potentials as well as to correct for double counting of spikes. In our analysis, we directly used the spikes provided after these steps through the aforementioned dataset.

Neuropixel probes were registered to a common co-ordinate framework[88]. Each recorded unit was assigned to a recording channel corresponding to the maximum spike amplitude. Hence each

unit inherited the brain region corresponding to the channel on the probe where its spike amplitude was largest.

Stationary epoch identification

To eliminate the confounding effects of changes in behavioral state associated with running, we restricted our analysis to stationary epochs. These were identified as epochs when running speed was below 2cm/sec for 5 seconds before as well as after the epoch in question. Analysis was restricted to sessions with at least 10 minutes of stationary epochs when computing SMS over 60 trials, and 5 minutes when using the first 20 trials or for the scrambled movie presentation.

Movie tuning quantification

Procedures similar to those used previously were used[72]. Frames of movie presented during stationary epochs were binned in 900 bins, corresponding to each distinct frame. This occupancy was used to normalize the corresponding binning of spikes for each individual neuron under consideration to obtain a tuning response which was smoothed with a Gaussian window of σ=67 ms or 2 frames. To quantify the degree of modulation we computed sparsity s of the tuning response where r_n is the firing rate corresponding to the nth frame:

$$s = 1 - \frac{1}{N}\frac{(\sum_n r_n)^2}{(\sum_n {r_n}^2)}$$

To assess the statistical significance of sparsity, we used a bootstrapping procedure, which does not assume a normal distribution. Briefly, for each cell, spike trains as a function of the frame number from each trial were circularly shifted by different amounts and the sparsity of the randomized data computed. This procedure was repeated 100 times with different sets of random value shifts. The mean value and standard deviation of the sparsity of randomized data was used to compute the z-scored sparsity of actual data using the function *zscore* in MATLAB. The observed sparsity was considered statistically significant if the z-scored sparsity of the observed spike train was greater 2, which corresponds to p<0.0228 in a one tailed t-test. Similar method was used to quantify significance of image tuning (119 bins for each distinct image shown) as well as scrambled movie tuning. Smoothing in scrambled movie tuning was performed over frames in the order they were presented which was different from their order in the actual

sequential movie. Scrambled movie frames where obtained by randomly re-arranging the frames of the original movie, but the same random sequence was presented on all trials.

Full Width at Half Maxima (FWHM) calculation

For neurons which were deemed to have significant movie tuning, we quantified the mean, peak, and minimum rates across 60 trials. Peak-FWHM was identified as all frames where the tuning response was above (peak+mean)/2 rate. Similarly, trough-FWHM was identified as frames where the tuning response was below (minimum+mean)/2 rate. This definition allowed for FWHM to consist non-contiguous frames, since majority of neurons had multiple peaks.

Identifying frames with significant response

The above definition of FWHM led to non-zero count of peaks from each cell since it relied on the maximum value of the tuning response to set the threshold (along with the mean response). This had no bearing on whether the peak (or trough) could be expected purely by chance. Hence, we used the bootstrap tuning curves obtained with the random shifts in each trial, to establish a mean±(2*std) level of the expected range of peaks and troughs by chance. Frames where the actual movie tuning response exceeded (either on the positive or negative side) this range was deemed as a 'significant response'. Peaks and troughs were identified amongst these significant responses using the *findpeaks* function in MATLAB. Peaks (troughs) were identified as to be within the significant response frames, have mean height (depth) of mean+2*std (mean-2*std for trough) and a minimum prominence of 2*std.

Stability quantification

All the trials were split into two blocks of 30 trials each, of which the latter 30 were presented after an intermittent gray screen presentation. Separate tuning curves computed for each half, with 900 bins used for occupancy and spiking, and resulting tuning response smoothed with a Guassian window of σ=67 ms or 2 frames. The correlation coefficient was computed between these two groups (C_{actual}), which is a measure of stability. This procedure was repeated for all cells in a given brain region. To compute the significance of stability, this procedure was repeated 50 times, with different random pairings, such that movie tuning response of $Neuron_i$ in the first block is paired with response from the second half from another randomly chosen

$Neuron_j$. This provided a distribution of 50 values of stability ($C_{shuffle}$). Mean and standard error across all neurons for C_{actual} were plotted in color and for $C_{shuffle}$ in gray in Fig. 4.3d.

Population vector decoding, decoding score metric

Procedures similar to those used previously were used[72]. All but one trials across all the neurons for each brain region were treated as the 'lookup trials' and these data were used to decode the firing rate maps from the remaining trial called 'observed data'. Both the observed and lookup trials were normalized between 0-1 and smoothed with a Gaussian window of 50 frames or 1.5seconds. At each frame (corresponding to 33ms) in the 'observed data', the correlation was computed between the observed population vector and the lookup population vectors for all frames. The matrix of these correlations is shown in Fig. 4.4b, c. The maximum correlation at each frame is denoted as the decoded value. The entire procedure was repeated at each frame and the error was computed as the root-mean square difference between the decoded and actual frame. For shuffle data, the above procedure was repeated 50 times, with different random pairings, such that the ordering of neurons in the lookup trials was randomly permuted.

The above procedure treated each frame independently without accounting for the similarity of visual content in different frames. To account for this, we developed the 'decoding score' metric. At each frame, the decoded value from above was used to obtain the correlation between input and decoded frames. Perfect decoding, led to high values of decoding score, which were capped at 1. This method accounted for the similarity of 2 frames even if they were presented temporally apart in the movie.

Eye movement bias

An IR dichroic mirror was placed in front the right eye to allow the eye tracking camera to operate without interference from the visual stimulus. Pupil movements were mapped onto the stimulus screen to obtain gaze locations on screen. Horizontal and vertical changes in gaze position were treated separately and binned with respect to the movie frames. Average gaze in horizontal and vertical dimension was computed over all stationary epochs and degree of modulation of gaze was computed using the sparsity metric, as described above. Significance of

the gaze-bias was quantified using bootstrapping methods, similar to that used for movie tuning quantification. Pupil area was analyzed in a similar fashion as gaze position on screen.

Extended Data Figures

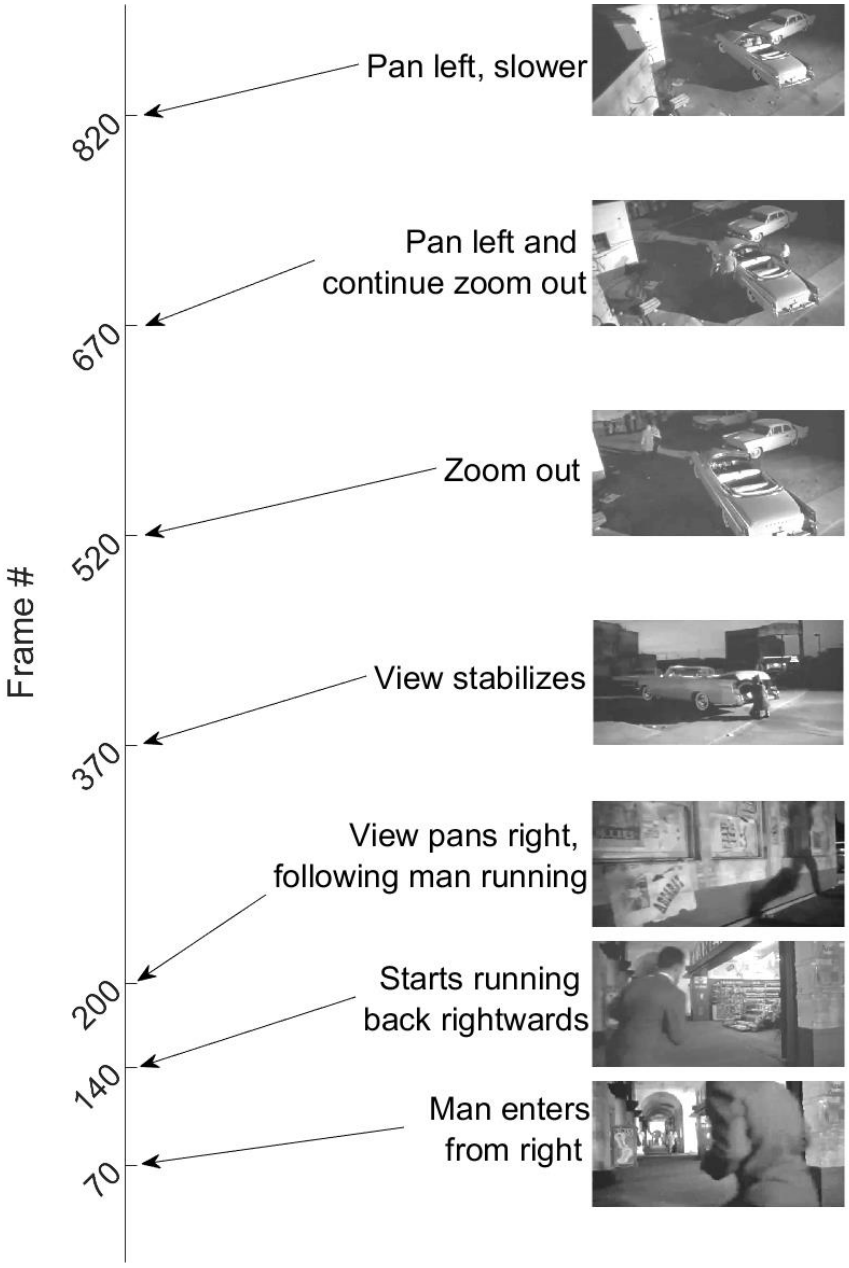

Extended Data Fig. 4.1 | Description of movie stimulus. Snippets of the 30 seconds clip from the movie and corresponding frame numbers.

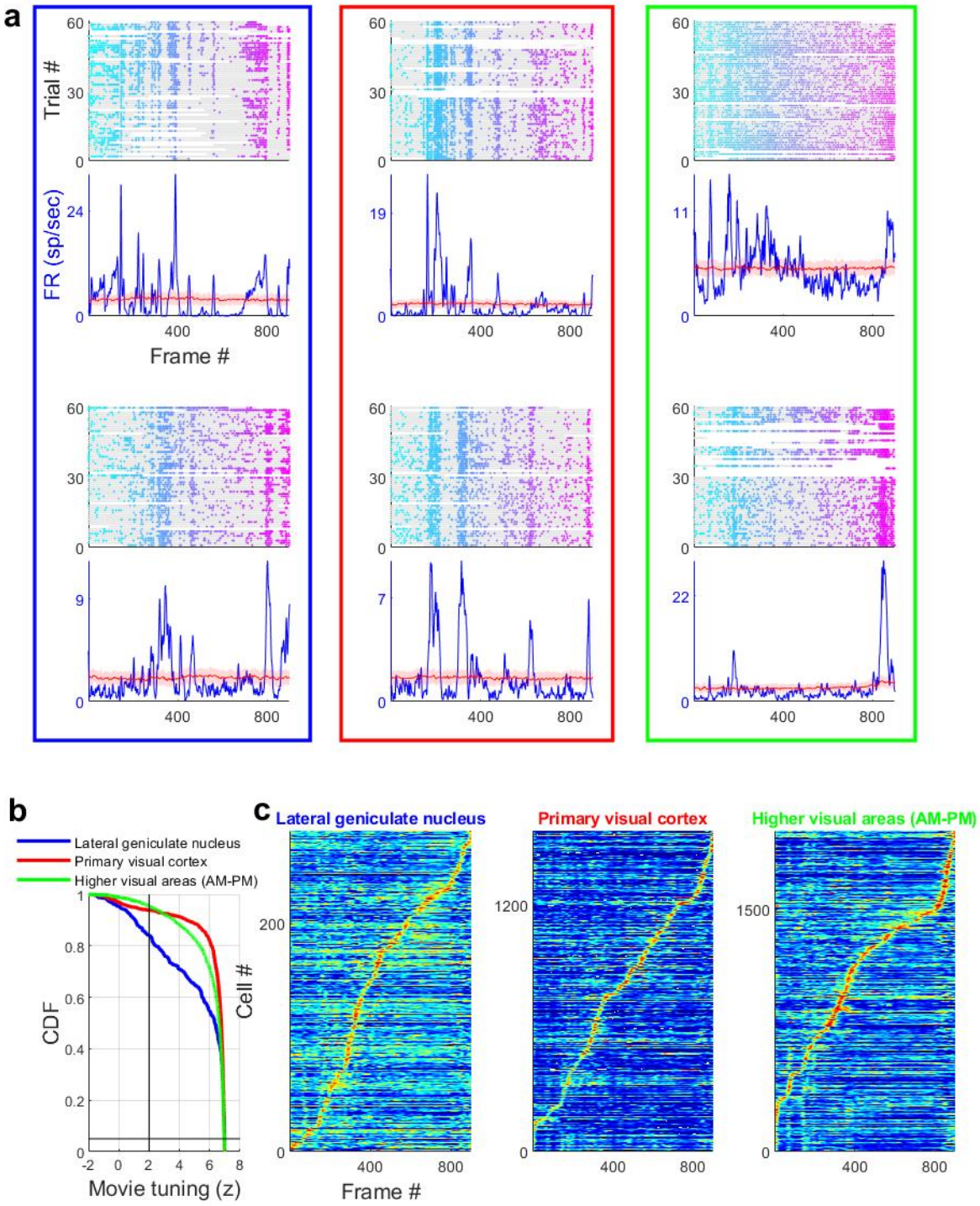

Extended Data Fig. 4.2 | Streaming movie selectivity (SMS) in visual neurons (a) Example raster plots (top) and mean rate responses (bottom) as a function of the frame of movie presented. Gray background in raster signifies the stationary epochs used in analysis to compute mean rate responses. Red line and shaded area signify mean and standard deviation of mean rate response expected by chance obtained by

bootstrapping (see *Methods*). 2 example cells each from dorsal lateral geniculate nucleus (blue, LGd), primary visual cortex (red, V1) and higher visual areas (green, anteromedial (AM) and posteromedial (PM)), showing increased spiking responses to different frames in the movie. **(b)** Large majority of neurons were tuned for the movie frames, with largest selectivity seen in higher visual areas (95.6%, 1988 out of 2080) followed closely by primary visual area (93.9%, 1563 out of 1665) and least by lateral geniculate nucleus (84.1%, 281 out of 334). Black vertical line indicates threshold of z>2 (see *Methods*) and the black horizontal line indicates chance level of 5%. **(c)** Stack plots of all tuned cells, arranged in the increasing order the frame corresponding to highest firing rates.

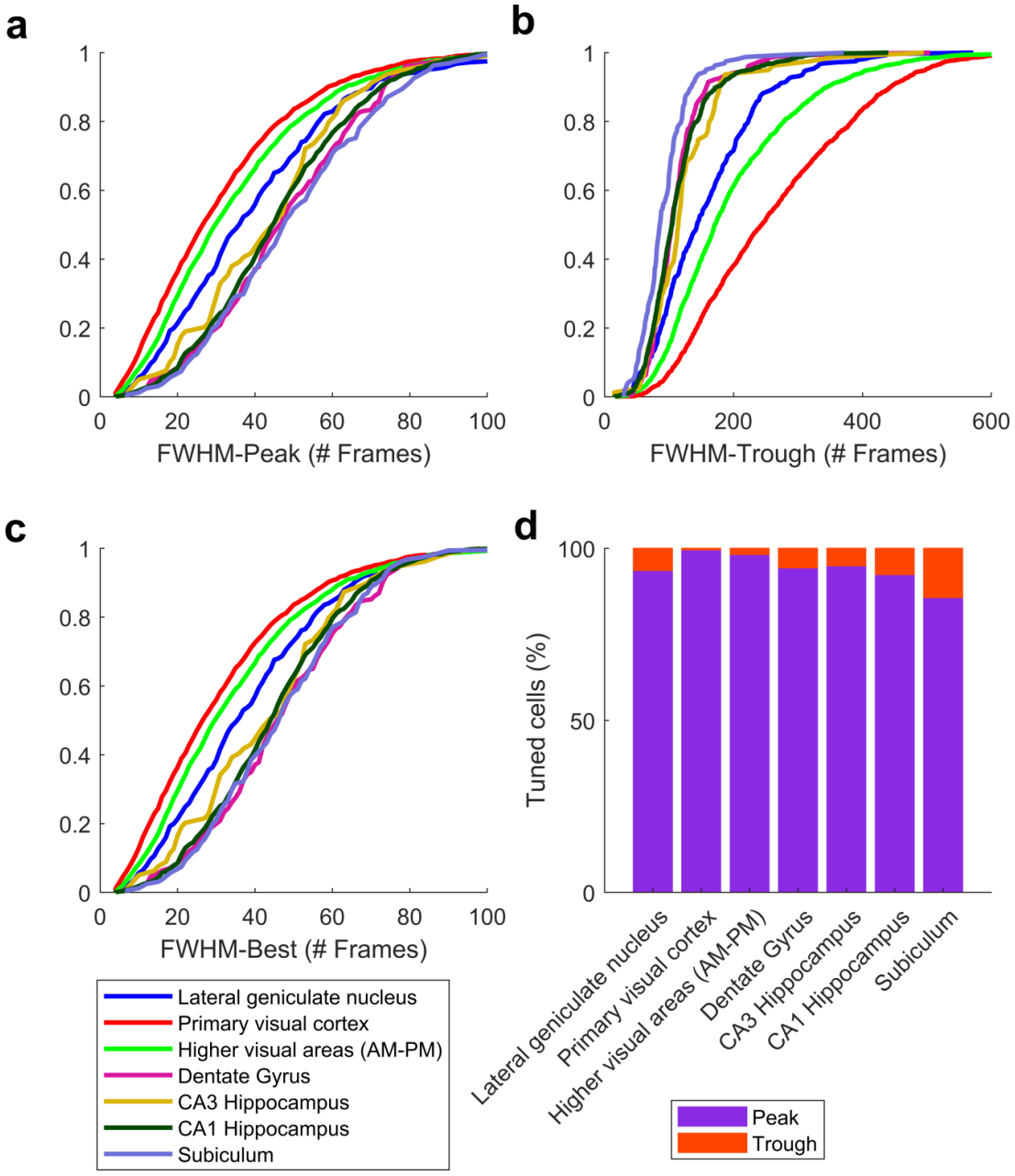

Extended Data Fig. 4.3 | peak-FWHMs were narrower than trough-FWHM (a) Cumulative histogram of peak-FWHM quantified as number of frames in FWHM zone, with narrowest peak in primary visual cortex (27/900, 3%) and the broadest in subiculum (47/900, 5.2%). **(b)** Same as (a), for troughs within FWH-minima, showing opposite trend and broader FWHM than peak-FWHM. **(c)** Best-FWHM was chosen as the narrower of peak or trough, and **(d)** was predominantly the peak-FWHM.

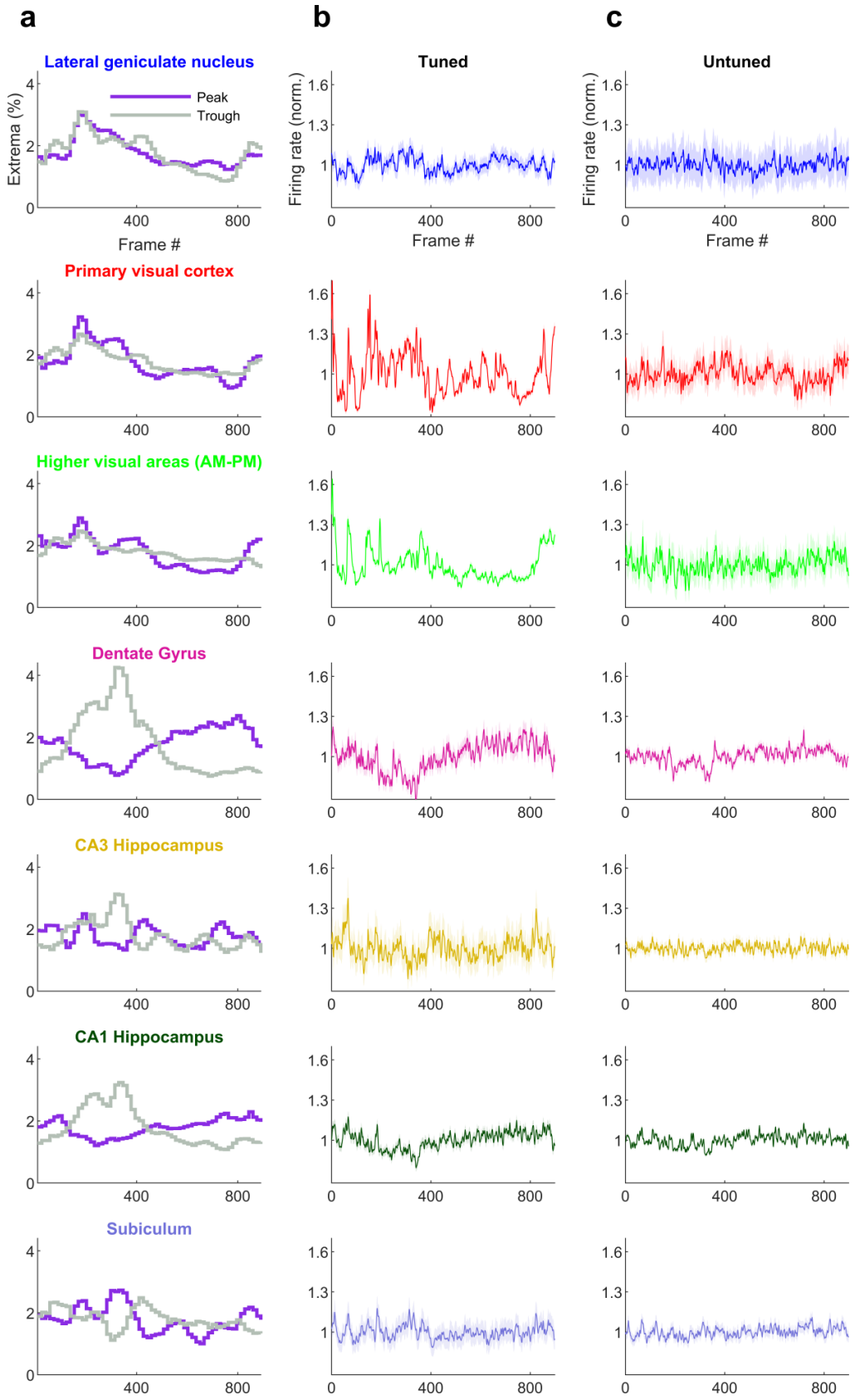
a
b
c
Lateral geniculate nucleus
Peak
Trough
Extrema (%)
Frame #
Tuned
Untuned
Firing rate (norm.)
Primary visual cortex
Higher visual areas (AM-PM)
Dentate Gyrus
CA3 Hippocampus
CA1 Hippocampus
Subiculum

Extended Data Fig. 4.4 | Distribution of peaks and troughs of SMS and average multi-unit response. (a) Distribution of peaks (purple) and troughs (gray) from the frames corresponding to significant responses (see *Methods*). Each neuron could contribute multiple peaks and troughs. Distribution of peaks and trough was correlated in visual areas (r>0.67 p<10^{-8}) but anti-correlated in hippocampal populations (r<-0.29 p<0.03). **(b)** Average multi-unit activity (MUA) for tuned neurons in different brain regions. For each tuned neuron, its response was smoothed with a Gaussian window of σ=330ms or 10 bins and normalized by its mean. MUA in primary visual cortex and AM-PM shows coordinated firing at the beginning of the movie, and around Frame #100. Dentate and CA1 MUAs show ensemble reduction in firing rates till ~Frame #370 after which the scene in movie stabilizes. **(c)** MUA of untuned neurons, showing largely uniform firing across movie frames for all brain regions.

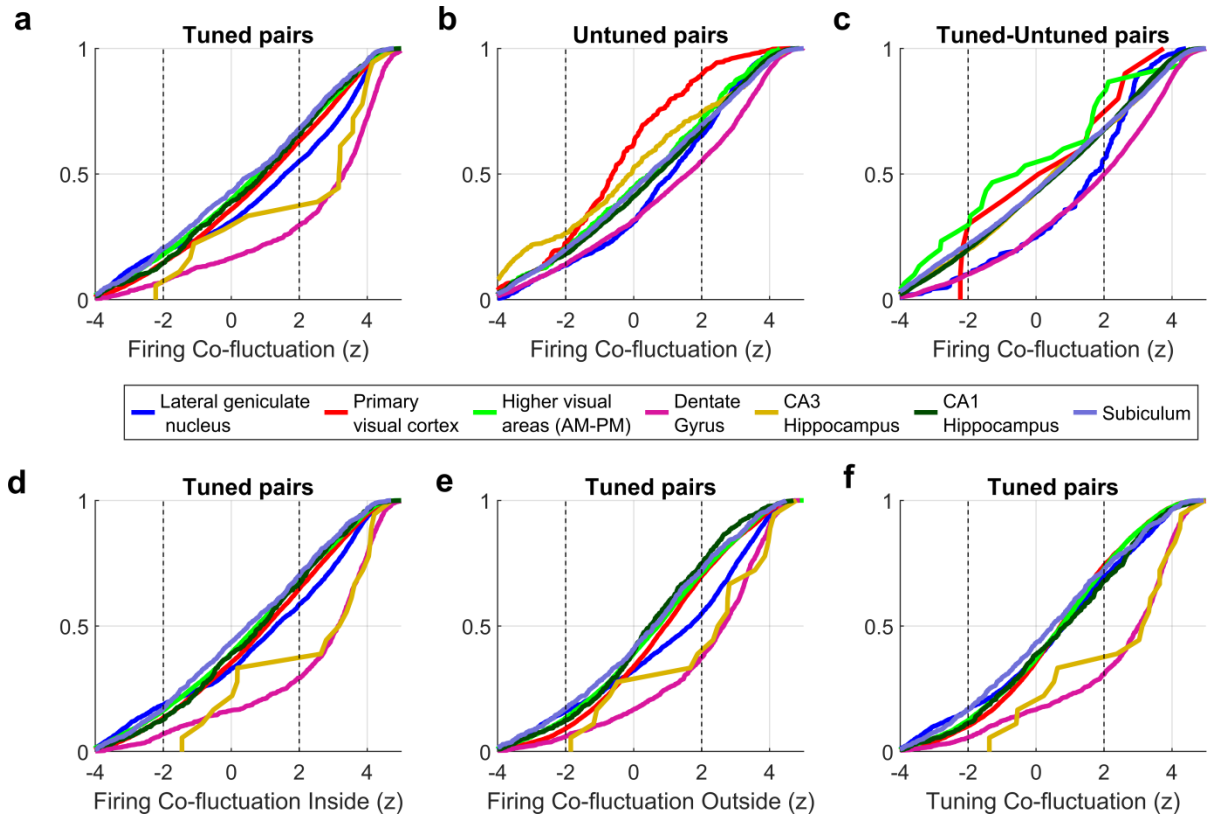

Extended Data Fig. 4.5 | Quantification of co-fluctuation of firing and SMS. (a) For simultaneously recorded pairs of cells, we computed a firing rate co-fluctuation metric as the correlation between mean firing across trials for different pairs of neurons (see *Methods*). This co-fluctuation was z-scored with shuffle data, where the order of trials for one neuron of the pair was mis-matched, to obtain significance levels. Significant co-fluctuation was widely prevalent in tuned cell pairs from dentate gyrus (70%) and CA3 (61%) compared to other regions. **(b)** Same as (a), for untuned cell pairs showing low co-fluctuation in primary visual cortex, compared to other regions. **(c)** Same as (a), for pairs of cells where one showed SMS (tuned) and the other did not. **(d)** For tuned cell pairs, we compared the co-fluctuation inside the SMS tuning zone, defined as the frames corresponding to mean firing response above 50 percentiles (to ensure equal number of bins inside and outside the tuning zone). Dentate gyrus neurons showed widespread co-fluctuation. **(e)** Same as (d), but for spikes outside the respective tuning zones of cell pairs. **(f)** Tuning co-fluctuation was defined analogously as firing co-fluctuation using the correlation between responses in a trial to the overall movie tuning response (see *Methods*). Significant tuning co-fluctuation was also widespread in dentate neuron cell pairs (69%), compared to other brain regions (26-32%)

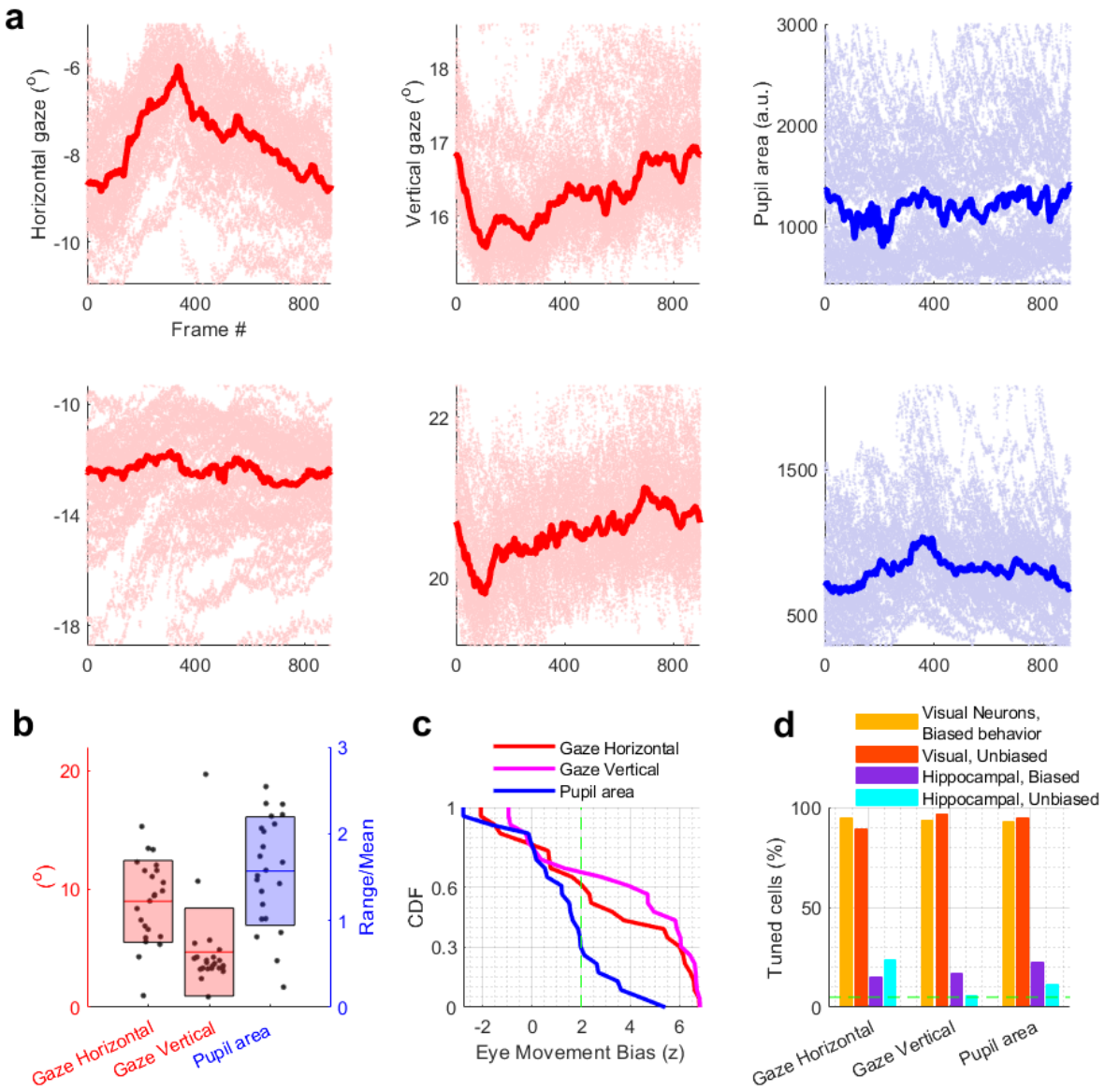

Extended Data Fig. 4.6 | Eye movement bias during movie presentation. (a) 2 example sessions with biased eye position on screen (gaze) as a function of movie frames. Dark traces correspond to mean responses across trials, light colors are each trial. Session on top has significant bias with horizontal as well as vertical gaze, whereas example session at the bottom has bias with pupil area and vertical gaze. **(b)** Across 23 sessions with eye movement recording, 99 percentile range of horizontal gaze movement was 8.9º (screen was 120º wide along horizontal), vertical gaze was 4.7º (screen: 95º) and average range/mean for pupil area was 1.6. **(c)** Cumulative distribution of eye movement bias (see *Methods* for quantification) across 23 sessions. Green dotted line indicates significance threshold of z=2 **(d)** Fraction of SMS tuned cells was separately computed for cells from sessions with and without significant behavioral

bias. Population distribution of SMS tuning was significantly different for visual as well as hippocampal regions for horizontal gaze (t-test $p<1.4x10^{-8}$). Vertical gaze and pupil area did not significantly affect visual cortical selectivity (t-test $p>0.12$), but biased behavior caused significantly more selectivity in hippocampal neurons (t-test $p<8.1x10^{-17}$). Total sessions used in eye movement bias analysis exceed those for computing SMS, since some sessions with insufficient stationary epochs were used here.

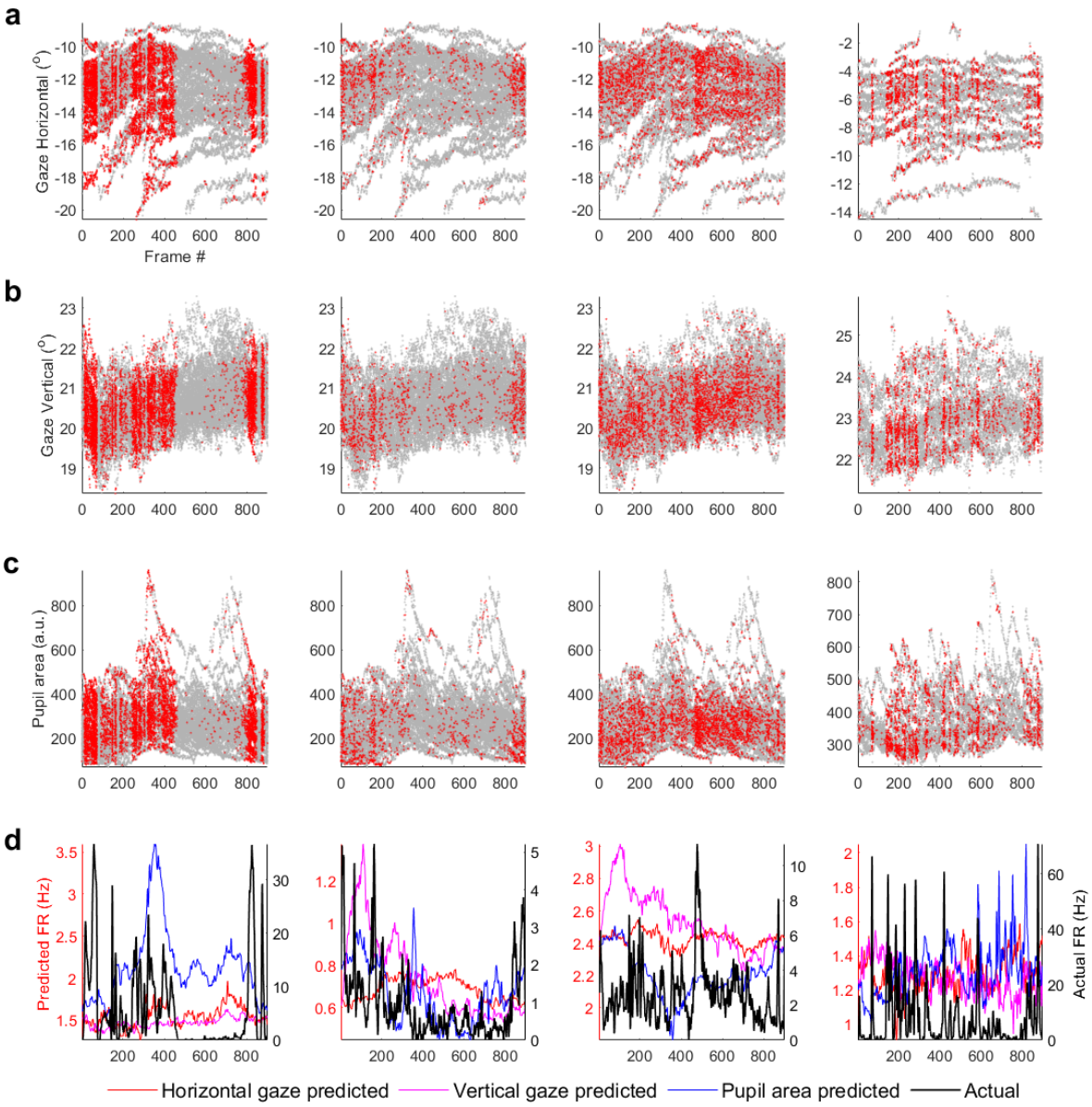

Extended Data Fig. 4.7 | Eye movements cannot explain streaming movie selectivity (SMS) (a) 4 example cells showing selective firing with respect to movie frame number, but no bias of firing with respect to gaze on screen along horizontal direction, resulting in vertical bands of spiking with little variance or dependence along the y-axis. **(b)** Same as (a) but comparing firing with respect to frame number and vertical gaze. **(c)** Same as (a) but comparing the effect of pupil dilation (quantified as pupil area), on firing of cells tuned for movie frames. **(d)** For the same example cells as a-c, Actual SMS response(black) is drastically different than the response predicted by eye movements, based on average response to horizontal and vertical eye movement and pupil dilation during stationary epochs in mean-luminance gray screen presentation (see *Methods*).

REFERENCES

1. Scoviille, W. B. & Milner, B. LOSS OF RECENT MEMORY AFTER BILATERAL HIPPOCAMPAL LESIONS. *J. Neurol. Neurosurg. Psychiat* (1957) doi:10.1136/jnnp.20.1.11.

2. Bliss, T. V. P. & L0mo, T. *LONG-LASTING POTENTIATION OF SYNAPTIC TRANSMISSION IN THE DENTATE AREA OF THE ANAESTHETIZED RABBIT FOLLOWING STIMULATION OF THE PERFORANT PATH*. *J. Physiol* vol. 232 (1973).

3. Parkinson, J. K., Murray, E. A. & Mishkin, M. A selective mnemonic role for the hippocampus in monkeys: Memory for the location of objects. *J. Neurosci.* **8**, 4159–4167 (1988).

4. Morris, R. G. M., Garrud, P., Rawlins, J. N. P. & O'Keefe, J. Place navigation impaired in rats with hippocampal lesions. *Nature* **297**, 681–683 (1982).

5. O'Keefe, J. & Nadel, L. *The hippocampus as a cognitive map*. (Clarendon Press, 1978).

6. Muller, R. U. *et al.* The effects of changes in the environment on the spatial firing of hippocampal complex-spike cells. *J. Neurosci.* **7**, 2008–2017 (1987).

7. Save, E., Cressant, A., Thinus-Blanc, C. & Poucet, B. *Spatial Firing of Hippocampal Place Cells in Blind Rats*. (1998).

8. Mittelstaedt, H. & Mittelstaedt, M.-L. Homing by Path Integration. in 290–297 (Springer, Berlin, Heidelberg, 1982). doi:10.1007/978-3-642-68616-0_29.

9. McNaughton, B. L., Battaglia, F. P., Jensen, O., Moser, E. I. & Moser, M.-B. Path integration and the neural basis of the 'cognitive map'. *Nat. Rev. Neurosci.* **7**, 663–678 (2006).

10. Taube, J. S., Muller, R. U. & Ranck Jr., J. B. Head-direction cells recorded from the

postsubiculum in freely moving rats. II. Effects of environmental manipulations. *J Neurosci* **10**, 436–47. (1990).

11. Sargolini, F. & Moser, E. Entorhinal Grid Cells and the Representation of Space. *Memories Mol. Circuits* (2007).

12. McNaughton, B. L. *et al.* Deciphering the hippocampal polyglot: the hippocampus as a path integration system. *J Exp Biol* **199**, 173–85. (1996).

13. Aronov, D. & Tank, D. W. Engagement of Neural Circuits Underlying 2D Spatial Navigation in a Rodent Virtual Reality System. *Neuron* **84**, 442–456 (2014).

14. Aghajan, Z. M. *et al.* Impaired spatial selectivity and intact phase precession in two-dimensional virtual reality. *Nat. Neurosci.* **18**, 121–128 (2015).

15. Danjo, T., Toyoizumi, T. & Fujisawa, S. Spatial representations of self and other in the hippocampus. *Science (80-.).* **359**, 213–218 (2018).

16. Omer, D. B., Maimon, S. R., Las, L. & Ulanovsky, N. Social place-cells in the bat hippocampus. *Science (80-.).* **359**, 218–224 (2018).

17. Mou, X. & Ji, D. Social observation enhances cross- environment activation of hippocampal place cell patterns. *Elife* **5**, (2016).

18. Aronov, D., Nevers, R. & Tank, D. W. Mapping of a non-spatial dimension by the hippocampal–entorhinal circuit. *Nature* **543**, 719–722 (2017).

19. Sakurai, Y. Coding of auditory temporal and pitch information by hippocampal individual cells and cell assemblies in the rat. *Neuroscience* **115**, 1153–1163 (2002).

20. Sakurai, Y. *Involvement of Auditory Cortical and Hippocampal Neurons in Auditory Working Memory and Reference Memory in the Rat*. *The Journal of Neuroscience* vol. 14 (1994).

21. Acharya, L., Aghajan, Z. M., Vuong, C., Moore, J. J. & Mehta, M. R. Causal Influence of Visual Cues on Hippocampal Directional Selectivity. *Cell* **164**, 197–207 (2016).

22. Hubel, D. H. & Wiesel, T. N. Receptive fields, binocular interaction and functional architecture in the cat's visual cortex. *J. Physiol.* **160**, 106 (1962).

23. O'Keefe, J. & Dostrovsky, J. The hippocampus as a spatial map. Preliminary evidence from unit activity in the freely-moving rat. *Brain Res* **34**, 171–5. (1971).

24. Fyhn, M., Molden, S., Witter, M. P., Moser, E. I. & Moser, M. B. Spatial representation in the entorhinal cortex. *Science (80-.).* **305**, 1258–1264 (2004).

25. Foster, T. C., Castro, C. A. & McNaughton, B. L. Spatial selectivity of rat hippocampal neurons: dependence on preparedness for movement. *Science (80-.).* **244**, 1580–2. (1989).

26. Itskov, P. M. *et al.* Sound sensitivity of neurons in rat hippocampus during performance of a sound-guided task Sound sensitivity of neurons in rat hippocampus during performance of a sound-guided task. 1822–1834 (2012) doi:10.1152/jn.00404.2011.

27. Taube, J. S. J. S., Muller, R. U. R. U., Ranck, J. B. J. & Ranck Jr., J. B. Head-direction cells recorded from the postsubiculum in freely moving rats. I. Description and quantitative analysis. *J. Neurosci.* **10**, 420–435 (1990).

28. Cushman, J. D. *et al.* Multisensory control of multimodal behavior: Do the legs know what the tongue is doing? *PLoS One* **8**, (2013).

29. Ravassard, P. *et al.* Multisensory control of hippocampal spatiotemporal selectivity. *Science* **340**, 1342–6 (2013).

30. Malpeli, J. G. & Baker, F. H. The representation of the visual field in the lateral geniculate nucleus of Macaca mulatta. *J. Comp. Neurol.* **161**, 569–594 (1975).

31. Mehta, M. R., Quirk, M. C. & Wilson, M. A. Experience-dependent asymmetric shape of hippocampal receptive fields. *Neuron* **25**, 707–15. (2000).

32. Ahmed, O. J. & Mehta, M. R. *The hippocampal rate code: anatomy, physiology and theory*. *Trends Neurosci* vol. 32 329–338 (2009).

33. de Vries, S. E. J. *et al.* A large-scale standardized physiological survey reveals functional

organization of the mouse visual cortex. *Nat. Neurosci.* **23**, 138–151 (2020).

34. Wilson, M. A. & McNaughton, B. L. Dynamics of the hippocampal ensemble code for space. *Science (80-.).* **261**, 1055–8. (1993).

35. Resnik, E., McFarland, J. M., Sprengel, R., Sakmann, B. & Mehta, M. R. The Effects of GluA1 Deletion on the Hippocampal Population Code for Position. *J. Neurosci.* **32**, 8952–68 (2012).

36. Stefanini, F. *et al.* A distributed neural code in the dentate gyrus and in CA1. *Neuron* (2020).

37. Battaglia, F. P., Sutherland, G. R. & McNaughton, B. L. Local sensory cues and place cell directionality: additional evidence of prospective coding in the hippocampus. *J Neurosci* **24**, 4541–4550 (2004).

38. Muller, R. U., Kubie, J. L., Bostock, E. M., Taube, J. S. & Quirk, G. J. Spatial firing correlates of neurons in the hippocampal formation of freely mfile:///C:/Users/mayank/Downloads/scholar (6).risoving rats. (1991).

39. Colgin, L. L., Moser, E. I. & Moser, M. B. Understanding memory through hippocampal remapping. *Trends Neurosci* **31**, 469–477 (2008).

40. Suzuki, W. A., Miller, E. K. & Desimone, R. Object and Place Memory in the Macaque Entorhinal Cortex. *J. Neurophysiol.* **78**, 1062–1081 (1997).

41. Pastalkova, E., Itskov, V., Amarasingham, A., Buzsaki, G. & Buzsáki, G. Internally generated cell assembly sequences in the rat hippocampus. *Science (80-.).* **321**, 1322–1327 (2008).

42. Saleem, A. B. *et al.* Coherent encoding of subjective spatial position in visual cortex and hippocampus. *Nature* **562**, 124–127 (2018).

43. Markus, E. J. *et al.* Interactions between location and task affect the spatial and directional firing of hippocampal neurons. *J Neurosci* **15**, 7079–94. (1995).

44. Ziv, Y. *et al.* Long-term dynamics of CA1 hippocampal place codes. (2013) doi:10.1038/nn.3329.

45. Geiller, T., Fattahi, M., Choi, J.-S. & Royer, S. Place cells are more strongly tied to landmarks in deep than in superficial CA1. *Nat. Commun.* **8**, 14531 (2017).

46. Felleman, D. J. & Van, D. C. E. Distributed hierarchical processing in the primate cerebral cortex. *Cereb. cortex (New York, NY 1991)* **1**, 1–47 (1991).

47. Quiroga, R. Q., Reddy, L., Kreiman, G., Koch, C. & Fried, I. Invariant visual representation by single neurons in the human brain. **435**, 1102–1107 (2005).

48. Hahn, T. T., Sakmann, B. & Mehta, M. R. Phase-locking of hippocampal interneurons' membrane potential to neocortical up-down states. *Nat Neurosci* **9**, 1359–1361 (2006).

49. Hahn, T. T., Sakmann, B. & Mehta, M. R. Differential responses of hippocampal subfields to cortical up-down states. *Proc Natl Acad Sci U S A* **104**, 5169–5174 (2007).

50. Hahn, T. T. G., McFarland, J. M., Berberich, S., Sakmann, B. & Mehta, M. R. Spontaneous persistent activity in entorhinal cortex modulates cortico-hippocampal interaction in vivo. *Nat Neurosci* **advance on**, (2012).

51. Beltramo, R. & Scanziani, M. *A collicular visual cortex: Neocortical space for an ancient midbrain visual structure*. http://science.sciencemag.org/.

52. Ji, D. & Wilson, M. A. Coordinated replay of awake experience in the cortex and hippocampus during sleep. *Nat Neurosci* **10**, 100–107 (2007).

53. Haggerty, D. C. & Ji, D. Activities of visual cortical and hippocampal neurons co-fluctuate in freely moving rats during spatial behavior. *Elife* **4**, e08902 (2015).

54. Royer, S. *et al.* Control of timing , rate and bursts of hippocampal place cells by dendritic and somatic inhibition. **15**, (2012).

55. Villette, V., Malvache, A., Tressard, T., Dupuy, N. & Cossart, R. Internally Recurring Hippocampal Sequences as a Population Template of Spatiotemporal Information. *Neuron*

88, 357–366 (2015).

56. Mishkin, M., Health, M., Mehta, M. R., Barnes, C. A. & McNaughton, B. L. Experience-dependent, asymmetric expansion of hippocampal place fields. *Proc Natl Acad Sci U S A* **94**, 8918–21. (1997).

57. Ringach, D. L., Shapley, R. M. & Hawken, M. J. Orientation selectivity in macaque V1: Diversity and laminar dependence. *J. Neurosci.* **22**, 5639–5651 (2002).

58. Ghodrati, M., Zavitz, E., Rosa, M. G. P. & Price, N. S. C. Contrast and luminance adaptation alter neuronal coding and perception of stimulus orientation. *Nat. Commun.* **10**, (2019).

59. Berens, P. CircStat : A MATLAB Toolbox for Circular Statistics . *J. Stat. Softw.* **31**, 1–21 (2009).

60. Knierim, J. J. *Dynamic Interactions between Local Surface Cues, Distal Landmarks, and Intrinsic Circuitry in Hippocampal Place Cells*. (2002).

61. Save, E., Nerad, L. & Poucet, B. *Contribution of multiple sensory information to place field stability in hippocampal place cells. Hippocampus* vol. 10 64–76 (2000).

62. McFarland, W. L., Teitelbaum, H. & Hedges, E. K. Relationship between hippocampal theta activity and running speed in the rat. *J. Comp. Physiol. Psychol.* **88**, 324–328 (1975).

63. Sławińska, U. & Kasicki, S. The frequency of rat's hippocampal theta rhythm is related to the speed of locomotion. *Brain Res.* **796**, 327–331 (1998).

64. Whishaw, I. Q. & Vanderwolf, C. H. Hippocampal EEG and behavior: Change in amplitude and frequency of RSA (Theta rhythm) associated with spontaneous and learned movement patterns in rats and cats. *Behav. Biol.* **8**, 461–484 (1973).

65. Safaryan, K. & Mehta, M. R. Enhanced hippocampal theta rhythmicity and emergence of eta oscillation in virtual reality. doi:10.1101/2020.06.29.178186.

66. Shin, J., Talnov, A., Matsumoto, G. & Brankack, J. Hippocampal theta rhythm and

running speed: A reconsideration using within-single trial analysis. *Neurocomputing* **38**–**40**, 1567–1574 (2001).

67. Skaggs, W. E., McNaughton, B. L., Wilson, M. A. & Barnes, C. A. Theta phase precession in hippocampal neuronal populations and the compression of temporal sequences. *Hippocampus* **6**, 149–172 (1996).

68. Bose, A., Booth, V. & Recce, M. *A Temporal Mechanism for Generating the Phase Precession of Hippocampal Place Cells*. *Journal of Computational Neuroscience* vol. 9.

69. Mehta, M. R., Lee, A. K. & Wilson, M. A. Role of experience and oscillations in transforming a rate code into a temporal code. *Nature* **417**, 741–746 (2002).

70. Kelemen, E. & Fenton, A. A. Coordinating different representations in the hippocampus. *Neurobiology of Learning and Memory* vol. 129 50–59 (2016).

71. Jezek, K., Henriksen, E. J., Treves, A., Moser, E. I. & Moser, M. B. Theta-paced flickering between place-cell maps in the hippocampus. *Nature* **478**, 246–249 (2011).

72. Purandare, C. S. *et al.* Moving bar of light generates angle, distance and direction selectivity in place cells.

73. Siegle, J. H. *et al.* Survey of spiking in the mouse visual system reveals functional hierarchy. *Nature* **592**, 86–92 (2021).

74. Niell, C. M. & Stryker, M. P. Modulation of Visual Responses by Behavioral State in Mouse Visual Cortex. *Neuron* **65**, 472–479 (2010).

75. Góis, Z. H. T. D. & Tort, A. B. L. Characterizing Speed Cells in the Rat Hippocampus. *Cell Rep.* **25**, 1872-1884.e4 (2018).

76. Wiener, S. I., Paul, C. A. & Eichenbaum, H. *Spatial and Behavioral Correlates of Hippocampal Neuronal Activity*. (1989).

77. Herikstad, R., Baker, J., Lachaux, J. P., Gray, C. M. & Yen, S. C. Natural movies evoke spike trains with low spike time variability in cat primary visual cortex. *J. Neurosci.* **31**,

15844–15860 (2011).

78. Yen, S.-C., Baker, J. & Gray, C. M. Heterogeneity in the Responses of Adjacent Neurons to Natural Stimuli in Cat Striate Cortex. *J Neurophysiol* **97**, 1326–1341 (2007).

79. Hoseini, M. S. *et al.* Dynamics and sources of response variability and its coordination in visual cortex. *Vis. Neurosci.* (2019) doi:10.1017/S0952523819000117.

80. Xia, J., Marks, T. D., Goard, M. J. & Wessel, R. Stable representation of a naturalistic movie emerges from episodic activity with 2 gain variability. (2021).

81. O'keefe, J. & Burgess, N. *Geometric determinants of the place fields of hippocampal neurons*.

82. Mountcastle, V. B. *MODALITY AND TOPOGRAPHIC PROPERTIES OF SINGLE NEURONS OF CAT'S SOMATIC SENSORY CORTEX1*.

83. Ringach, D. L. *et al.* Spatial clustering of tuning in mouse primary visual cortex. *Nat. Commun.* **7**, 1–9 (2016).

84. Strange, B. A., Witter, M. P., Lein, E. S. & Moser, E. I. Functional organization of the hippocampal longitudinal axis. *Nat. Publ. Gr.* **15**, (2014).

85. Jung, M. W., Wiener, S. I. & Mcnaughtonl, B. L. *Comparison of Spatial Firing Characteristics of Units in Dorsal and Ventral Hippocampus of the Rat*. *The Journal of Neuroscience* vol. 74 (1994).

86. Fanselow, M. S. & Dong, H. W. Are the Dorsal and Ventral Hippocampus Functionally Distinct Structures? *Neuron* vol. 65 7–19 (2010).

87. Mizuseki, K., Diba, K., Pastalkova, E. & Buzsáki, G. Hippocampal CA1 pyramidal cells form functionally distinct sublayers. *Nat. Neurosci.* **14**, 1174–1183 (2011).

88. Wang, Q. *et al.* The Allen Mouse Brain Common Coordinate Framework: A 3D Reference Atlas ll The Allen Mouse Brain Common Coordinate Framework: A 3D Reference Atlas. doi:10.1016/j.cell.2020.04.007.

89. Fenton, A. A. & Muller, R. U. *Place cell discharge is extremely variable during individual passes of the rat through the firing field*. *Czech Academy of Sciences* vol. 95 www.pnas.org. (1998).

90. Carandini, M. Amplification of trial-to-trial response variability by neurons in visual cortex. *PLoS Biol.* **2**, e264 (2004).

91. Churchland, M. M. *et al.* Stimulus onset quenches neural variability: A widespread cortical phenomenon. *Nat. Neurosci.* **13**, 369–378 (2010).

92. Kampa, B. M. *et al.* Representation of visual scenes by local neuronal populations in layer 2/3 of mouse visual cortex. (2011) doi:10.3389/fncir.2011.00018.

93. Masseck, O. A. & Hoffmann, K. P. Comparative neurobiology of the optokinetic reflex. in *Annals of the New York Academy of Sciences* vol. 1164 430–439 (Blackwell Publishing Inc., 2009).

94. Stringer, C. *et al.* Spontaneous behaviors drive multidimensional, brainwide activity. doi:10.1126/science.aav7893.

95. Larsen, R. S. & Waters, J. Neuromodulatory Correlates of Pupil Dilation. *Front. Neural Circuits* **12**, 21 (2018).

96. J de Vries, S. E. *et al.* A large-scale, standardized physiological survey reveals 1 higher order coding throughout the mouse visual cortex. doi:10.1101/359513.

97. Foster, D. J. & Knierim, J. J. Sequence learning and the role of the hippocampus in rodent navigation. *Current Opinion in Neurobiology* vol. 22 294–300 (2012).

98. Buzsáki, G. & Tingley, D. Space and Time: The Hippocampus as a Sequence Generator. *Trends in Cognitive Sciences* vol. 22 853–869 (2018).

99. Mehta, M. R. *From synaptic plasticity to spatial maps and sequence learning*. *Hippocampus* vol. 25 756–762 (2015).

100. Saleem, A. B., Diamanti, E. M., Fournier, J., Harris, K. D. & Carandini, M. Coherent

representations of subjective spatial position in primary visual cortex and hippocampus. *bioRxiv* 1–19 (2017) doi:10.1101/235648.

101. Rutishauser, U., Mamelak, A. N. & Schuman, E. M. Single-trial learning of novel stimuli by individual neurons of the human hippocampus-amygdala complex. *Neuron* **49**, 805–813 (2006).

102. Silson, E. H., Zeidman, P., Knapen, T. & Baker, C. I. *Representation of contralateral visual space in the human hippocampus 1 2*. (2021). doi:10.1101/2020.07.30.228361.

103. Nishimoto, S. *et al.* Reconstructing visual experiences from brain activity evoked by natural movies. *Curr. Biol.* **21**, 1641–1646 (2011).